Department of Materials Science

**PhD program in Materials Science and Nanotechnology
Cycle XXX – Industrial Curriculum**

BIOFILLERS FROM RENEWABLE LIGNOCELLULOSIC FEEDSTOCK FOR ELASTOMERS

Syed Danish Ali

Reg. No. 799145

Tutor/Supervisor: Prof. Marco Emilio Orlandi

Co-tutor: Dott. Luca Castellani

Coordinator: Prof. Marco Bernasconi
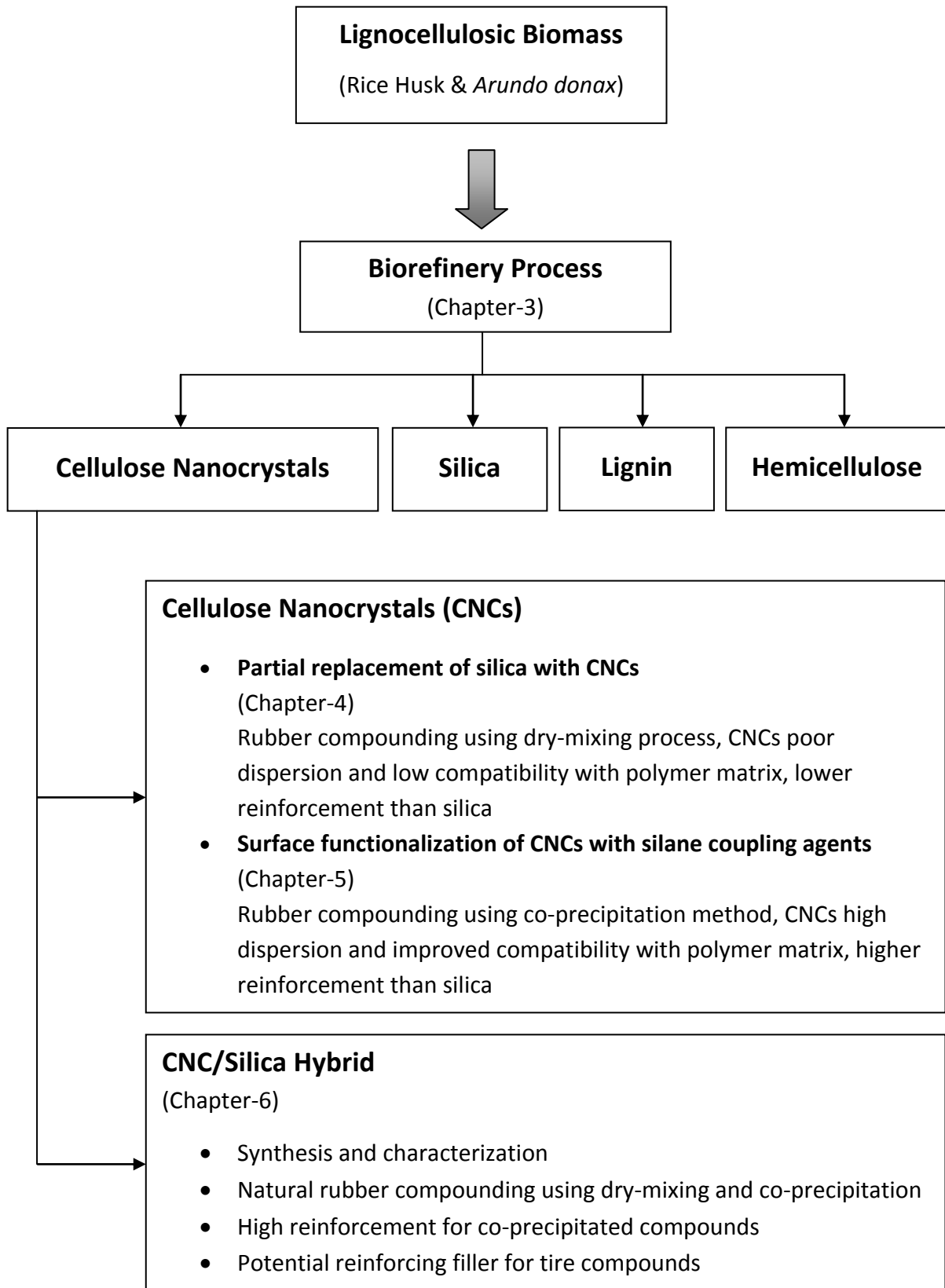
Feb 2018

Abstract

Reinforcing fillers are the primary component of rubber compounds which are added to improve the properties of elastomers. Carbon black and silica are the most commonly used reinforcing fillers in the tire industry due to their outstanding reinforcing effects. Despite the high reinforcing effects, the production of carbon black from non-renewable fossil fuels and high densities of these two fillers make the density of final product relatively high and impart a negative effect on the fuel efficiency of automobiles. These challenges have triggered the increasing concerns for the development of low-density, eco-friendly, sustainable, and renewable materials. Lignocellulosic biomasses have been emerged as potential renewable resources due to their annual renewability and large biomass stock and can be fractionated into value-added products. The work presented in this thesis was started by setting up an integrated biorefinery process for the simultaneous recovery of lignin, hemicelluloses, silica, and cellulose nanocrystals (CNCs) from two lignocellulosic biomasses; *Arundo donax* and rice husk. The CNCs extracted from these lignocellulosic biomasses can be used as promising reinforcing filler due to their fascinating properties, such as renewability, biodegradability, low density, high aspect-ratio, and high mechanical properties.

The feasibility of using CNCs instead of or along with silica in the rubber compounds was studied by investigating the effect of CNCs incorporation on the final properties of the rubber compounds. The incorporation of CNCs in rubber compounds was carried out using three approaches. In the first approach, silica was partially replaced with CNCs in natural rubber compounds prepared through the dry-mixing process. An investigation of the dynamic and tensile mechanical properties of the prepared compounds demonstrated a decrease in the reinforcement of the rubber compounds with the increase of CNCs contents. The tendency of CNCs to form aggregates due to strong hydrogen bonding between hydroxyl groups of CNCs resulted in poor dispersion in the polymer matrix and the dry-mixing process was not strong enough to break down these aggregates, hence reduced mechanical properties were observed. In the second approach, to enhance the filler dispersion and interfacial interaction between CNCs and polymer, the surface of CNCs

was functionalized with six different silane coupling agents and the rubber compounds were prepared through the co-precipitation method. The functionalization was carried out by two different strategies: pre-functionalization of CNCs in ethanol/water mixture before preparing the rubber compound and post-functionalization of CNCs by adding silane coupling agents during the compounding process in the internal mixer. The compounds filled with post-functionalized CNCs showed much higher reinforcement than the silica-filled compound. The mixing of CNCs suspension with natural rubber latex improved the dispersion of CNCs particles in matrix and silane coupling agents enhanced the interfacial interaction between the CNCs and the polymer, resulting in the improved reinforcing effect of CNCs.

In the third approach, the CNC/Silica hybrid was prepared using CNCs as a template and decorating the surface of CNCs with a layer of silica. The hybrid material produced by combining organic and inorganic phases at nanoscale provided unique properties acquired by the synergistic combination of organic and inorganic components with complementary properties. The microscopic and surface area analyses confirmed the rod-like morphology and the core-shell structure of the prepared hybrid. The incorporation of CNC/Silica hybrid in natural rubber significantly improved the mechanical properties of the resulting compounds. The CNC/Silica hybrid demonstrated much higher reinforcement than silica-filled compounds, however much lower density of the final compound. Thus, the prepared hybrid can be used as potential reinforcing filler to replace traditional silica filler in the tire compounds.

Thesis Organizational Chart

Lignocellulosic Biomass

(Rice Husk & *Arundo donax*)

↓

Biorefinery Process

(Chapter-3)

Cellulose Nanocrystals | **Silica** | **Lignin** | **Hemicellulose**

Cellulose Nanocrystals (CNCs)

- **Partial replacement of silica with CNCs**
  (Chapter-4)
  Rubber compounding using dry-mixing process, CNCs poor dispersion and low compatibility with polymer matrix, lower reinforcement than silica
- **Surface functionalization of CNCs with silane coupling agents**
  (Chapter-5)
  Rubber compounding using co-precipitation method, CNCs high dispersion and improved compatibility with polymer matrix, higher reinforcement than silica

CNC/Silica Hybrid

(Chapter-6)

- Synthesis and characterization
- Natural rubber compounding using dry-mixing and co-precipitation
- High reinforcement for co-precipitated compounds
- Potential reinforcing filler for tire compounds

Dedication

This thesis is dedicated to my parents

Acknowledgments

Up and above anything else, all gratitude and praises are due to almighty ALLAH alone, the most gracious, merciful and compassionate, the creator of the universe, Who enabled me to complete this research work successfully. All respects and gratitude for Holy Prophet Hazrat Muhammad (P.B.U.H.) who enabled us to recognize our creator and showed us the way to success.

It is a matter of great pleasure for me to express my deep sense of gratitude to my supervisor Prof. Marco Emilio Orlandi for his supervision, guidance, and support throughout the whole journey. My very special and sincere thanks to Dr. Luca Zoia for his scholarly guidance, encouragements, cooperation, invaluable discussions, and suggestions during the whole course of my research work. I would like to extend my sincere thanks to my industry supervisor Mr. Luca Castellani for his time, guidance, suggestion, and continuous support throughout my research work.

I would like to express my special thanks to Prof. Alain Dufresne, for providing me the opportunity to work under his supervision for six months at LGP2 Pagora, Grenoble Institute of Technology, Grenoble, France. He always remained very supportive, helpful, and available for valuable discussions during my stay at LGP2.

Sincere thanks to my group fellows Eeva Liisa, Anika, and Davide for providing a pleasant and stimulating atmosphere for work. It would be worthwhile to acknowledge the services provided by the lab staff of Pirelli.

I would like to express my thanks to Dr. Sara Qaiser, Director, Nanoscience and Technology Department, and Dr. Hafeez R. Hoorani, DG, National Centre for Physics, Islamabad, Pakistan, for providing leave from my job to complete my PhD study.

I would like to pay my special and heartiest thanks to my beloved fiancée Rumana for her support, encouragement, and affection throughout my PhD study.

In giving appreciation, I must acknowledge my parents, sisters, and brothers. Without their love, encouragement, motivation, support, sacrifice and endless prayers, the present work was impossible.

Contributions of Co-Authors

Prof. Marco Emilio Orlandi and Dr. Luca Zoia were involved in supervising this work and revising of all chapters.

Dr. Davide Barana and Dr. Anika Salanti contributed to the recovery and characterization of lignin and hemicellulose in the biorefinery process of the rice husk and the *Arundo donax*.

Luca Castellani was involved in supervising and designing the formulations of rubber compounds.

Table of Contents

List of Abbreviations

6PPD	N-(1,3-Dimethylbutyl)-N'-phenyl-p-phenylenediamine
ΔM	Degree of crosslinking
AD	*Arundo donax*
AFM	Atomic force microscope
APS	3-aminopropyltriethoxysilane
BET	Brunauer-Emmett-Teller
BR	Butadiene rubber
CBS	N-cyclohexyl-2-benzothiazylsulfenamide
CNCs	Cellulose nanocrystals
CrI	Crystallinity index
CRI	Curing rate index
CSH	CNC/Silica hybrid
CTAB	Cetyltrimethylammonium bromide
DLS	Dynamic light scattering
DP	Degree of polymerization
EDX	Energy dispersive X-ray
F-CNCs	Functionalized cellulose nanocrystals
FESEM	Field emission scanning electron microscopy
FTIR	Fourier-transform infrared
G'	Storage modulus
G'_o	Storage modulus at 1 % strain
G'_∞	Storage modulus at 100 % strain
G''	Loss modulus
GPC	Gel permeation chromatography
ICP-OES	Inductively coupled plasma- Optical emission spectroscopy
LCCs	Lignin-carbohydrate complexes
LODP	Level-off degree of polymerization
MCC	Microcrystalline cellulose
M_H	Maximum torque

M_L	Minimum torque
Mn	Number-average molecular weight
Mp	Peak molecular weight
MPS	3-methacryloxypropyltriethoxysilane
MRPS	3-mercaptopropyltrimethoxysilane
Mw	Weight-average molecular weight
NR	Natural rubber
PLA	Polylactic acid
phr	Parts per hundred parts of rubber
SANS	Small-angle neutron scattering
RH	Rice husk
SBR	Styrene butadiene rubber
SEM	Scanning electron microscope
SEM-FEG	Scanning electron microscope-Field emission gun
SR	Synthetic rubber
T_{90}	Optimum cure time
TCF	Total chlorine free
TEM	Transmission electron microscope
TEMPO	2,2,6,6-tetramethylpiperidine-1-oxyl
TESPD	Bis[3-(triethoxysilyl)propyl]disulfide
TESPT	Bis[3-(triethoxysilyl)propyl]tetrasulfide
T_g	Glass transition temperature
TGA	Thermal gravimetric analysis
TMQ	2,2,4-trimethyl-1,2-dihydroquinoline
Ts2	Scorch time
VTES	Vinyltriethoxysilane
XRD	X-ray diffraction

Chapter 1

Lignocellulosic Biomass: A way to Bio-Based Economy

Syed Danish Ali, Luca Zoia, Marco Emilio Orlandi

1.1 Fossil to Natural Resources

The industrial production of wide range of chemicals and materials are heavily based on fossil resources [1]. The future of the chemical industry is under threat due to the decline of these fossil resources along with their alarming environmental problems, such as greenhouse gas emission and global warming. Henry Ford proposed in the start of the 19th century that the establishment of a bio-based economy is a rational and important alternative for the development of any civilization; however, the lower price of oil than any other product deferred this establishment. From the last century, the depletion of fossil fuel resources causing an increase in the price of the fuel and the cost-effectiveness of these fossil resources is vanishing [2]. On the other hand, the severe ecological problems caused by the substantial use of these fossil resources are serious threats to our society. These devastating issues have triggered the increasing concerns for the development of green, sustainable, eco-friendly, and renewable products. The European Union has already approved laws for the conservation of the environment and initiated greater efforts for developing environmental-friendly materials based on natural resources. Hence, there is great demand to decrease the dependence on non-renewable fossil resources and build up some alternative solutions for the development of materials from natural resources [3,4].

Lignocellulosic biomass has been considered as one of the most promising alternative natural resources for the fossil resources [5,6]. It is a renewable, bio-degradable, cost-effective and most abundant biomass available on earth. It is not only an abundant renewable feedstock but also available globally [7,8]. It is produced naturally through a biological photosynthesis process, consuming water, atmospheric carbon dioxide and sunlight, the only source of sustainable organic carbon and the ideal analogs to fossil

resources for the production of green chemicals and materials without net carbon emission [9,10]. A huge potential of lignocellulosic biomass for sustainable production of fuels, chemicals, and materials have been revealed in many studies [7,8]. Lignocellulosic biomass, having higher oxygen contents than fossil resources, has been expected as an ample carbon-neutral natural resource, which can reduce carbon dioxide emission and environmental concerns. It is a potential substitute to limit the use of fossil resources and can be used to produce biofuels, biochemicals, and bio-materials. Thus, the abundant availability, chemical composition, and cost-effectiveness make the lignocellulosic biomass a promising feedstock for the production of value-added products [11–13].

During the last few decades, a lot of studies have been done on the production of biofuels, chemicals, and materials from renewable biomass, however, there are serious concerns about their sustainability, for example, bioethanol is currently produced from starch and sugar crops. The production of bioethanol from these crops can result in a shortage of food [14]. The key advantage of lignocellulosic biomass on other biomass feedstocks is that these are from a non-edible part of the plants and crops, thus do not come in competition with food supplies [15]. Another economic benefit of lignocellulosic biomass on other important agricultural biomass is that it can be produced in shorter time and at a lower cost. Furthermore, a large volume of agroforestry, agro-industrial and agricultural lignocellulosic wastes are collected every year and disposed to soil and landfill, causing critical environmental problems. These lignocellulosic wastes can be used for the production of numerous value-added chemicals and products [16]. Despite the interesting advantages of lignocellulosic biomass, the development of technologies for the transformation of lignocellulosic biomass to value-added chemicals and products is challenging [9]. Lignocellulosic feedstocks are not easily degradable and show resistance to chemical and enzymatic degradation [13]. Although the lignocellulosic feedstocks are abundantly available and cheap, however, their pretreatment is not cheap from cost and energy point of view and their conversion to fine chemicals and materials at low cost with high yield and selectivity is a serious challenge. An effective and inexpensive production of value-added products from the lignocellulosic biomass mainly relies on the development of an efficient pretreatment system. A lot of research work at present is being carried out throughout the world to give a strong answer to this problem [17,18].

1.2   Structure of Lignocellulosic Biomass

Lignocellulosic biomass is mostly consisting of three components: cellulose, hemicellulose and lignin, a minute quantity of some other components such as extractives, minerals, and acetyl groups are also present. Fig. 1.1 shows the main components present in lignocellulosic biomass. The chemical composition and arrangement of these components of lignocellulosic biomass into the complex irregular three-dimensional formation of varying degree depends on the source of lignocellulosic biomass [13].
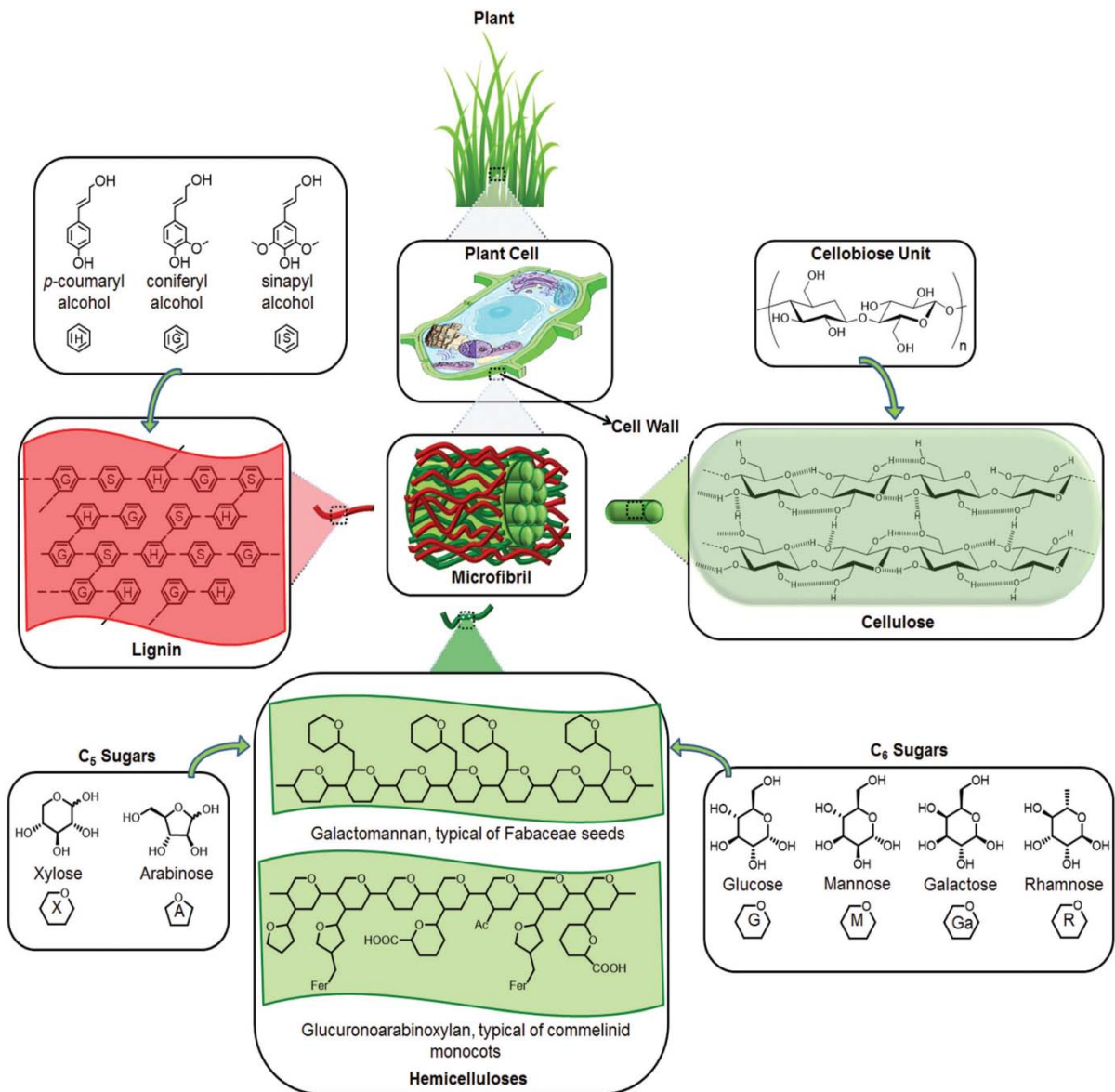
Figure 1.1: The main components of lignocellulosic biomass found in plants cell wall [19]

Lignocellulosic biomass is not easily degradable and shows resistance to degradation, this recalcitrance and toughness are due to the high crystallinity of cellulose, encapsulation of cellulose by hemicelluloses-lignin complex, and hydrophobicity of lignin [13,20,21]. The distribution of cellulose, hemicelluloses, and lignin in the plant cell wall is not uniform and the percentage composition and structure of these components differ according to the source of lignocellulosic biomass [13]. Typically, lignocellulose comprises of 10-25 % lignin, 20-35 % hemicellulose, and 35-50 % cellulose. Other extractives, oil, and minerals from the remaining fraction [17]. Table 1.1 shows the chemical composition of different sources of lignocellulosic biomass.

Table 1.1: The chemical composition of different types of lignocellulosic biomass [19]

Lignocellulosic Biomass		Cellulose (%)	Hemicellulose (%)	Lignin (%)
Hardwood	Poplar	50.8–53.3	26.2–28.7	15.5–16.3
	Oak	40.4	35.9	24.1
	Eucalyptus	54.1	18.4	21.5
Softwood	Pine	42.0–50.0	24.0–27.0	20.0
	Douglas fir	44.0	11.0	27.0
	Spruce	45.5	22.9	27.9
Agricultural Waste	Wheat Straw	35.0–39.0	23.0–30.0	12.0–16.0
	Barley Hull	34.0	36.0	13.8-19.0
	Barley Straw	36.0–43.0	24.0–33.0	6.3–9.8
	Rice Straw	29.2–34.7	23.0–25.9	17.0–19.0
	Rice Husk	28.7–35.6	12.0–29.3	15.4–20.0
	Oat Straw	31.0-–35.0	20.0–26.0	10.0–15.0
	Corn Cobs	33.7–41.2	31.9–36.0	6.1–15.9
	Corn Stalks	35.0–39.6	16.8–35.0	7.0–18.4
	Sugarcane Bagasse	25.0–45.0	28.0–32.0	15.0–25.0
	Sorghum Straw	32.0–35.0	24.0–27.0	15.0–21.0
Grasses	Grasses	25.0–40.0	25.0–50.0	10.0–30.0
	Switchgrass	35.0–40.0	25.0–30.0	15.0–20.0

1.2.1 Cellulose

Cellulose is the major constituent of lignocellulosic biomass and one of the most important natural polymers. The total production of cellulose is more than 7.5×10^{10} tons per year, which makes it the most abundant renewable organic polymer produced in the world [22]. Generally, cellulose can be defined as a water-insoluble, tough, and fibrous material that plays an important part in retaining the structure of plant cell wall. Since the discovery and isolation of cellulose in 1838, a lot of research work is constantly being carried out to study the chemical and physical properties of cellulose, its assembly and biosynthesis, and structural features [23]. Many reviews have already been published on this interesting renewable material [24–33].

Cellulose is a high molecular weight homopolymer composed of repeating unit of β-1,4 glucose linked by glycosidic linkage, in which every repeating unit is corkscrewed 180° with respect to its neighbor. The repeating unit is often considered to be a dimer of glucose, known as cellobiose, as shown in Fig. 1.2. The two ends of the cellulose chain are chemically different from each other, one end has a hemiacetal unit, the reducing end, and the other end is a nonreducing functionality having a hydroxyl group. Usually, the cellulose chains have about 20,000 repeating glucose units or polymerization degree, however, the primary cell wall of the plant can have short chains of cellulose. All the β-D-glucopyranose rings in the cellulose chain take a $^{4}C_{1}$ chair conformation, which resulted in the equatorial position of the hydroxyl groups and vertical position of the hydrogen atoms. The strong intramolecular hydrogen bonding network between hydroxyl groups and oxygen atoms stabilizes this conformation.

Naturally, cellulose does not exist as discrete molecules, but it occurs in the form of cellulose fiber containing the chains of cellulose molecules. During the biosynthesis process, the individual cellulose molecules go through the spinning in a hierarchical order and elementary fibrils are formed by usually 36 individual cellulose molecules. These elementary fibrils make the microfibrils which sequentially built the cellulose fibers. This packing of elementary fibrils in cellulose fibers may differ in different sources depending on the conditions of biosynthesis [34]. The diameter of cellulose microfibrils depends on the origin of cellulose and range from 2 to 20 nm. The aggregation of cellulose chain to

microfibrils happens due to van der Waals forces and strong hydrogen bonding network, both inter- and intra-molecular hydrogen bonding. The microfibrils have both crystalline and amorphous domains depending on the extent of hydrogen bonding.
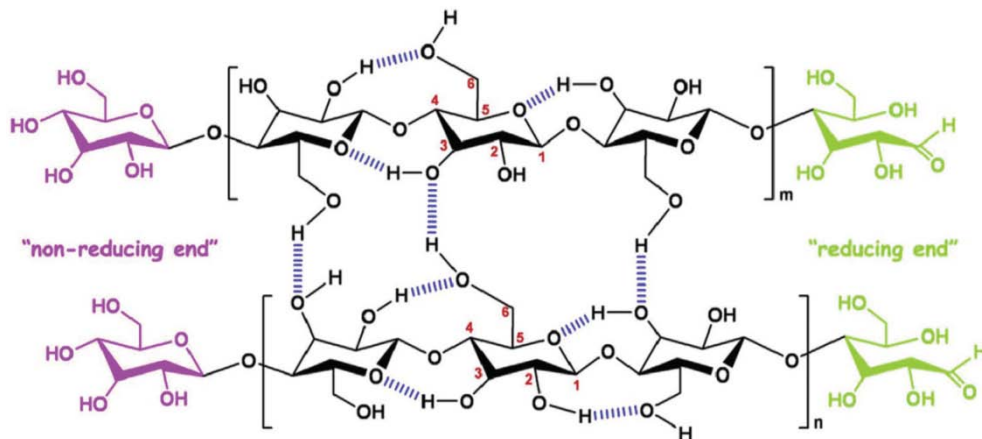
Figure 1.2: Chemical structure, and inter- and intra-molecular hydrogen bonding network in cellulose [35]

1.2.2 Hemicellulose

Hemicellulose is the second most abundant polymer produced in the biosphere and composed of many heteropolymers such as glucomannan, glucuronoxylan, galactomannan, xylan, arabinoxylan, and xyloglucan. Monomers of five and six carbon atoms, such as galactose, glucose, mannose, arabinose, xylose and acetylated sugars, made the heteropolymers of the hemicellulose. Partial molecular structure of O-acetyl-4-methyl glucuronoxylan is shown in Fig. 1.3. The composition of hemicellulose depends on the source of hemicellulose, e.g. softwood hemicelluloses usually comprise glucomannans, hardwood hemicelluloses typically have xylans, and straws and grasses mostly contain xylan, galactan, and arabinan [19,20,36]. The monomers which made the heteropolymers can be used as fundamental, cheap, and scale-up raw materials for the production of a lot of chemicals.

Unlike cellulose, hemicellulose does not have crystalline domains and have amorphous and regular structure. Hemicellulose creates a strong and complex bonding network with

cellulose microfibrils and lignin and contributes to the structural strength of plant cell wall. The complex bonding network provides a protective cover against the hydrolysis and makes it challenging for the synthesis of a large number of biochemicals. Before the synthesis of chemicals, the lignocellulosic fraction of the plant is subjected to pre-treatment to separate it from lignin and cellulose. The removal of lignin from lignocellulosic biomass exposes the hemicellulose part and enhances the efficiency of hydrolysis process to transform hemicellulose fraction to xylose [37].
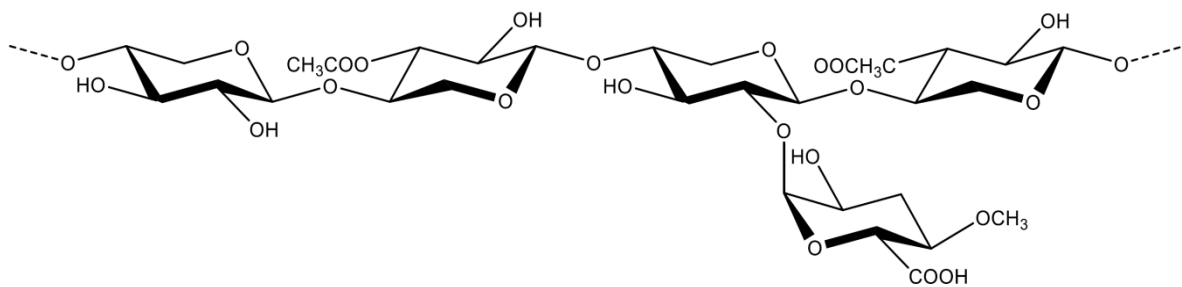
Figure 1.3: Partial molecular structure of O-acetyl-4-methyl glucuronoxylan [38]

1.2.3 Lignin

Lignin is the third most abundant polymer found in nature. It is a three dimensional, complex heterogeneous, amorphous, high molecular structure polymer composed of three phenolic monomers which are linked through alkyl-alkyl, alkyl-aryl or aryl-aryl ether bond. Lignin comprises about 15-30 % of lignocellulosic biomass and it is an aromatic-based cross-linked heteropolymer, which plays an important role in water transportation and provides structural strength to plant. It acts like glue which binds the different component of cell wall together and imparts structural strength to plant tissues and fibers, rigidity to the cell wall, and resistance to the attack of microbes and pathogens [39]. Lignin is the only scalable renewable raw material composed of aromatic building blocks and can be used for the production of value-added bio-products [40]. The three phenylpropanolic building blocks monolignols, those are: coumaryl alcohol (p-hydroxyphenyl propanol), coniferyl alcohol (guaiacyl propanol) and sinapyl alcohol (syringyl alcohol) form the structure of lignin [41]. The composition of these monolignols monomers varies depending on the

plant species. Hardwood lignins contain sinapyl alcohol and coniferyl alcohol, softwood lignins mostly have coniferyl alcohol, and herbaceous plants like grasses usually contain all the three monomers [42]. The structural motifs of softwood lignin are shown in Fig. 1.4. The content of monomers has a great effect on the bond formation in the polymerization process of lignin, for example, softwood has more carbon-carbon bond than hardwood [43]. Hence, it becomes really difficult to identify the precise chemical structure of every lignin due to various chemical bond and contents of monomers.
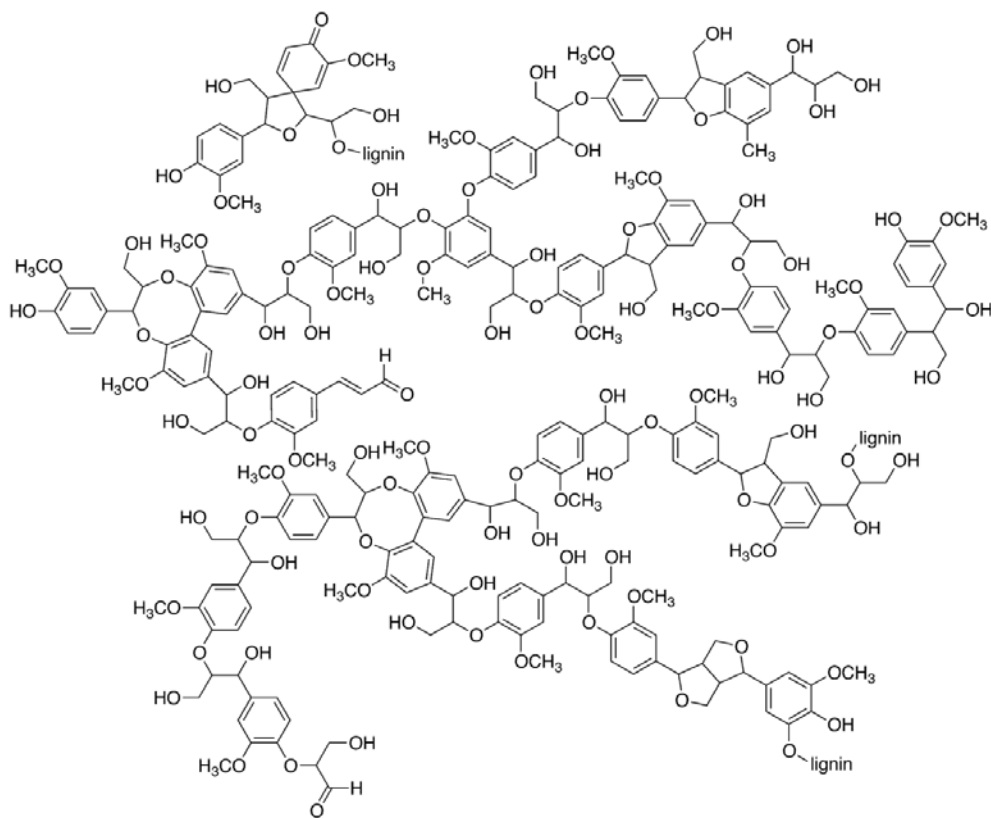
Figure 1.4: Structural motifs of softwood lignin [44]

1.3   Biorefinery of Lignocellulosic Biomass

The establishment of bio-based industries by utilizing the different constituents of lignocellulosic biomass for the production of many value-added materials of commercial value has been acknowledged as the most promising approach. This integrated strategy, known as "biorefinery", has become apparent since the late 20th century and represents a

key piece toward sustainability. The concept of the biorefinery is acquiring growing interest all over the world both academically and commercially. There are various definitions for biorefinery from different organizations such as, The International Energy Agency (IEA), The US Department of Energy (DOE), American National Renewable Energy Laboratory (NREL), but generally, the term biorefinery is referred to as a facility or network of facilities that integrate biomass in a range of bio-based products (for example, human food, materials, and chemicals) and bio-energy (heat, power, and fuels) in a sustainable and economical way [45–48]. The concept of the biorefinery is similar to today's petroleum refinery which produces multiple products such as fuels, chemicals, and materials as shown in Fig. 1.5.
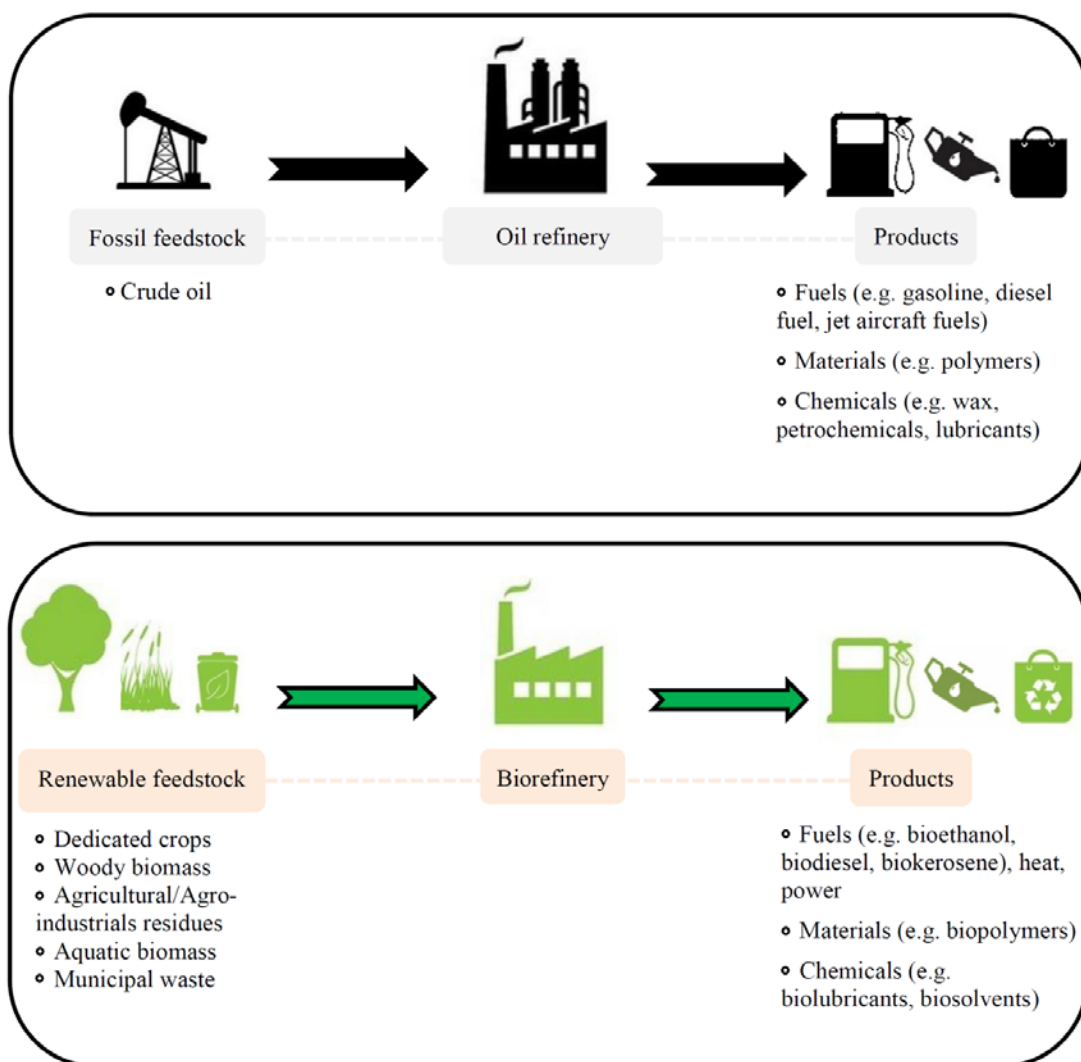
Figure 1.5: Comparison between oil and biorefinery [49]

In a conventional oil refinery, the crude oil is transformed to multiple fuels, building blocks of different chemicals, and materials. While in a biorefinery, the different renewable lignocellulosic biomass such as dedicated energy crops and residues, agricultural waste, forestry, industrial and municipal solid waste, and marine resources are converted into many products of market value. These multiple products include products having low-volume but high-value such as fine chemicals for cosmetic and pharmaceutical industries, chemicals for special use like cleaning materials and food additives; also the products having high-volume but low-value such as biofuels (e.g. biogas and bioethanol), materials and chemicals in bulk like acetic acid [14]. Fig. 1.6 shows a value pyramid of a number of products obtained from the biorefinery of biomass as a function of their market value and the volume produced. Many factors such as availability, composition, the price of the raw material, market value and market needs, pretreatments required for selected biomass, and regulations, should be considered to point out the most promising product with significant economic value for a biorefinery.
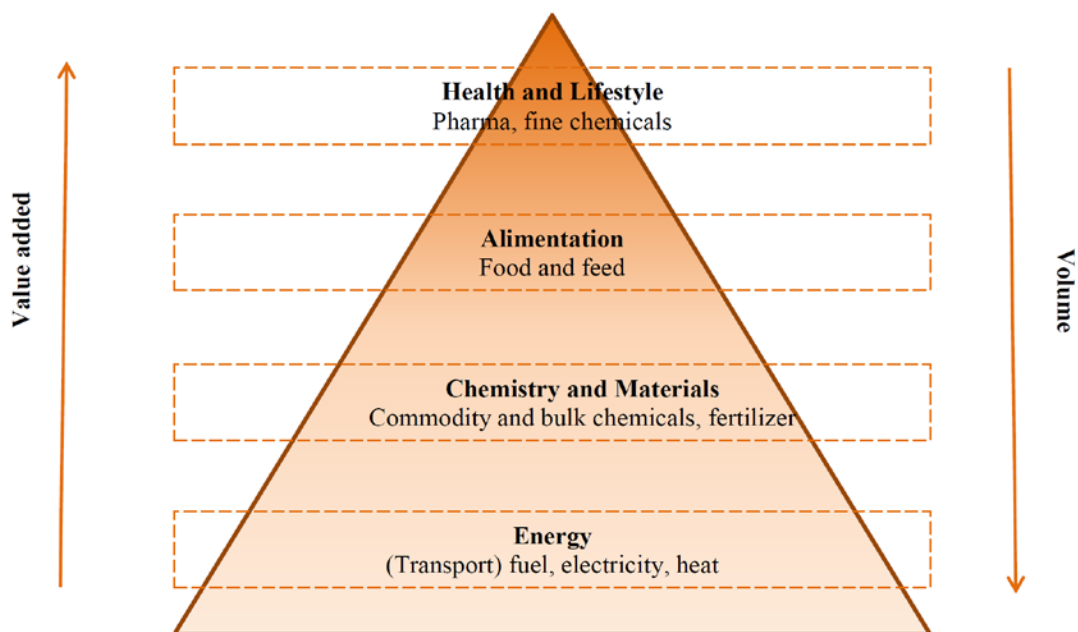
Figure 1.6: Value pyramid of different biomass applications [49]

Biorefinery can be divided into two groups depending on the major product produced from the renewable biomass: energy-driven and material-driven [50]. In an energy-driven

biorefinery, the biomass is mainly utilized to make multiple biofuels, heat, and power while the by-products are used to make value-added chemicals and materials to get additional benefits. In a materials-driven biorefinery, the biomass is mainly utilized to make fine chemical and materials of high commercial value and the by-products are used to make fuel, heat, and power. Maximum economic benefits from biomass can be obtained using this promising approach. The carbohydrate fraction of the lignocellulosic biomass such as cellulose and hemicellulose can you converted through the chemical and biological process into various promising building blocks. These building blocks, having many functional groups, can be used to produce multiple value-added chemicals, materials, and products [51].

1.4 Cellulose Nanocrystals

In nature, cellulose exists in the form of fibers which are composed of chains of cellulose molecules. The chains of cellulose molecules are aggregated into the elementary fibrils, known as protofibrils, due to the strong inter- and intra-molecular hydrogen bonding and van der Waals forces. These elementary fibrils are packed into microfibrils which in turn form the cellulose fibers. If the terminal complexes are not disturbed, an unlimited number of nanofibrils with only a limited number of amorphous regions and defects can be generated [34,52]. The amorphous regions are spread through the segments of elementary fibrils as chain dislocations where the microfibrils are distorted due to internal strain in the cellulose fiber [53]. In the crystalline regions, chains of cellulose are tightly packed stabilized by the complex and strong network of inter- and intra-molecular hydrogen bonding. The crystal size and degree of crystallinity depend on the cellulose origin, for example, the degree of crystallinity differ from 50 % in mostly plant to 60 % in bacterial cellulose, 80 % in tunicates, and 90 % in some algae [54]. The transverse degradation of cellulose fibers at the amorphous regions results in defect-free highly crystalline rod-like nanoparticles, known as cellulose nanocrystals.

Cellulose nanocrystals (CNCs), an emerging class of extremely interesting bio-based nano-materials, have gained tremendous level of attention in both academic and industrial communities due to its fascinating physiochemical properties such as renewability,

biodegradability, biocompatibility, sustainability, optical transparency, flexible surface chemistry, low density, high surface area, and better mechanical properties [55,56]. The CNCs are usually isolated from the cellulose fibers by controlled acid hydrolysis. This idea of acid hydrolysis was presented for the first time by Nickerson and Habrle in 1947 [57] and then confirmed by Ränby in 1950, who prepared a cellulose colloidal suspension by controlled acid hydrolysis of cellulose fibers using sulfuric acid [58,59]. The transmission electron microscopic analysis of the dried colloidal suspension of CNCs showed the presence of rod-like nanoparticles and electron diffraction analysis revealed that both needle-like crystals and original cellulose fibers have the same crystalline structure [60]. Later, Marchessault et al. in 1959 demonstrated the nematic liquid crystalline ordering of CNCs in colloidal suspension [61]. The interest in CNCs, however, started to increase after the discovery of reinforcement of nanocomposites with CNCs by Favier et al. in 1995 and a lot of research has been focused on CNCs nanocomposites due to the increasing interest in the preparation of functional materials from renewable resources [62,63].

1.4.1 Dimensions and Morphology of Cellulose Nanocrystals

Cellulose nanocrystals are highly crystalline needle-like or rod-like nanoparticles having high surface area and can be obtained from many natural resources. The dimensions (length and width) of the CNCs depend on the origin of cellulose as well as the hydrolysis conditions to isolate the CNCs. The diffusion-controlled behavior of the acid hydrolysis process plays a role in such differences in dimensions. These diversities in the dimension of the CNCs, prepared from a given source of cellulose using hydrolysis process, can be minimized by including filtration, differential centrifugation or ultracentrifugation [63–65]. Usually, the CNCs isolated from terrestrial woody biomass have a short length, while on the other hand, CNCs obtained from tunicates and bacteria have higher length. The dimensions of the CNCs vary from few nanometers in width and from tens of nanometers to several micrometers in length. Fig. 1.7 shows the TEM images of CNCs isolated from different sources. The accurate morphological characterizations of CNCs are typically carried out by advanced analytical techniques such as microscopy (AFM, TEM) [66], dynamic light scattering [67], and small angle neutron scattering [68]. In the TEM analysis, the drying step during the sample preparation cause the aggregation of CNCs, additionally,

instrumental artifacts result in overestimation of CNCs dimensions. The aggregation of CNCs can be avoided by using the TEM in cryogenic mode [63]. A rapid and efficient surface morphology analysis of CNCs at ambient conditions can be done by using atomic force microscope (AFM) up to the angstrom level [66,69–71]. Although, rounded cross-section profiles may observe in AFM topography which may be due to AFM tip and tip-broadening effects. The use of AFM for the measurement of mechanical properties of CNCs has also been reported [72].
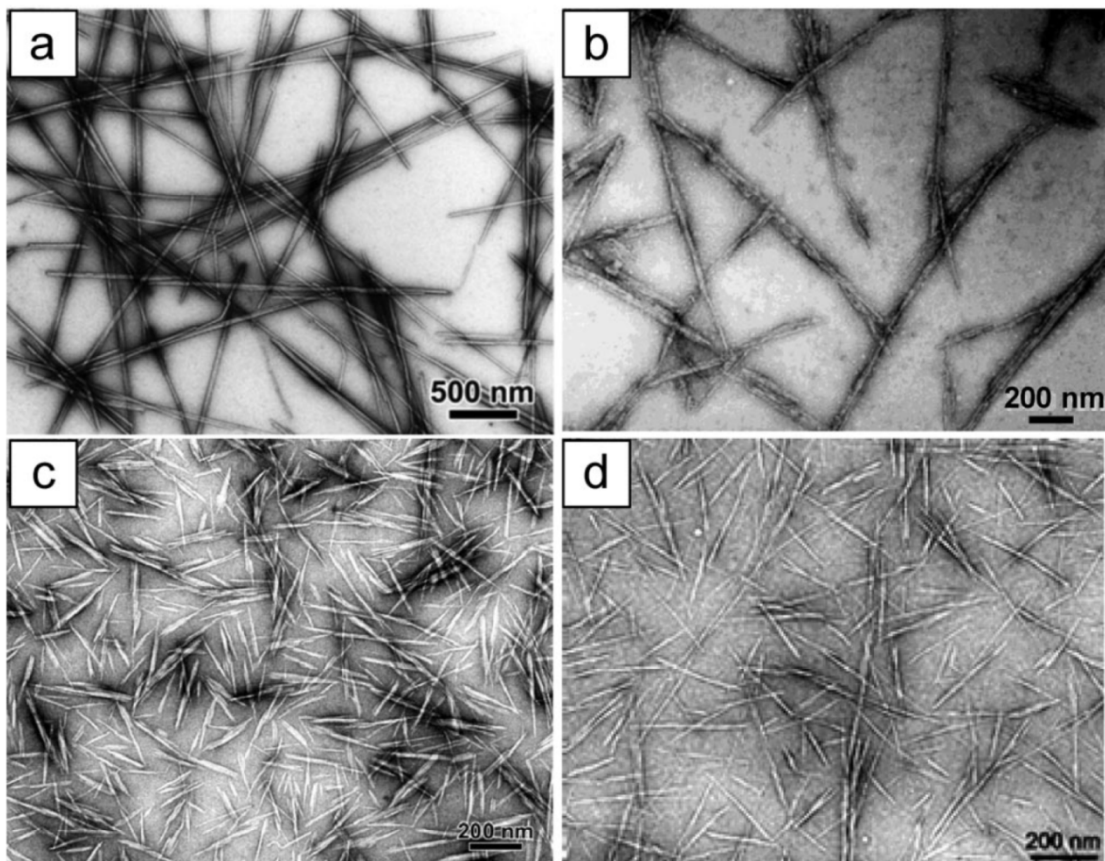
Figure 1.7: TEM images of CNCs obtained from, (a) tunicate [63], (b) bacterial [73], (c) ramie [74], and (d) sisal [75]

The typical dimensions of the CNCs obtained from different sources vary from few nanometers in width and tens of nanometers to several micrometers in length. Typical dimensions of CNCs isolated from a variety of cellulose sources and measured by different techniques are outlined in Table 1.2. The CNCs obtained from wood have a width of 3-5

nm and length of 100-200 nm, while CNCs isolated from cotton are 5-10 nm in width and 100-300 in length. The length-to-width ratio (aspect ratio) of CNCs ranges from 10 to 30 for cotton and 70 for tunicate.

Table 1.2: Dimensions of CNCs obtained from various cellulose sources

Source	Length (nm)	Width (nm)	Technique	Ref
Bacterial	100-1000	10-50	TEM	[76]
	100-1000	5-10	TEM	[73]
Cotton	100-150	5-10	TEM	[77]
	70-170	~7	TEM	[78]
	200-300	8	TEM	[79]
	255	15	DLS	[67]
	150-210	5-11	AFM	[66]
Cotton linter	100-200	10-20	SEM-FEG	[80]
	25-320	6-70	TEM	[63]
	300-500	15-30	AFM	[81]
MCC	35-265	3-48	TEM	[63]
	250-270	23	TEM	[82]
	~500	10	AFM	[83]
Ramie	150-250	6-8	TEM	[74]
	50-150	5-10	TEM	[84]
Sisal	100-500	3-5	TEM	[75]
	150-280	3.5-6.5	TEM	[85]
Tunicate	1160	16	DLS	[67]
	500-1000	10	TEM	[86]
	1000-3000	15-30	TEM	[87]
	100-1000	15	TEM	[79]
	1073	28	TEM	[63]
Valonia	>1000	10-20	TEM	[88]
Softwood	100-200	3-4	TEM	[89]
	100-150	4-5	AFM	[90]
Hardwood	140-150	4-5	AFM	[90]

The cross-section morphology of CNCs is also dependent on the source of the cellulose fibers. During the biosynthesis process, the terminal complexes are supposed to be the source of the morphological shape of the cross-section. It has been reported that the terminal complexes are arranged in different manners based on the origin of the cell wall, which resulted in different geometries of the cellulose crystals [34]. The TEM analysis showed that *Valonia* has the cellulose crystallites with a square cross-sectional shape having an average length of 18 nm [88]. On the other hand, TEM and SANS analysis revealed a rectangular (8.8 × 18.2 nm) cross-sectional shape for CNCs obtained from tunicate [68,91].

1.4.2 Preparation of Cellulose Nanocrystals

Acid hydrolysis is the most common method used for the preparation of CNCs from cellulose fibers. During the acid hydrolysis process, the amorphous or paracrystalline regions in cellulose fibers are more available to acid attack and preferentially hydrolyzed, on the other hand, crystalline regions show high resistance to acid attack and isolated in the form of cellulose nanocrystals as shown schematically in Fig. 1.8 [92,93]. The acid molecules preferentially attack the amorphous regions of the cellulose fibers and get diffused into the cellulose microfibrils, causing the breakage of glycosidic bonds within cellulose chains. This process leads to the destruction of the hierarchical structure of microfibrils into the CNCs [94].
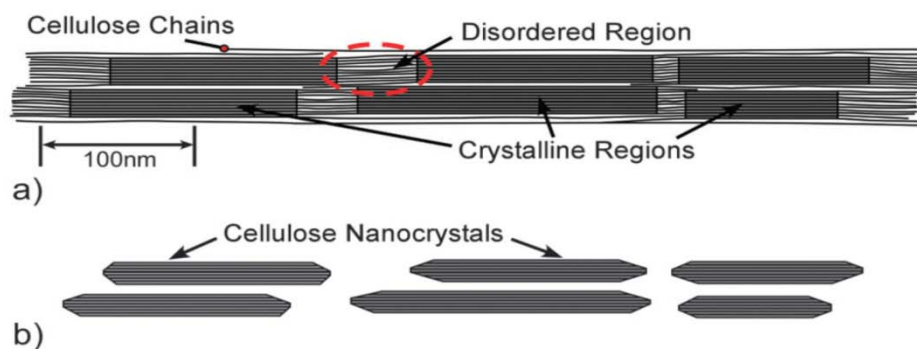
Figure 1.8: Schematics of (a) Cellulose microfibrils having crystalline and amorphous regions (b) cellulose nanocrystals obtained after acid hydrolysis [95]

The selective acid cleavage of cellulose chains takes place due to the difference in kinetics of hydrolysis between the crystalline and amorphous regions [96]. The acids used in the hydrolysis process releases the hydronium ions, which reacts with the oxygen atom of glycosidic linkage between the two glucose monomers, resulting in the cleavage of glycosidic bonds of the amorphous domains [97]. Generally, the degree of polymerization (DP) of cellulose rapidly starts decreasing during the acid hydrolysis and reached to the level-off degree of polymerization (LODP). The LODP is related to the source of cellulose fibers, typically, it is reported that the LODP value for cotton is 250 [98], 140-200 for wood pulp [99], and 300 for ramie [100].

In a typical hydrolysis process, highly concentrated acid and distilled water are mixed with the cellulosic material under firmly controlled conditions. Many researchers have reported the effect of different operating parameters on the physiochemical, mechanical, and thermal properties of the obtained CNCs. The temperature, agitation speed, hydrolysis time, concentration and nature of acid used, moreover, the ratio of acid-to-cellulosic fibers play a key role in the dimensions, crystallinity, morphology, mechanical properties, and thermal stability [90,101–103]. At the end of the hydrolysis process, the suspension is subjected to centrifugation and repeated washing with distilled water. Dialysis against deionized water is also carried out to remove any traces of free acid. Additionally, sonication treatment has also been reported to get stable and homogeneous CNCs dispersion in water [104–106].

Sulfuric acid and hydrochloric acids are the most commonly used acids in the hydrolysis process however many other acids such as hydrobromic acid, phosphoric acid, hydrogen peroxide, and maleic acid have also been studied for the preparation of CNCs [107–109]. When hydrochloric acid is used in the hydrolysis process, the obtained CNCs have very low surface charge density which results in the limited dispersion and flocculation in the aqueous suspensions [110]. However, when sulfuric acid is used in hydrolysis, a highly dispersed CNCs aqueous suspension is obtained which is due to the high surface charge density of the isolated CNCs owing to the reaction between hydroxyl groups of the cellulose and sulfuric acid resulting in highly charged sulfate esters [95,97]. The thermostability of the CNCs is compromised due to presence sulfate groups on the CNCs

surface, in fact, the sulfate moieties catalyze and start to degrade the CNCs especially at high temperatures [73]. A two-steps hydrolysis process, using hydrochloric acid in the first step and sulfuric acid in the second step in a controlled manner, gives the opportunity to tune the surface charge density, although having the same morphology and dimensions of CNCs as those directly prepared from sulfuric acid hydrolysis [89,111].

1.4.3 Chemical Modifications of Cellulose Nanocrystals

The presence of numerous hydroxyl groups on the surface of CNCs provides active sites for chemical modification. Many chemical modifications of CNCs such as etherification, esterification, silylation, oxidation, cationization, polymer grafting, etc, have been reported [112–118]. Fig. 1.9 shows the common chemical modifications of the CNCs. Between the three types of hydroxyl in the cellulose structure, the hydroxyl group of the primary alcohol at sixth carbon is more susceptible to chemical modification [119]. The hydrophilic character of hydroxyl groups resulted in the imperfect dispersion of CNCs in non-polar solvents and hydrophobic polymer matrices. Different chemical functionalities are introduced onto the CNCs surface to have either, stable and homogeneous dispersion in non-polar solvents by creating positive or negative electrostatic charges, or a better dispersion and improved compatibility with polymer matrices, especially with hydrophobic and non-polar matrices. However, the preservation of native morphology and crystallinity of the CNCs, while functionalizing the surface only, is the main challenge in the chemical modification of CNCs. The chemical modifications of CNCs is gaining increasing research interests due to promising mechanical properties of CNCs and potential applications of modified CNCs in nanocomposites, biomedical, etc.

Non-covalent surface modifications of CNCs are usually carried out by surfactant adsorption on the surface through van der Waals forces, hydrogen bonding, electrostatic attractions or hydrophilic affinity. Heux et al, reported for the first time the use of surfactants phosphoric acid ester with alkylphenol tails to modify the CNCs surface [79]. The results revealed that the coated layer of surfactant on the CNCs surface has a thickness of about 1.5 nm and resulting modified CNCs have a very high dispersion in a non-polar solvent [79,120].
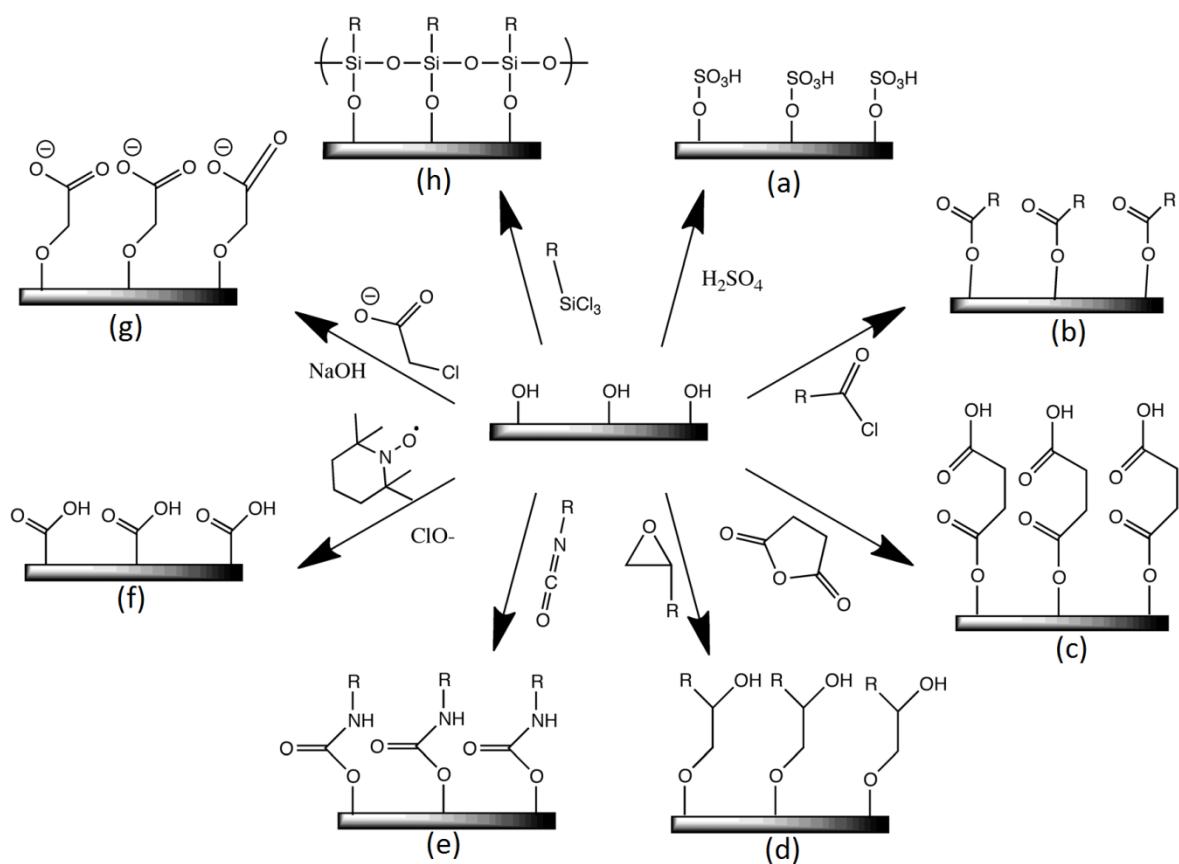
Figure 1.9: Common modification chemistries of CNCs surfaces: (a) sulfuric acid treatment provides sulfate esters, (b) carboxylic acid halides create ester linkages, (c) acid anhydrides create ester linkages, (d) epoxides create ether linkages, (e) isocyanates create urethane linkages, (f) TEMPO mediated hypochlorite oxidation creates carboxylic acids, (g) halogenated acetic acids create carboxymethyl surfaces, and (h) chlorosilanes create an oligomeric silylated layer [95].

The primary hydroxyl groups present on the surface of CNCs are converted to carboxyl form by a simple and green TEMPO (2,2,6,6-tetramethylpiperidine-1-oxyl)-mediated oxidation process. This process uses the stable nitroxyl radical (TEMPO) in the environment of NaOCl and NaBr. This technique was first time developed by De Nooy et al. in 1994 and demonstrated the oxidation of only primary hydroxyl groups of polysaccharides, whereas the secondary hydroxyl groups left unchanged [121]. The crystal axis and morphology of the CNCs restrict the accessibility of hydroxymethyl groups for oxidation and only half of the hydroxymethyl groups undergo the oxidation process, while the remaining half is buried in the crystal structure as shown in Fig. 1.10 [122].
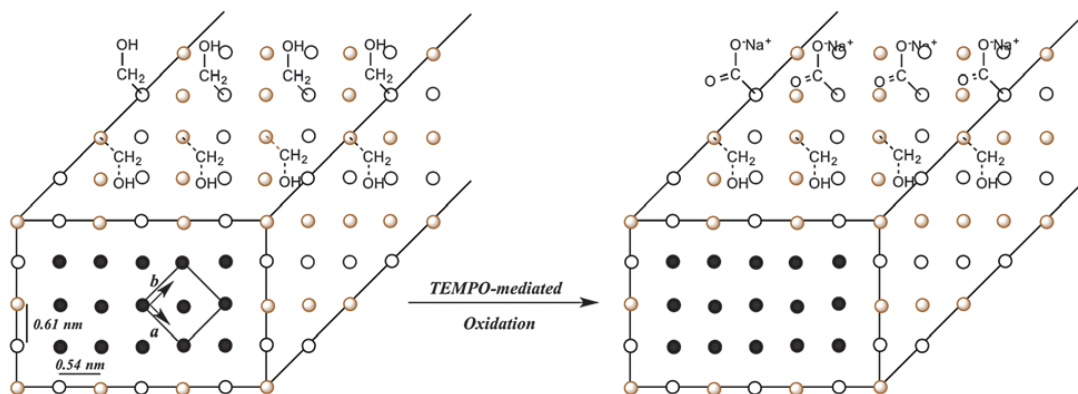
Figure 1.10: Schematic representation of a CNC cross-section illustrating the selective TEMPO-mediated oxidation of primary hydroxyl groups at the surface of the crystal [122].

Araki et al. reported the TEMPO-mediated oxidation of CNCs prepared through the hydrochloric acid hydrolysis and demonstrated a stable and homogeneous dispersion of modified CNCs in water [77]. Habibi et al. reported the TEMPO-mediated oxidation of CNCs prepared from tunicate through the hydrochloric acid hydrolysis and revealed that the original morphology of the CNCs was not compromised [122].

The silylation of CNCs with different alkyldimethylchlorosilanes, with alkyl moieties ranging from small to long-chain carbon backbone such as isopropyl, n-butyl, n-dodecyl, etc, have been reported [123]. It has been reported that a stable suspension of the modified CNCs can be obtained in low polarity solvents with a degree of substitution ranging between 0.6 and 1, also the CNCs maintained their morphological integrity. On the other hand, a higher degree of substitution (greater than 1) results in degradation of crystals and hence loss of morphological integrity. Frone et al. studied the functionalization of CNCs with 3-aminopropyltriethoxysilane and reported the increased compatibility of modified CNCs with PLA which resulted in remarkable improvement in mechanical properties of the nanocomposites [124].

The chemical modification of CNCs through esterification has been widely studied due to easy and simple modification process. Both phosphorylation and sulfonation, during the acid hydrolysis of CNCs, are the examples of esterification reactions. The acetylation of CNCs is the most extensively studied among the esterification reactions. Sassi and Chanzy reported the acetylation of the model CNCs isolated from tunicate and *Valonia* using acetic

anhydride and acetic acid and verified two mechanisms for acetylation; homogeneous and heterogeneous acetylation [91]. The homogeneous acetylation proceeds through a non-swelling mechanism and acetylated cellulose chains are dissolved in the reaction medium, resulting in a reduction of crystal dimensions. While in heterogeneous acetylation, that contains a diluent like toluene, acetylated cellulose chains remain insoluble and surround the unreacted cellulose chains of the crystalline core. The one-pot reaction for simultaneous hydrolysis of amorphous cellulose and Fischer esterification of hydroxyl groups has been reported by Braun and Dorgan as shown in Fig. 1.11 [125].
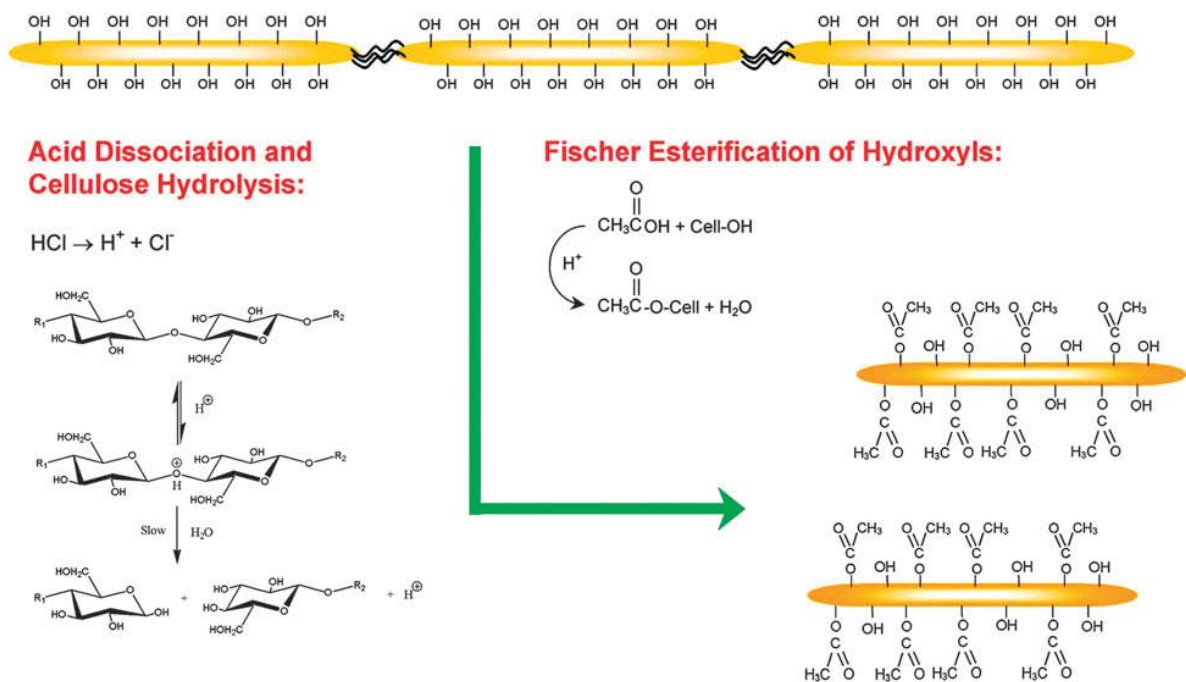
Figure 1.11: Reaction scheme illustrating the one-pot cellulose hydrolysis and esterification of hydroxyl groups [125]

1.4.4 Applications of Cellulose Nanocrystals in Polymer Composites

CNCs is a promising renewable nanomaterial for a large number of applications, such as drug delivery, biosensing, green catalysis, synthesis of antimicrobial and medical materials, enzyme immobilization, etc [126]. Since the introduction of CNCs for the first time as reinforcing filler in poly (styrene-*co*-butyl acrylate) (poly (S-*co*-BuA)) based composites by

Favier et al. [62], CNCs have gained a high level of attention in polymer composites field owing to their fascinating inherent properties such as renewability, biodegradability, unique morphology, nanoscale dimensions, low density, high surface area, ease of chemical modification, and high mechanical properties. A lot of studies have been reported to incorporate CNCs in number of polymer matrices, such as polyurethane [127], poly (vinyl chloride) [128,129], polypropylene [130], polyethylene [84], epoxides [93], poly (ethylene-vinyl acetate) [131], poly (vinyl acetate) [75], poly (vinyl alcohol) [132], carboxymethyl cellulose [133], cellulose acetate butyrate [134], poly (oxyethylene) [135], styrene-butyl acrylate latex [136], poly (caprolactone) [74], polysulfonates [137], polysiloxanes [138], and bio-based polymers, such as polyhydroxybutyrates [139], poly (hydroxyoctanoate) [140], poly (lactic acid) [141], chitosan [81], and starch-based polymers [92,142].

The nanoscale dimensions, high aspect ratio, and fascinating mechanical properties of the CNCs make them an ideal candidate for enhancement of mechanical properties of the host material. Theoretically, CNCs have the axial Young's modulus equal to that of Kevlar but higher than steel. A theoretical study shows that a perfect crystal of cellulose has Young's modulus value of 167.5 GPa [143]. Recently, Sturcova et al [144] and Rusli et al [145] used Raman spectroscopy for the measurement of elastic modulus of CNCs isolated from tunicate and cotton, respectively, and showed elastic modulus value of 143 GPa for tunicate and 105 GPa for cotton. Favier et al. for the first time incorporated CNCs, obtained from tunicate, as reinforcing filler in Poly(S-Co-BuA) and dynamic mechanical analysis showed a significant increase in the storage modulus of the nanocomposites even at low contents of CNCs [62,146]. It was established that the reinforcing effect of CNCs in the polymers composites is due to the development of a rigid percolating filler network [147,148]. The formation and extent of percolation network play an important role in the mechanical properties of composites and are affected by the filler properties such as the dimension of the filler, filler-filler and filler-polymer interactions. The aspect ratio (length to diameter ratio, L/d) of CNCs decides the percolation threshold value and determines the mechanical properties of the composites. A high aspect ratio of CNCs provides high reinforcement to nanocomposites as low volume of filler is required to attain the percolation. Samir et al. studied the use of CNCs, extracted from tunicate ($L/d \sim 67$),

bacterial ($L/d \sim 60$), and Avicel ($L/d \sim 10$), in poly(S-*co*-BuA) polymer matrix and reported the highest value of modulus for tunicate CNCs that have higher aspect ratio than other two [149]. De Rodriguez et al. used sisal CNCs with high aspect ratio as reinforcing filler in polyvinyl acetate and reported that high aspect ratio ensures percolation and provided thermal stability and mechanical improvement at lower filler contents [75].

The final properties of the polymer composites largely depend on the processing techniques. The processing technique is selected while considering the inherent properties of CNCs, their surface characteristics (chemically modified or not), the nature of polymer matrix (degradation, dispersibility, and solubility), and required final properties of the composite material. The formation of a rigid network of CNCs is the origin for improvement in mechanical properties of the polymer composites. The formation of this network is influenced by both the surface chemistry of the CNCs and nature of the polymer matrix and strongly affects the mechanical performance. To obtain the optimum mechanical properties, interfacial interactions between CNCs-CNCs and CNCs-matrix should be compromised [150]. Poor interactions between CNC and matrix result in significant decrease in the mechanical properties because CNCs are typically released from the matrix. Unexpectedly, when composites are prepared through casting method, very strong interactions between CNCs and matrix cause a decrease in the elastic modulus which is most probably due to the fact that the CNCs mobility is restricted and they could not form the percolation network. This behavior was clearly shown in the case of composite formed using CNCs prepared from cottonseed linters as reinforcing filler in glycerol-plasticized starch [142]. Although, this behavior is not observed when polymer composites are prepared through a sol-gel process where percolation is formed before the addition of polymer solution. In this case, strong CNCs-matrix interactions increase the nonlinear mechanical properties particularly ultimate strength when CNCs are modified chemically with long-chain molecules such as polymer chains [151,152], fatty acids [84], N-octadecyl isocyanate [85], or surfactants [153]. In addition, if the grafted chains and the matrix are the same, better compatibilization can be obtained due to the formation of a co-continuous phase.

References

[1]   J.C. Serrano-Ruiz, R. Luque, A. Sepúlveda-Escribano, Chem. Soc. Rev. 40 (2011) 5266.

[2]   L.A. Lucia, BioResources 3 (2008) 981–982.

[3]   Y. Ahn, S.H. Lee, H.J. Kim, Y.-H. Yang, J.H. Hong, Y.-H. Kim, H. Kim, Carbohydr. Polym. 88 (2012) 395–398.

[4]   K.G. Satyanarayana, G.G.C. Arizaga, F. Wypych, Prog. Polym. Sci. 34 (2009) 982–1021.

[5]   C.-H. (Clayton) Zhou, J.N. Beltramini, Y.-X. Fan, G.Q. (Max) Lu, Chem. Soc. Rev. 37 (2008) 527–549.

[6]   G.W. Huber, S. Iborra, A. Corma, Chem. Rev. 106 (2006) 4044–4098.

[7]   C. Somerville, H. Youngs, C. Taylor, S.C. Davis, S.P. Long, Science (80-.). 329 (2010) 790–792.

[8]   E. Taarning, C.M. Osmundsen, X. Yang, B. Voss, S.I. Andersen, C.H. Christensen, Energy Environ. Sci. 4 (2011) 793–804.

[9]   C.-H. Zhou, X. Xia, C.-X. Lin, D.-S. Tong, J. Beltramini, Chem. Soc. Rev. 40 (2011) 5588.

[10]   A.J. Ragauskas, C.K. Williams, B.H. Davison, G. Britovsek, J. Cairney, C.A. Eckert, W.J. Frederick, J.P. Hallett, D.J. Leak, C.L. Liotta, J.R. Mielenz, R. Murphy, R. Templer, T. Tschaplinski, Science (80-.). 311 (2006) 484–489.

[11]   P. Mäki-Arvela, I. Anugwom, P. Virtanen, R. Sjöholm, J.P. Mikkola, Ind. Crops Prod. 32 (2010) 175–201.

[12]   N. Sun, H. Rodríguez, M. Rahman, R.D. Rogers, Chem. Commun. 47 (2011) 1405–1421.

[13]   A. Barakat, H. de Vries, X. Rouau, Bioresour. Technol. 134 (2013) 362–373.

[14]   F. Cherubini, Energy Convers. Manag. 51 (2010) 1412–1421.

[15]   Y. Sun, J. Cheng, Bioresour. Technol. 83 (2002) 1–11.

[16]   M.J. Taherzadeh, K. Karimi, Int. J. Mol. Sci. 9 (2008) 1621–1651.

[17]   B. Saha, in:, C.T. Hou (Ed.), Handb. Ind. Catal., 1st ed., CRC Press, 2005, pp. 1–12.

[18]   D.M. Alonso, S.G. Wettstein, J.A. Dumesic, Green Chem. 15 (2013) 584.

[19]   F.H. Isikgor, C.R. Becer, Polym. Chem. 6 (2015) 4497–4559.

[20]   V.B. Agbor, N. Cicek, R. Sparling, A. Berlin, D.B. Levin, Biotechnol. Adv. 29 (2011) 675–685.

[21] S. Moraïs, E. Morag, Y. Barak, D. Goldman, Y. Hadar, R. Lamed, Y. Shoham, D.B. Wilson, E.A. Bayera, MBio 3 (2012) e00508-12.

[22] A.D. French, N.R. Bertoniere, R.M. Brown, H. Chanzy, D. Gray, K. Hattori, W. Glasser, Kirk-Othmer Encyclopedia of Chemical Technology., John Wiley & Sons, Inc., New York, 2004.

[23] A. Payen, Comptes Rendus 7 (1838) 1052–1056.

[24] R.H. Atalla, in:, Compr. Nat. Prod. Chem., Elsevier, 1999, pp. 529–598.

[25] R.H. Atalla, J.W. Brady, J.F. Matthews, S.Y. Ding, M.E. Himmel, in:, Biomass Recalcitrance Deconstructing Plant Cell Wall Bioenergy, Blackwell Publishing Ltd., Oxford, UK, 2009, pp. 188–212.

[26] D. Fengel, G. Wegener, Wood—chemistry, Ultrastructure, Reactions, Walter de Gruyter, New York, 1984.

[27] D.N.-S. Hon, N. Shiraishi, Wood and Cellulosic Chemistry, M. Dekker, New York, 1991.

[28] R.H. Marchessault, P.R. Sundararajan, in:, G.O. Aspinall (Ed.), The Polysaccharides, Elsevier, 1983, pp. 11–95.

[29] A.C. O'sullivan, Cellulose 4 (1997) 173–207.

[30] A. Sarko, in:, J.F. Kennedy (Ed.), Wood Cellul. Ind. Util. Biotechnol. Struct. Prop., Ellis Horwood, Chichester, U.K., 1987.

[31] S. Salmon, S. Hudson, Polym. Rev. 37 (1997) 199–276.

[32] D. Klemm, B. Heublein, H.P. Fink, A. Bohn, Angew. Chemie - Int. Ed. 44 (2005) 3358–3393.

[33] R.D. Preston, in:, R.A. Young, R.M. Rowell (Eds.), Cellul. Struct. Modif. Hydrolys., John Wiley and Sons, New York, 1986, p. 379.

[34] R.M. Brown, J. Macromol. Sci. Part A 33 (1996) 1345–1373.

[35] N. Lin, A. Dufresne, Eur. Polym. J. 59 (2014) 302–325.

[36] J.S. Brigham, W.S. Adney, M.E. Himmel, in:, C.E. Wyman (Ed.), Bioethanol Prod. Util., Taylor & Francis, Washington, DC, 1996, pp. 119–141.

[37] C.E. Wyman, Biotechnol. Prog. 19 (2003) 254–262.

[38] A.S. Mamman, J.M. Lee, Y.C. Kim, I.T. Hwang, N.J. Park, Y.K. Hwang, J.S. Chang, J.S. Hwang, Biofuels, Bioprod. Biorefining 2 (2008) 438–454.

[39] E.M. Rubin, Nature 454 (2008) 841–845.

[40] C.O. Tuck, E. Perez, I.T. Horvath, R.A. Sheldon, M. Poliakoff, Science (80-.). 337 (2012) 695–699.

[41] A.M. Abdel-Hamid, J.O. Solbiati, I.K.O. Cann, Adv. Appl. Microbiol. 82 (2013) 1–28.

[42] E. Dorrestijn, L.J.J. Laarhoven, I.W.C.E. Arends, P. Mulder, J. Anal. Appl. Pyrolysis 54 (2000) 153–192.

[43] T. Nguyen, E. Zavarin, E.M. Barrall, J. Macromol. Sci. Part C 20 (1981) 1–65.

[44] A. Sakakibara, Wood Sci. Technol. 14 (1980) 89–100.

[45] M. Fatih Demirbas, Appl. Energy 86 (2009) S151–S161.

[46] E. Shahbazali, Green Process. Synth. 2 (2013) 87–88.

[47] Y.H.P. Zhang, J. Ind. Microbiol. Biotechnol. 35 (2008) 367–375.

[48] M.E. Himmel, Biomass Recalcitrance Deconstructing the Plant Cell Wall for Bioenergy, Blackwell Pub, Oxford, UK, 2008.

[49] S.I. Mussatto, G.M. Dragone, in:, Biomass Fractionation Technol. a Lignocellul. Feed. Based Biorefinery, Elsevier, Netherlands, 2016, pp. 1–22.

[50] J.-L. Wertz, O. Bédué, Lignocellulosic Biorefineries, 1st ed., EFPL Press, Lausanne, 2013.

[51] E. De Jong, A. Higson, P. Walsh, M. Wellisch, Biofuels, Bioprod. Biorefining 6 (2012) 606–624.

[52] R.M. Brown, in:, J. Polym. Sci. Part A Polym. Chem., Wiley Subscription Services, Inc., A Wiley Company, 2004, pp. 487–495.

[53] S.P. Rowland, E.J. Roberts, J. Polym. Sci. Part A-1 Polym. Chem. 10 (1972) 2447–2461.

[54] J.M. Dugan, J.E. Gough, S.J. Eichhorn, Nanomedicine (Lond). 8 (2013) 287–98.

[55] J.P.F. Lagerwall, C. Schütz, M. Salajkova, J. Noh, J. Hyun Park, G. Scalia, L. Bergström, NPG Asia Mater. 6 (2014) e80.

[56] N. Lin, J. Huang, A. Dufresne, Nanoscale 4 (2012) 3274.

[57] R.F. Nickerson, J.A. Habrle, Ind. Eng. Chem. 39 (1947) 1507–1512.

[58] B.G. RANBY, E. RIBI, Experientia 6 (1950) 12–14.

[59] B.G. Ranby, Discuss. Faraday Soc. 11 (1951) 158–164.

[60] S.M. Mukherjee, H.J. Woods, Biochim. Biophys. Acta 10 (1953) 499–511.

[61] R.H. Marchessault, F.F. Morehead, N.M. Walter, Nature 184 (1959) 632–633.

[62] V. Favier, H. Chanzy, J.Y. Cavaille, Macromolecules 28 (1995) 6365–6367.

[63]   S. Elazzouzi-Hafraoui, Y. Nishiyama, J.L. Putaux, L. Heux, F. Dubreuil, C. Rochas, Biomacromolecules 9 (2008) 57–65.

[64]   W. Bai, J. Holbery, K. Li, Cellulose 16 (2009) 455–465.

[65]   M. Miriam de Souza Lima, R. Borsali, Langmuir 18 (2002) 992–996.

[66]   A.F.M. and, A.M. Donald*, (2003).

[67]   M.M. De Souza Lima, J.T. Wong, M. Paillet, R. Borsali, R. Pecora, Langmuir 19 (2003) 24–29.

[68]   P. Terech, L. Chazeau, J.Y. Cavaille, Macromolecules 32 (1999) 1872–1875.

[69]   S. HANLEY, J. GIASSON, J. REVOL, D. GRAY, Polymer (Guildf). 33 (1992) 4639–4642.

[70]   S. Hanley, J.-F. Revol, L. Godbout, D. Gray, Cellulose 4 (1997) 209–220.

[71]   I. Kvien, B.S. Tanem, K. Oksman, Biomacromolecules 6 (2005) 3160–3165.

[72]   R.R. Lahiji, R. Reifenberger, A. Raman, A. Rudie, R.J. Moon, in:, NSTI Nanotechnol. Conf. Trade Show, 2008, pp. 704–707.

[73]   M. Roman, W.T. Winter, Biomacromolecules (2004) 1671–1677.

[74]   Y. Habibi, A.-L. Goffin, N. Schiltz, E. Duquesne, P. Dubois, A. Dufresne, J. Mater. Chem. 18 (2008) 5002.

[75]   N.L. Garcia de Rodriguez, W. Thielemans, A. Dufresne, Cellulose 13 (2006) 261–270.

[76]   J. Araki, S. Kuga, Langmuir 17 (2001) 4493–4496.

[77]   J. Araki, M. Wada, S. Kuga, Langmuir 17 (2001) 21–27.

[78]   X.M. Dong, T. Kimura, J.-F. Revol, D.G. Gray, Langmuir 12 (1996) 2076–2082.

[79]   L. Heux, G. Chauve, C. Bonini, Langmuir 16 (2000) 8210–8212.

[80]   M. Roohani, Y. Habibi, N.M. Belgacem, G. Ebrahim, A.N. Karimi, A. Dufresne, Eur. Polym. J. 44 (2008) 2489–2498.

[81]   Q. Li, J. Zhou, L. Zhang, J. Polym. Sci. Part B Polym. Phys. 47 (2009) 1069–1077.

[82]   J.R. Capadona, K. Shanmuganathan, S. Trittschuh, S. Seidel, S.J. Rowan, C. Weder, in:, Biomacromolecules, American Chemical Society, 2009, pp. 712–716.

[83]   L. Pranger, R. Tannenbaum, Macromolecules 41 (2008) 8682–8687.

[84]   A. Junior de Menezes, G. Siqueira, A.A.S. Curvelo, A. Dufresne, Polymer (Guildf). 50 (2009) 4552–4563.

[85]   G. Siqueira, J. Bras, A. Dufresne, Biomacromolecules 10 (2009) 425–432.

[86]   M.N. Anglès, A. Dufresne, Macromolecules 33 (2000) 8344–8353.

[87]   F. Kimura, T. Kimura, M. Tamura, A. Hirai, M. Ikuno, F. Horii, Langmuir 21 (2005)

2034–2037.

[88] J.F. Revol, Carbohydr. Polym. 2 (1982) 123–134.

[89] J. Araki, M. Wada, S. Kuga, T. Okano, J. Wood Sci. 45 (1999) 258–261.

[90] S. Beck-Candanedo, M. Roman, D.G. Gray, Biomacromolecules 6 (2005) 1048–1054.

[91] J.F. Sassi, H. Chanzy, Cellulose 2 (1995) 111–127.

[92] M.N. Anglès, A. Dufresne, Macromolecules 34 (2001) 2921–2931.

[93] M.M. Ruiz, J.Y. Cavaillé, A. Dufresne, J.F. Gérard, C. Graillat, Compos. Interfaces 7 (2000) 117–131.

[94] M. Mariano, N. El Kissi, A. Dufresne, J. Polym. Sci. Part B Polym. Phys. 52 (2014) 791–806.

[95] R.J. Moon, A. Martini, J. Nairn, J. Simonsen, J. Youngblood, Chem. Soc. Rev. 40 (2011) 3941.

[96] A. Dufresne, Nanocellulose: From Nature to High Performance Tailored Materials, Walter de Gruyter, 2013.

[97] H.M. Ng, L.T. Sin, T.T. Tee, S.T. Bee, D. Hui, C.Y. Low, A.R. Rahmat, Compos. Part B Eng. 75 (2015) 176–200.

[98] O.A. Battista, Ind. Eng. Chem. 42 (1950) 502–507.

[99] O.A. Battista, S. Coppick, J.A. Howsmon, F.F. Morehead, W.A. Sisson, Ind. Eng. Chem. 48 (1956) 333–335.

[100] Y. Nishiyama, U.J. Kim, D.Y. Kim, K.S. Katsumata, R.P. May, P. Langan, Biomacromolecules 4 (2003) 1013–1017.

[101] A. Dufresne, Nanocellulose: From Nature to High Performance Tailored Materials, Walter de Gruyter GmbH Co.KG, [s.l.] :, 2012.

[102] D. Bondeson, A. Mathew, K. Oksman, Cellulose 13 (2006) 171–180.

[103] X.M. Dong, J.-F. Revol, D.G. Gray, Cellulose 5 (1998) 19–32.

[104] V. Kumar T, Nanocellulose Polymer Nanocomposites: Funadamentals and Applications, 2015.

[105] M. Jonoobi, R. Oladi, Y. Davoudpour, K. Oksman, A. Dufresne, Y. Hamzeh, R. Davoodi, Cellulose 22 (2015) 935–969.

[106] N.F. Vasconcelos, J.P.A. Feitosa, F.M.P. da Gama, J.P.S. Morais, F.K. Andrade, M. de S.M. de Souza Filho, M. de F. Rosa, Carbohydr. Polym. 155 (2017) 425–431.

[107] T. Koshizawa, Japan Tappi J. 14 (1960) 455–458,475.

[108] M. Usuda, O. Suzuki, J. Nakano, N. Migita, Kogyo Kagaku Zasshi 70 (1967) 349–352.

[109] I. Filpponen, The Synthetic Strategies for Unique Properties in Cellulose Nanocrystal Materials, North Carolina State University, Raleigh, NC, 2009.

[110] J. Araki, M. Wada, S. Kuga, T. Okano, Colloids Surfaces A Physicochem. Eng. Asp. 142 (1998) 75–82.

[111] J. Araki, M. Wada, S. Kuga, T. Okano, Langmuir 16 (2000) 2413–2415.

[112] B. Sun, Q. Hou, Z. Liu, Y. Ni, Cellulose 22 (2015) 1135–1146.

[113] A. Salam, L.A. Lucia, H. Jameel, Cellulose 22 (2015) 397–406.

[114] B. Sun, Q. Hou, Z. Liu, Z. He, Y. Ni, Cellulose 21 (2014) 2879–2887.

[115] U.D. Hemraz, K.A. Campbell, J.S. Burdick, K. Ckless, Y. Boluk, R. Sunasee, Biomacromolecules 16 (2015) 319–325.

[116] J.-L. Huang, C.-J. Li, D.G. Gray, RSC Adv. 4 (2014) 6965.

[117] J. Yang, C.-R. Han, J.-F. Duan, M.-G. Ma, X.-M. Zhang, F. Xu, R.-C. Sun, X.-M. Xie, J. Mater. Chem. 22 (2012) 22467.

[118] A. Villares, C. Moreau, A. Dammak, I. Capron, B. Cathala, Soft Matter 11 (2015) 6472–6481.

[119] D. Roy, M. Semsarilar, J.T. Guthrie, S. Perrier, Chem. Soc. Rev. 38 (2009) 2046.

[120] C. Bonini, L. Heux, J.Y. Cavaillé, P. Lindner, C. Dewhurst, P. Terech, Langmuir 18 (2002) 3311–3314.

[121] A.E.J. de Nooy, A.C. Besemer, H. van Bekkum, Recl. Des Trav. Chim. Des Pays???Bas 113 (1994) 165–166.

[122] Y. Habibi, H. Chanzy, M.R. Vignon, Cellulose 13 (2006) 679–687.

[123] C. Goussé, H. Chanzy, G. Excoffier, L. Soubeyrand, E. Fleury, Polymer (Guildf). 43 (2002) 2645–2651.

[124] A.N. Frone, S. Berlioz, J.F. Chailan, D.M. Panaitescu, D. Donescu, Polym. Compos. 32 (2011) 976–985.

[125] B. Braun, J.R. Dorgan, Biomacromolecules 10 (2009) 334–341.

[126] E. Lam, K.B. Male, J.H. Chong, A.C.W. Leung, J.H.T. Luong, Trends Biotechnol. 30 (2012) 283–290.

[127] N.E. Marcovich, M.L. Auad, N.E. Bellesi, S.R. Nutt, M.I. Aranguren, J. Mater. Res. 21 (2006) 870–881.

[128] L. Chazeau, J.Y. Cavaillé, P. Terech, Polymer (Guildf). 40 (1999) 5333–5344.

[129] L. Chazeau, J.Y. Cavaill??, J. Perez, J. Polym. Sci. Part B Polym. Phys. 38 (2000) 383–392.

[130] C. Bonini, Study of the Role of Fiber/fiber and Fiber/matrix Interactions in Nanocomposites with Cellulose Reinforcement and Apolar Matrix, Joseph Fourier University, Grenoble, France, 2000.

[131] G. Chauve, L. Heux, R. Arouini, K. Mazeau, Biomacromolecules 6 (2005) 2025–2031.

[132] S.A. Paralikar, J. Simonsen, J. Lombardi, J. Memb. Sci. 320 (2008) 248–258.

[133] Y. Choi, J. Simonsen, J. Nanosci. Nanotechnol. 6 (2006) 633–639.

[134] L. Petersson, A.P. Mathew, K. Oksman, J. Appl. Polym. Sci. 112 (2009) 2001–2009.

[135] M.A.S. Azizi Samir, F. Alloin, J.Y. Sanchez, A. Dufresne, Polymer (Guildf). 45 (2004) 4149–4157.

[136] M. Paillet, A. Dufresne, Macromolecules 34 (2001) 6527–6530.

[137] S. Noorani, J. Simonsen, S. Atre, in:, 2006, pp. 209–220.

[138] M. Grunert, W.T. Winter, Polym. Mater. Sci. Eng. 82 (2000) 232. Spring.

[139] Long Jiang, E. Morelius, Jinwen Zhang, M. Wolcott, J. Holbery, J. Compos. Mater. 42 (2008) 2629–2645.

[140] D. Dubief, E. Samain, A. Dufresne, Macromolecules 32 (1999) 5765–5771.

[141] L. Petersson, I. Kvien, K. Oksman, Compos. Sci. Technol. 67 (2007) 2535–2544.

[142] Y. Lu, L. Weng, X. Cao, Macromol. Biosci. 5 (2005) 1101–1107.

[143] K. Tashiro, M. Kobayashi, Polymer (Guildf). 32 (1991) 1516–1526.

[144] A. Šturcová, G.R. Davies, S.J. Eichhorn, Biomacromolecules 6 (2005) 1055–1061.

[145] R. Rusli, S.J. Eichhorn, Appl. Phys. Lett. 93 (2008) 33111.

[146] V. Favier, G.R. Canova, J.Y. Cavaillé, H. Chanzy, A. Dufresne, C. Gauthier, Polym. Adv. Technol. 6 (1995) 351–355.

[147] V. Favier, G.R. Canova, S.C. Shrivastava, J.Y. Cavaillé, Polym. Eng. Sci. 37 (1997) 1732–1739.

[148] L. Flandin, G. Bidan, Y. Brechet, J.Y. Cavaille, Polym. Compos. 21 (2000) 165–174.

[149] M.A.S. Azizi Samir, F. Alloin, A. Dufresne, Biomacromolecules 6 (2005) 612–626.

[150] A. Dufresne, J. Nanosci. Nanotechnol. 6 (2006) 322–330.

[151] Y. Habibi, A. Dufresne, Biomacromolecules 9 (2008) 1974–1980.

[152] X. Cao, Y. Habibi, L.A. Lucia, J. Mater. Chem. 19 (2009) 7137.

[153] N. Ljungberg, J.Y. Cavaillé, L. Heux, Polymer (Guildf). 47 (2006) 6285–6292.

Chapter 2

Science and Technology of Rubber Compounds

Syed Danish Ali, Luca Zoia, Marco Emilio Orlandi

2.1   Rubber Compounds

Rubbers, commonly known as elastomers, are an important class of polymers and one of the most useful materials in science and technology. Really interesting properties of these materials, such as mechanical strength, flexibility, curing behavior, flexural properties, etc, make them significantly important. Filler particles and various other ingredients are added to the rubber matrices to not only increase the existing properties but also to attain new qualities, for instance, impermeability, conductivity, etc. Two major constituents of rubber compounds are filler and rubber itself, and their composition relies on the final products. The properties of the rubber compounds are largely affected by the nature of rubber and filler, dispersion of the filler in the rubber matrix, their compatibility, and filler-rubber interactions. Carbon black, carbon nanotubes, silica, clay, and bio-nanofibers are the commonly used fillers in the rubber compounds and they play an important role in regulating the final properties [1–7].

Rubber compounds have many fascinating properties which are not present in other materials, for example, abrasion resistance, high elasticity, and damping properties. Therefore, rubber compounds have much promising application in automotive industry, railways, domestic appliances, electrical and electronics, civil and mechanical engineering sectors. The most common and important application of rubber compounds is in tire manufacturing. Reduced rolling resistance, high mechanical properties, maximum traction in dry and wet environments, and optimized performance are the main objective in the tire industry. Careful selection of one or more rubber matrices, together with appropriate amount and type of filler makes it possible to obtain all the required objectives [8]. It has been reported that same reinforcement can be obtained with only 6 phr of nano-clay as

compared to 40 phr of carbon filled compounds with superior dynamic properties and lower heat production [9]. The rubber compounds used in different application, for instance, in the tire industry are composed of different ingredients, which can be divided into five categories; polymers, fillers, vulcanization system, stabilizer system and special materials.

2.1.1 Polymers

Polymers are the main ingredient of the rubber compounds which could be either natural or synthetic polymer. Polymers are the high molecular weight materials, which are composed of long chains of molecules made up of repeating unit of one or more type of polymerized monomers. These chains of polymers are long and flexible having tens of thousands of monomer units. The chains in the polymers are distributed randomly which are coiled and entangled with the neighboring chains restricting their motion. Polymers display combinations of very important properties, most significantly their elasticity and resilience. They show the ability to return to their original shape after being deformed by stretching or compression and display a high level of extensibility.
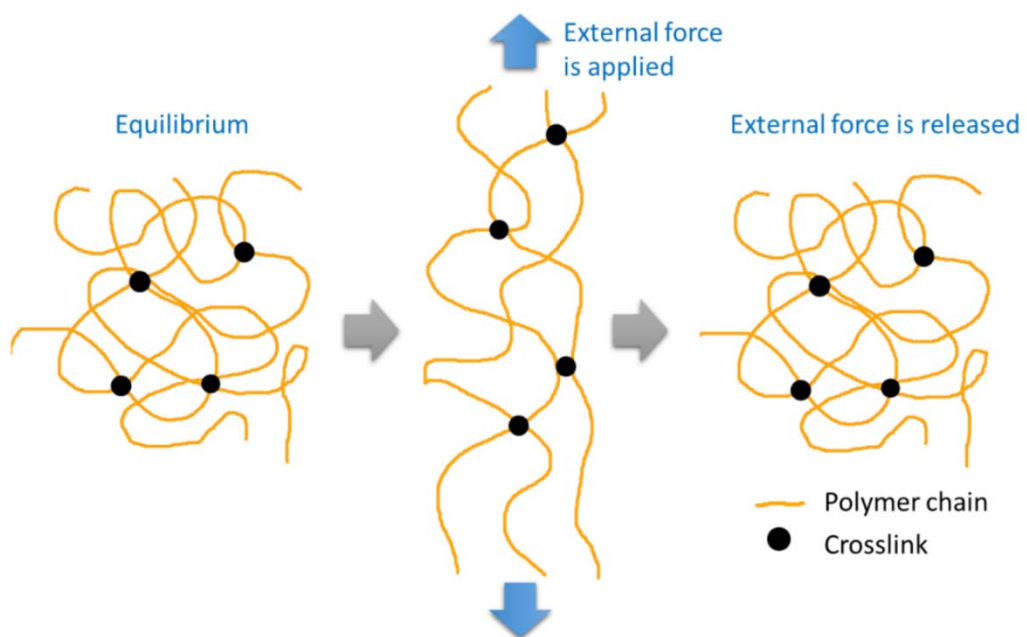
Figure 2.1: Schematic representation of elasticity of crosslinked polymer chains [10]

On a molecular level, the random polymer chains in the cured polymer are crosslinked at some points and when stress is applied, the chains are uncoiled and aligned in the direction of applied force. When the stress is released, the chains gain their original random uncoiled shape as represented in Fig. 2.1. This characteristic of polymer results in some really important properties, for instance, high elongation at break, high elasticity, and low hardness [11].

The molecular weight and configuration of the constituent atoms have a significant effect on the physical properties of the polymers. Chain entanglements increase with increasing molecular weight, resulting in the stiffness at high elongations [12–14]. The restricted rotation of the carbon bonds of the polymer chain cause an increase in the stiffness of the obtained product, for instance, polystyrene is much stiffer than polyethylene due to the steric hindrance of side groups [15]. Highly pure and regular structure of polymer chains results in the crystalline nature of the polymer. At high elongation, the polymer chains align in the direction of applied force and can also originate crystallinity, which results in an increase in the strength and stiffness [16–18]. Polymers are sensitive to temperature and show a change in elastic properties with thermal agitation. Generally, with a decrease in temperature, the stiffness increases, until the polymer gains a glass-like stability at a certain temperature, known as glass transition temperature, T_g, this results in an increase of hysteresis and internal viscosity. The size and number of side groups on the polymer chains affect the glass transition temperature of the polymer. The T_g increase with increasing the size and number of side groups such as chlorine, benzene rings or vinyl groups, etc. Therefore, high hysteresis is related to the high glass transition temperature and consequently high friction and low air permeability [19].

Polymers can be divided into two general categories; natural rubber and synthetic rubber. Typically, natural rubber is obtained from the rubber tree, *Hevea Brasiliensis*, and synthetic rubbers are prepared from different monomers produced through petroleum refining and cracking. Natural rubber accounts for about 46 % of total world rubber consumption while the remaining are synthetic rubbers, out of which about 18 % is constituted by styrene butadiene rubber (SBR) [20]. In the tire industry, up to 30 different kinds of synthetic rubber and 8 kinds of natural rubber are used in the formulation of rubber compounds,

and synthetic rubber accounts for about 60 % of total rubber used in the tire industry [21,22].

2.1.1.1 Natural Rubber

Natural rubber (NR) is a biopolymer of high commercial value with interesting properties such as high elasticity, efficient heat dispersion, and resilience [23]. Chemically, it is composed of long polymeric chains of *cis*-1,4-poly(isoprene), the chemical structure is shown in Fig. 2.2. About 300 to 70,000 Isoprene molecules are coupled in the form of random irregular chains with a rubbery texture and amorphous structure, having an average molecular weight of natural rubber between 100,000 to 1,000,000 g/mol [24–26].
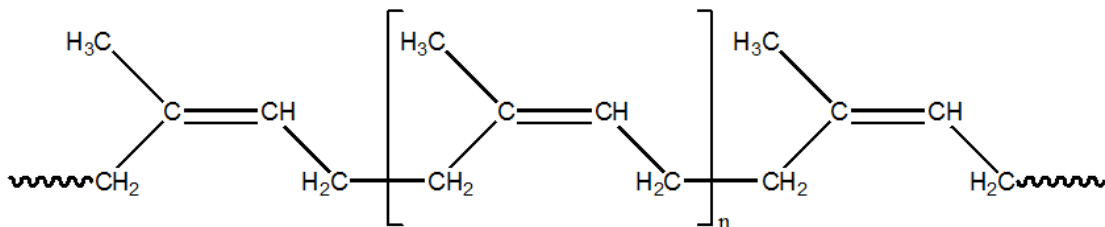
Figure 2.2: Chemical structure of natural rubber [*cis*-1,4-poly(isoprene)]

Natural rubber is obtained in the form of a milky aqueous suspension, commonly known as NR latex, from the sap of many plants (up to 2500 species) [26]. Currently, high-quality NR in viable quantities with high commercial value is obtained from *Hevea brasiliensis* tree [27]. Natural rubber produced from *Hevea brasiliensis* tree is mainly *cis* isomer however *trans* isomer can be found in the latex obtained from genus *Dichopsis*. *Hevea brasiliensis* tree is indigenous to Brazil, however, it is cultivated as a valuable crop in both tropical and subtropical counties. Currently, Malaysia, Indonesia, Thailand, China, and India are the main NR-producing countries with a total world natural rubber production of about 89 % in 2005 [28]. During the harvesting and processing of NR latex, along with NR, some other non-rubber components are also extracted. The obtained latex contains about 94 % NR contents and 6 % non-rubber contents, such as 2 % of resins, 1-2 % of proteins and

phosphoproteins, 1 % of carbohydrate, 1 % of fatty acids, and 0.5 % of inorganic salts [29]. It is believed that these components play their role in the extraordinary characteristics of the NR [24]. The NR latex contains micron size natural rubber particles which are stabilized by the protein anions. These negatively charged particles form a stable colloidal suspension which protects the latex from coagulation. The exposure of NR latex to air causes the decomposition of proteins by enzymes and bacteria and results in its coagulation. Commercially, NR latex is stabilized by the addition of ammonia to prevent the growth of microorganisms and maintained an alkaline environment [30,31].

Natural rubber is a general purpose elastomer and its outstanding properties makes it ideal rubber material for many important applications. The presence of double bonds in the chemical structure of NR provides the reactive sites for the attachment of functional groups, grafting or crosslinking. Another important property of NR is its ability to undergo strain-induced crystallization. Under a high strain, the polymeric molecular chains are aligned in the direction of deformation, resulting in the formation of crystalline domains which act as a filler. This phenomenon increases the reinforcement of the material [32–34]. The high elasticity, resilience, low heat build-up, low hysteresis, good abrasion resistance, outstanding dynamic properties along with excellent processability of natural rubber make it ideal rubber for automotive tires. The use of NR has increased significantly in modern tires and accounts for 75 % of total natural rubber consumption. Other common applications of NR include mechanical products, medical and health-related products, anti-vibration mountings, load-bearing components, flexible couplings, etc [35,36].

2.1.1.2 Synthetic Rubber

Synthetic rubbers (SR) are the artificial elastomers which are commonly synthesized from the monomers derived from petroleum. Isoprene, butadiene, styrene, propylene, ethylene, isobutylene, and acrylonitrile are the most commonly used monomers. The development of synthetic rubber was started in 20th century in order to fulfill the increasing demand of elastomeric materials and also to improve the final properties of the rubber compounds. Currently, there are more than 20 different varieties of SR, which could provide the desired set of properties required for a specific application [37].

Polyisoprene (IR), polybutadiene (BR), styrene butadiene rubber (SBR), etc are the general purpose SR. These rubbers are characterized by the presence of chemical unsaturation (diene functionality) in their backbones, which makes them much likely to be attacked by oxygen or ozone. The special purpose SR, in contrast to general purpose SR, have inherent properties of resistance to high temperature, ozone, and oil depending on the repeating unit [38].

SBR is a copolymer of styrene and butadiene and the most commonly used synthetic rubber. Chemical structure of the SBR is shown in Fig. 2.3. It has really interesting properties, such as high skid and abrasion resistance, high reinforcement with reinforcing filler, and low cost with the only drawback of high heat generation. It is synthesized by either solution or emulsion process. The microstructure of polymer (i.e. the arrangement of monomers in polymer chains) is difficult to control in emulsion process, which results in the less pure final product as compared to solution process. Nevertheless, emulsion SBR demonstrates higher tear strength and tensile strength, and easy processability, and finds its applications in the tire tread, breaker compounds of bias tires, ply, bead wire insulation, sidewalls, and conveyors belt covers. The solution SBR is commonly used in tire tread of light truck and passenger tires, large off-the-road tires, and tire tread of radial medium truck tires [39].
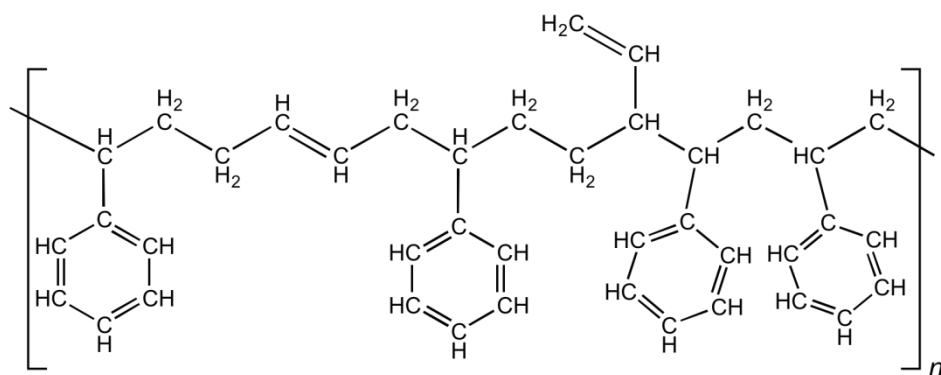
Figure 2.3: Chemical structure of styrene butadiene rubber

Among the world total SR production, 60 % is consumed in the tire industry. SBR accounts for the largest volume which is 65 % and butadiene rubber (BR) has the second largest

contribution of SR used in tires [40]. BR presents high abrasion resistance, cut growth resistance, and tread wear performance and commonly used in the tire tread, sidewalls and some casing part of the tire. A blend of BR with NR has been reported in many studies to improve the resistance of cut growth and better fatigue [41]. Regarding the microstructure, butadiene can take three configurations, *cis*-(1,4), *trans*-(1,4), and *vinyl*-(1,2) as shown in Fig. 2.4 and relative percentage of these three isomers have a substantial effect on the performance of rubber compounds. High-*cis* BR (92 % *cis*) demonstrate improved abrasion resistance but their processing is difficult at factory processing temperature. High-*trans* BR (93 % *trans*) show high toughness and crystallinity at room temperature and high-*vinyl* BR compounds display superior wet traction and wet skid performance in tire treads [39,41–43].
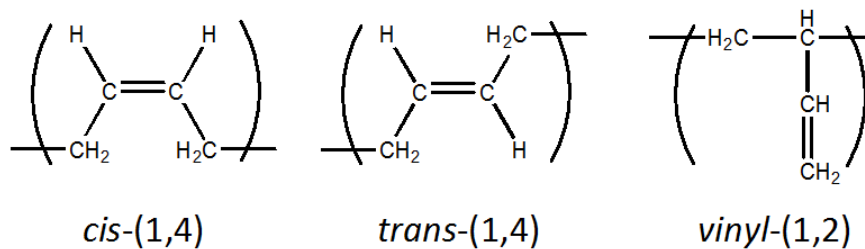
Figure 2.4: Polymer microstructure: possible configurations for butadiene in SBR and BR

2.1.2 Fillers

The filler is a very important component of rubber compounds, which is added to enhance the properties and reduce the cost of the rubber compounds. Fillers are divided into three general categories depending on their effect on the physical properties of the rubber compounds, i.e. non-reinforcing, semi-reinforcing and reinforcing fillers. Fillers such as chalk powder, clay, calcium carbonate, etc, are non-reinforcing, which do not show any reinforcement effect and only used to lower the cost of final product. The addition of reinforcing fillers, such as carbon black, silica, etc, improve the mechanical properties of the vulcanized rubber compounds such as tensile strength, modulus, stiffness, abrasion resistance, elongation at break, heat build-up, and rolling resistance [44–46]. The extent of reinforcement in rubber compounds is related to the innate properties of the filler used.

Some important properties of the fillers, which determine their performance are chemical composition, particle size, particle shape, structure, aspect ratio, surface area, surface chemistry, and density [40,47].

The most important property of fillers which significantly influence the reinforcement of rubber compounds is the particle size. Fillers having a particle diameter greater than 1 μm usually do not show any reinforcing effect. Fillers with particle size ranging from 100 nm to 1 μm are moderate reinforcing, while those ranging from 1 to 100 nm offer very high reinforcement and significantly enhance the mechanical properties of the rubber compounds [11]. The morphological characteristics such as surface area and structure of the reinforcing fillers are critically significant for their reinforcing ability. The surface area is directly related to the particle size of the filler. A small particle size, high surface area and the high surface area-to-volume ratio of filler improves the mechanical properties of the rubber compounds without altering their bulk properties such as density or light transmission. The surface area is very important because it defines the extent of interactions between the filler and polymer. The smaller the primary particle size, the higher surface area, which results in extension of interface [48–50]. The polymer chains are adsorbed on the filler surface either through physical interaction, such as Van der Waals forces, or chemical interactions by making a chemical bond with the functional groups on the filler surface. A high surface area of the filler particles results in more polymers chains to be adsorbed on the surface, restricting the chains mobility under strain, consequently high reinforcement effect of rubber compounds [11]. The fraction of the polymer chains adsorbed on the filler surface is known as bound rubber as represented in Fig. 2.5 and it is related to the surface activity of the filler. The surface activity of the filler defines the two types of interactions; filler-rubber and filler-filler, which greatly influence the viscoelastic behavior of the rubber compounds [51–53]. Fillers with high surface activity can induce high reinforcement in the rubber compounds. High surface-active fillers have many functional groups on the surface with a strong affinity toward the rubber and chemically react with the polymeric chains, which results in improvement in mechanical properties. The enhancement of filler-rubber interactions by a coupling agent is frequently used in rubber industry. Coupling agents have two chemical functionalities which react chemically with both filler and rubber [46,54,55]. Filler-filler interactions play an important

role in the formation of strong filler-network which affects the physical properties of the rubber compounds. Above the percolation threshold, the filler particles are interconnected in a three-dimensional network through the polar or hydrogen bonds. The breakage of the filler-network under the cyclic deformation results in a non-linear viscoelastic behavior, known as the Payne effect. Filler-filler interactions also define the dispersion of the filler in a polymer matrix, and good dispersion is a key property to achieve reinforcement in rubber compound [56–58]. In a rubber compound, a fraction of the polymer matrix can be mechanically interlocked in voids between the filler particles. This fraction of rubber, known as the occluded rubber (as shown in Fig. 2.5), causes an increase in the modulus of the rubber compounds, which is due to the fact that the occluded rubber is shielded from deformation and acts as a filler. The effective volume of the filler is increased; therefore, the concentration of the filler affects the modulus of the rubber compounds [11,52,59,60].
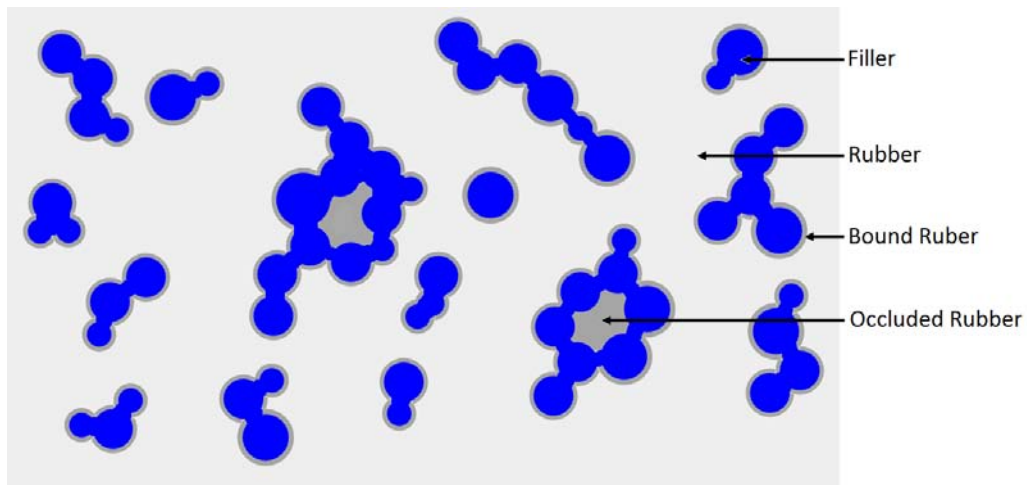
Figure 2.5: Schematic representation of filler dispersion in rubber

The structure is also an important property of the filler which plays an important role in reinforcement. The spherical filler particles are partially fused to form irregular chainlike or branched aggregates. During the processing of rubber compounds, these aggregates are unbreakable and act as actual reinforcing objects. The branched and chainlike structures of aggregates make them bulky and their effective volume in rubber compounds is much higher than the actual volume of aggregates, which determine the extent of strain

amplification in deformable phase [48,61]. The shape of the filler also influences the reinforcement; filler with high aspect ratio shows the higher reinforcing effect than spherical filler. An increase in viscosity was observed for clay-reinforced compounds when the shape was changed from spherical to platelets to needles [44].

2.1.2.1 Carbon Black

Carbon black is one of the most commonly used reinforcing fillers in the rubber industry. Three processes are commonly known for the production of carbon black; the channel process, the thermal process, and the furnace process, however about 97 % of the carbon black is produced through the furnace process. In a typical furnace process, the heavy fraction of crude oil is partially pyrolyzed in the vapor phase in a heated chamber under controlled conditions. The properties of carbon black such as particle size, surface activity, and structure can be modified by controlling the process conditions. The carbon black is produced in spherical primary particles and many functional groups, such as carboxylic acids, phenols, quinines, ketones, and lactones, are introduced on the surface during the production process as shown in Fig. 2.6. Carbon black interacts with rubber through the chemical reactions of these functional groups with curing agents and reactive moieties present in polymeric chains [62–64].
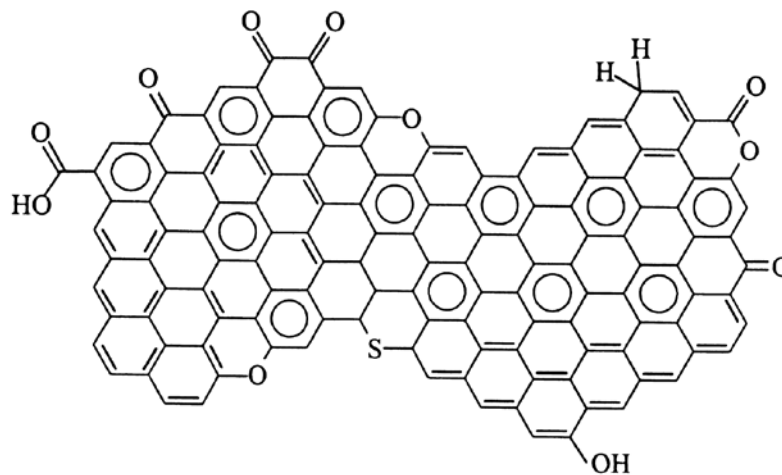
Figure 2.6: Chemical functions on carbon black surface [65]

As the particle size and surface area are the most important properties of the fillers, so these two properties were chosen by the American Society of Testing Materials (ASTM) for the classification of carbon black, as shown in Table 2.1. The ASTM nomenclature format consists of four characters; the first character is a letter, either "N" or "S", which is related to the effect of carbon black on curing rate of the rubber compounds. The letter "N" represents the normal curing and "S" represents the slow curing rate. Other three characters are digits; the first digit indicates the primary particle diameter and surface area of the carbon black, and other two digits are randomly assigned [66]. Each carbon black provides specific characteristics to rubber compounds and the right selection of carbon black is very important in order to obtain the required performance.

Table 2.1: ASTM nomenclature of carbon black

ASTM number	Primary Particle Diameter (nm)	Average Nitrogen Surface Area (m^2/g)
900-999	201-500	0-10
800-899	101-200	11-20
700-799	61-100	21-32
600-699	49-60	33-39
500-599	40-48	40-49
400-499	31-39	50-69
300-399	26-30	70-99
200-299	20-25	100-120
100-199	11-19	121-150
000-099	1-10	>150

Generally, it is considered that the reinforcement of carbon black-filled rubber compounds is the result of adsorption of polymer chains on the carbon black surface. Polymeric chains are strongly bonded on to the carbon black surface due to its high surface energy and significantly restrict their motion. Some general trends for effect of carbon black properties on physical properties of the rubber compounds have been reported. The fatigue resistance and cut growth are improved by the increase of carbon black structure. As the particle size decreases, the tear strength and abrasion resistance increase, however

heat build-up and hysteresis also increase. An increase of carbon black loading causes an increase in hardness, heat build-up, rolling resistance, and wet-skid properties. Abrasion resistance, compound processability, and tensile strength achieve an optimal value and then start decreasing [1,67–69].

2.1.2.2 Silica

Silica is also most widely used reinforcing filler in the rubber industry. The use of silica in rubber compounds is not new but started from the beginning of 20th century [70]. At that time it was used as a non-reinforcing filler along with carbon black. Two most important breakthroughs, the development of silica-silane technology and demonstration of reinforcing capability of silica in the elastomers, transformed the silica into a reinforcing filler [71]. Silica provides the same reinforcement as carbon black, additionally low hysteresis which is especially required for tire applications. The silica used in rubber industry is mainly produced through precipitation. In a typical process, the alkaline solution of sodium silicate is precipitated with the addition of acid solution under controlled conditions of temperature, pH, and concentration of acid and salt solutions [57,72]. Precipitation recipe and drying conditions of silica are very important to obtain the highly dispersible reinforcing silica [57,73].

The precipitated silica is obtained with primary particle size ranging in nanometer scale, typically from 5 to 50 nm. The nanoparticles are fused together through siloxane bonds in the form of aggregates (100-500 nm in size) characterized by the high structure. Due to the presence of numerous silanol groups on the silica surface, silica aggregates tend to agglomerate due to strong hydrogen bonding and are poorly dispersed in a hydrophobic polymer, resulting in non-reinforcing behavior. In order to increase the dispersion and to improve the compatibility with the polymeric matrix, the surface of silica is functionalized with specific coupling agents. Bis[3-(triethoxysilyl)propyl]tetrasulfide (TESPT) is the most commonly used silane coupling agent. TESPT coupling agent has two functional groups, triethoxysilyl moiety react with silanol groups on silica surface and tetrasulfide react with polymer chains (as shown in Fig. 2.7), which improve the compatibility of silica with elastomer [75]. Hence, compatibilized silica as a filler provides an improvement in tear

strength, wet traction, and hysteresis, and reduction in heat build-up, and utilized in rubber compounds for tires, industrials rubber goods and shoe soles [76,77].
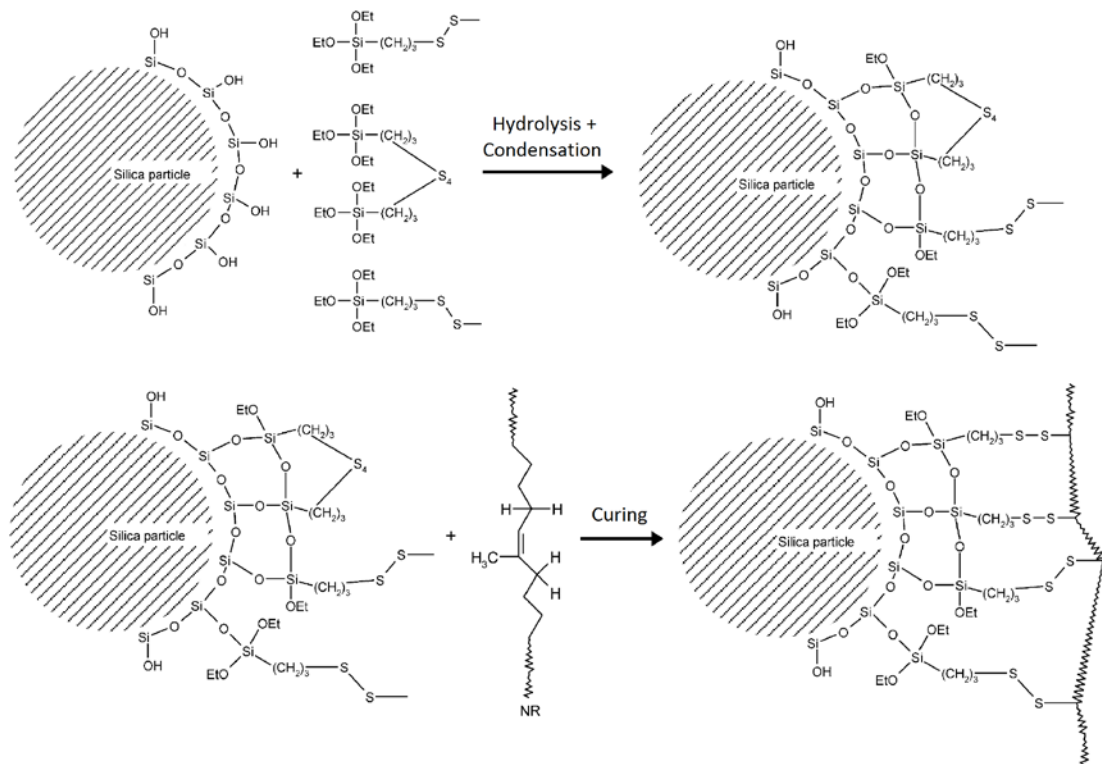
Figure 2.7: Silica surface functionalization with silane coupling agent and formation of silica-to-rubber bond [74]

2.1.3   Vulcanization System

Vulcanization is a chemical process in which the polymer chains of the rubber are crosslinked to introduce valuable mechanical properties to the rubber. The process was introduced for the first time by Charles Goodyear in 1839 [78]. The production of many valuable rubber products such as the tires, mechanical goods, etc, would not be possible without vulcanization. Generally, rubber itself is very soft and suffers from very poor physical properties, sensitive to extreme temperatures, swelling in solvents, poor resistance to light, and cannot sustain its shape after high strains. Vulcanization decreases the plasticity, stickiness, hot and cold flow of the rubber and enhances the elasticity by

forming a three dimensional crosslinked elastic network as shown in Fig. 2.8 [47]. At a molecular level, during the vulcanization, junctures (crosslinks) are formed along the rubber molecules and the average spacing between the crosslinks is represented in the form of molecular weight between the junctures, which range from 4,000 to 10,000 daltons. Due to the formation of this network, it is no more possible for the rubber to be solubilized in a solvent or processed by any mean which needs it to flow. Therefore, it is necessary to make the final shape of the product before the vulcanization.
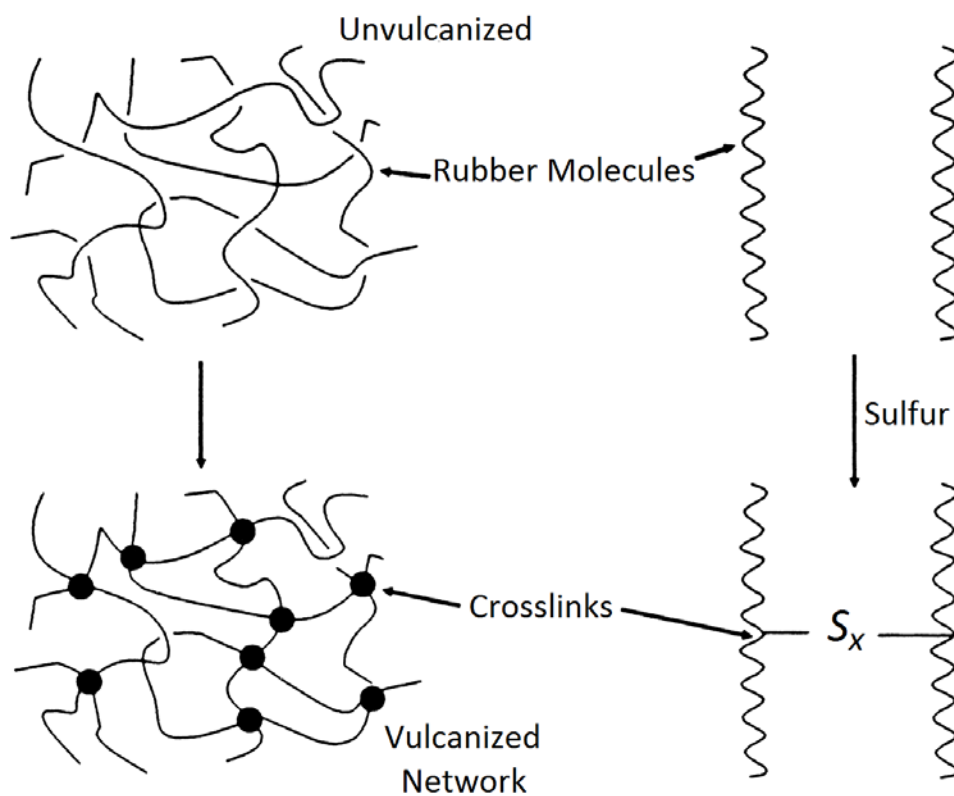
Figure 2.8: Schematic representation of crosslinks formation during vulcanization [47]

A vulcanization system in a rubber compound is composed of three main components; vulcanizing agents, activators, and accelerators. Sulfur and peroxides are the two most commonly used vulcanizing agents. Initially, the vulcanization was carried out by heating the rubber with 8 parts per 100 parts of rubber (phr) of elemental sulfur at 140 $^{\circ}$C. The process required 5 hours to complete, the addition of zinc oxide reduced the time to 3 hours. Later on, the introduction of only 0.5 phr of accelerator during vulcanization

reduced the vulcanization time to just 1 to 3 minutes. Hence, sulfur vulcanization without an accelerator does not have any commercial importance. Oenslager discovered the aniline as the first accelerator for sulfur vulcanization in 1906 [79]. A lot of research work after that has been carried out on the development of accelerators for sulfur vulcanization [80,81]. Accelerators are usually organic compounds when added during the vulcanization process increase the rate of vulcanization reactions and crosslink density. Based on the function, they are classified as primary and secondary accelerators. Primary accelerators provide medium to fast curing and scorch delay while secondary accelerators are scorchy, and provide very fast cure [82]. The commonly used accelerators in vulcanization belong to the eight groups; thioureas, thiurams, thiazoles, guanidines, dithiocarbamates, sulfonamides, aldehydeamines, and xanthates. Accelerators are used in combination with activators during vulcanization to gain the full potential of accelerators. Zinc oxide and stearic acid are the commonly used activators in the vulcanization system. A typical concentration of 5 and 2 phr for zinc oxide and stearic acid, respectively, is considered
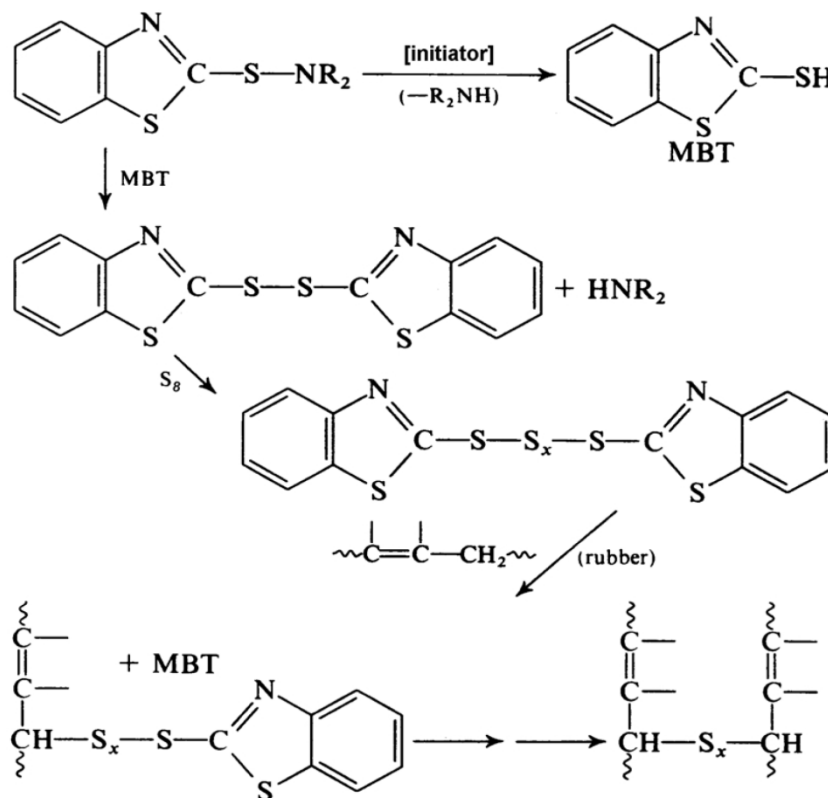
Figure 2.9: Reaction path of accelerated-sulfur vulcanization [47]

sufficient to obtain the optimum properties of the rubber compounds and widely accepted in the rubber industry. Accelerated-sulfur vulcanization is the most widely used method and employed to vulcanize the rubbers which have unsaturation. The general reaction pathway of sulfur vulcanization using benzothiazole is shown in Fig. 2.9. Initially, a monomeric polysulfide having Ac-S_x-Ac structure is formed by the reaction of the accelerator with sulfur, where Ac represents a radical generated from the accelerator. Then a polymeric polysulfide of the structure, rubber-S_x-Ac, is formed by the reaction between rubber and monomeric polysulfide. Finally, a crosslink, rubber-S_x-rubber, is formed by either direct reaction between two polymeric polysulfides or through an intermediate [47,83–86].

Vulcanization greatly influences the properties of the vulcanizate. The effect of extent of vulcanization on the physical properties of the vulcanized compounds is shown in Fig. 2.10. It should be noted that hysteresis decreases with increasing the crosslink density. Hysteresis represents the deformation energy that is lost as heat. At low crosslinking the properties those are linked with breaking energy, such as tear strength, fatigue life, and toughness, increase but further crosslinking causes a decrease in these properties. An increase of crosslink density and hysteresis cause an increase in the properties that are
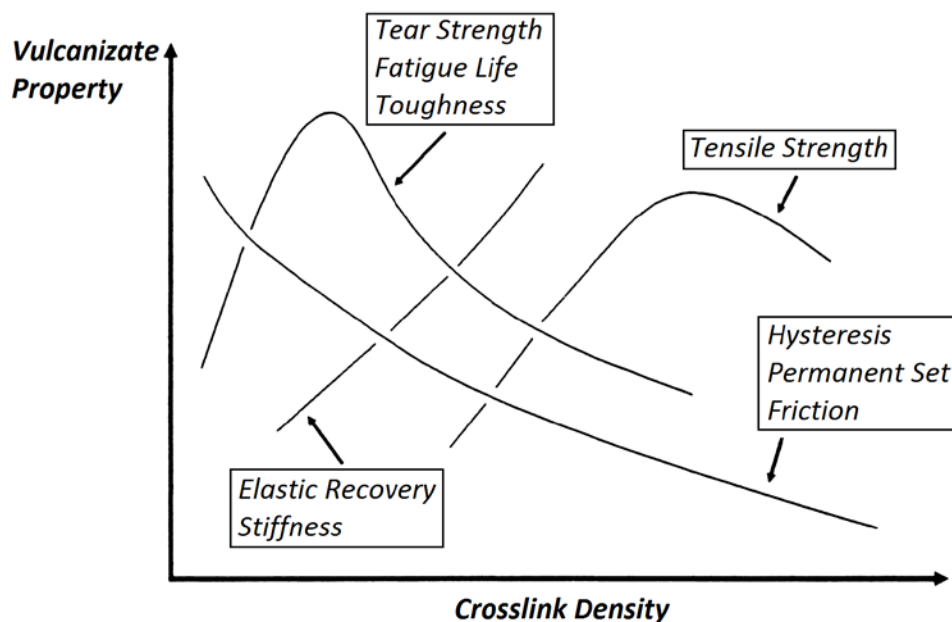
Figure 2.10: Effect of extent of vulcanization on vulcanizate properties [47]

45

related to energy-at-break. Since hysteresis decreases with increasing the crosslink density, so these properties are maximized at some intermediate crosslink density [47,87].

2.1.4 Stabilizer Systems

The unsaturation nature of natural and synthetic rubbers provides them unique viscoelastic properties, although these rubbers containing carbon-carbon double bond are more prone to attack by ozone, oxygen, and thermal degradation. Oxidation and ozonation are accelerated by light, heat, solvents, moisture, sulfur, dynamic fatigue and heavy metal contamination. Hence, in order to provide the required service life to vulcanized rubber products, it is essential to protect them from ozone, oxygen, heat, and light. The oxidation
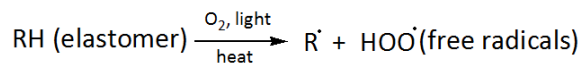
Figure 2.11: Oxidation and ozonation mechanisms of rubber degradation

of the rubber takes place through a free radical process. The process is carried out in three steps; initiation, propagation, and termination, as shown in Fig. 2.11. The energy supplied by the light, heat or shear cause the breakage of the bond, resulting in free radical formation. Ozonation takes place through the attack of ozone on the carbon-carbon double bonds of the polymeric chains, resulting in the formation of ozonides which promptly decompose causing the chain cleavage. This cleavage of polymer chains results in the surface cracks of the rubber compounds [40,47].

Antioxidants or antiozonants are added to rubber compounds to protect the degradation of vulcanized rubber products. Antioxidants protect the rubber from oxidation by reacting with oxygen and free radicals. Antioxidants are generally grouped in primary and secondary antioxidants; primary antioxidants act as a chain terminator and secondary antioxidants act as hydroperoxide decomposer. Three types of antioxidants; phenolic, aromatic amine, and hydroperoxide decomposing antioxidants are commonly used. The antioxidation mechanism of hindered phenolics is shown in Fig. 2.12. Antiozonants protection mechanism of rubber is described by four principal theories. The first theory suggests the competitive reaction of antiozonants with rubber for ozone. The second theory describes the formation of a protective layer of ozonized antiozonant on the rubber surface, which protects the further attack of ozone. The third theorizes the reaction of antiozonants with ozonized rubber fragments and restoring the rubber chains by relinking
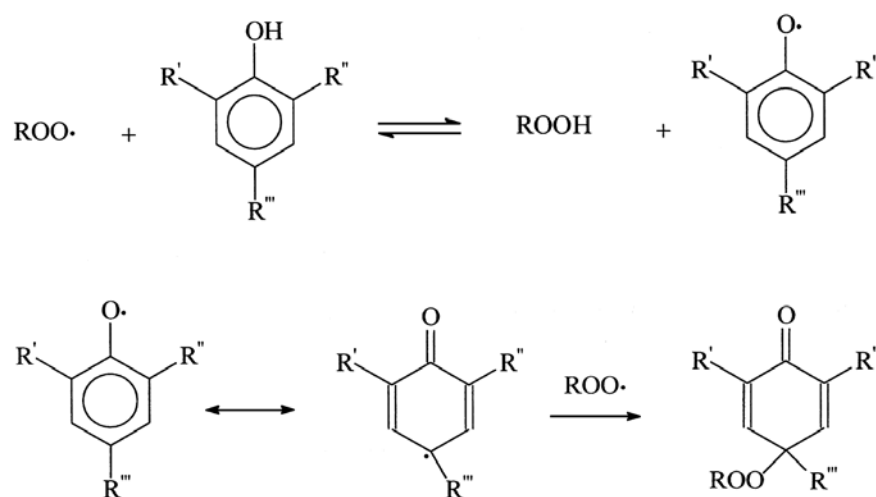
Figure 2.12: Chain termination by hindered phenolics [40]

47

them. The fourth postulates the formation of Criege zwitterions from the ozonized products. Along with antioxidants and antiozonants, waxes are also frequently used in rubber compounds as protective agents. The solubility of the waxes is very poor in the rubber, so they migrated to the surface of rubber products and protect them from the attack of ozone by making a protective layer on the surface [40,47].

2.1.5   Special Compounding Ingredients

Polymers, fillers, vulcanization system and stabilizer system are the primary ingredients of the rubber compounds. In addition to these, some secondary ingredients are also added to rubber compounds such as processing oils, plasticizers, coloring agents, and resins. Processing oils are added to improve the processing of rubber compounds and classified as aromatic, naphthenic, and paraffinic. For the proper action of processing oils, they must be compatible with the polymer; otherwise, they will result in loss of properties of the rubber compounds. The properties of the processing oil, such as molecular composition, molecular weight, and viscosity, determine the compatibility with polymers. Additionally, the stability of the processing oil against oxidation is very important for the performance of the final product. Plasticizers are added to enhance the flexibility and processing of the rubber compounds. In most cases, plasticizers cause a decrease in tensile strength and static modulus but an improvement in low-temperature flexibility and elongation at break. Waxes and processing oils can be considered as a plasticizer but this term is commonly used in rubber industry for compounds which comprise low-molecular-weight polyethylene, tans, pine, and esters. Different kind of resins, such as processing or extending resins, curing resins, and tackifying resins are also added to rubber compounds. They provide an improvement in tensile strength, tack, dispersion of filler, and resistance to fatigue and cut growth [47,88].

2.2   Application of Rubber Compounds in Tires

The tire is an important part of the vehicle which provides dampening and cushioning, traction, load carrying capacity, cornering force, minimizes vibrations and noise, and transmits driving and braking torque. The first pneumatic tire was patented by Robert

Thomson in 1845. Over the decades, tires have gone through a lot of developments. Before the development of radial tires, ply bias tires were mainly used, which use an innertube to retain the air. Safety, fuel consumption, and mileage were greatly improved by tubeless radial tires. A tire must deliver a high abrasion resistance, high traction in both wet and dry conditions, and low rolling resistance. A high abrasion resistance provides a good durability and low wear of the tire and tire can show improved mileage. A high traction on wet and dry roads offers a high grip between the road and the tread and avoids the slippage while running on the road. Rolling resistance is also an important property of the tread and influences the fuel consumption. Low rolling resistance results in better fuel-consumption performance. Interesting properties of the rubber compounds, such as elasticity, mechanical properties, deformability and recovery, and dampening characteristics, make it possible to obtain the required functions of the tires [40,47,89–91].

2.2.1 Tire Structure and Components

Tread and casing are the two main areas of a pneumatic tire. Tread come in contact with ground and casing transmit power to tread and support the load. These two areas are composed of many other components, each one with some specific properties. All of these basic components are made of different rubber compounds which interact with each other for high performance of tires. These rubber compounds held all the components of tire together and act as one structural unit; furthermore, they protect the belts, steel or fabric breakers, steel beads, and textile, which provide the ultimate strength to the tire. The cross-section showing the structure and different components of a radial tire is shown in Fig. 2.13. Each component plays a particular function in the performance of a tire. Tread is the component of the tire which comes in direct contact with the road, so its formulation is designed to provide low rolling resistance, good wet skid, traction, abrasion resistance, cornering characteristics, low heat build-up, and minimum generation of noise. Tread can be a compound of NR, SBR, BR, with silica, carbon blacks, vulcanizing chemicals, and oils. Tread shoulder influences the cornering properties and heat dissipation of tread. Tread base is formulated to provide low rolling resistance, good dissipation and good adhesion of tread with belts. Sidewall provides the support to tread and casing durability by protecting from scratch. It must be resistant to the environment, tearing and abrasion. The sidewall is

formulated by adding NR, BR, SBR, together with carbon black, various processing oils and other organic chemicals. The layers of steel belts or textiles, which are enclosed in rubber compounds, and lying below the tread, provide protection and strength to plies. Additionally, they provide stiffness to the casing which results in enhanced handling performance, and resistance to wear and damage.
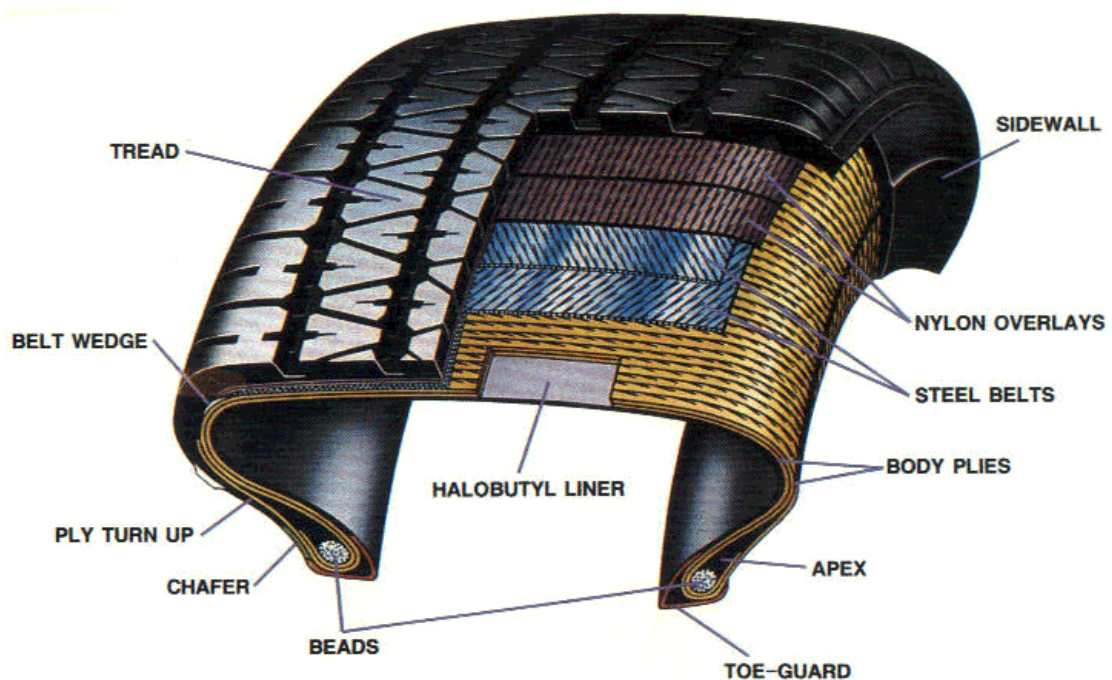
Figure 2.13: Cross-section of a high-performance passenger car tire [47]

Ply cords, either textile for passenger tire or steel for truck tires, extend from one bead to the other act as a primary reinforcing component of the tire casing. Beads are loops of steel wires fasten the plies and hold the tire in the rim. Apex compounds must be dynamically stiff to provide good handling performance and make the stress to be distributed easily. The belt wedge compounds are designed to have high adhesion between the casing and belt and provide better durability and wear properties to tread. Innerliner maintains the air pressure inside the tire, and the compounds of butyl rubber or their halogenated derivatives are usually used to obtain the good resistance to air-permeability [39,47,89].

References

[1]   W.M. Hess, W.K. Klamp, Rubber Chem. Technol. 56 (1983) 390–417.

[2]   S. Hui, T.K. Chaki, S. Chattopadhyay, J. Appl. Polym. Sci. 110 (2008) 825–836.

[3]   A. Bertora, M. Castellano, E. Marsano, M. Alessi, L. Conzatti, P. Stagnaro, G. Colucci, A. Priola, A. Turturro, Macromol. Mater. Eng. 296 (2011) 455–464.

[4]   M. Bhattacharya, M. Maiti, A.K. Bhowmick, Rubber Chem. Technol. 81 (2008) 782–808.

[5]   G. Ramorino, F. Bignotti, S. Pandini, T. Riccò, Compos. Sci. Technol. 69 (2009) 1206–1211.

[6]   V. Favier, G.R. Canova, J.Y. Cavaillé, H. Chanzy, A. Dufresne, C. Gauthier, Polym. Adv. Technol. 6 (1995) 351–355.

[7]   M.A.S. Azizi Samir, F. Alloin, A. Dufresne, Biomacromolecules 6 (2005) 612–626.

[8]   J.L. Leblanc, Prog. Polym. Sci. 27 (2002) 627–687.

[9]   J. Ayippadath Gopi, S.K. Patel, A.K. Chandra, D.K. Tripathy, J. Polym. Res. 18 (2011) 1625–1634.

[10]   D. Barana, Lignin-Based Elastomeric Composites for Sustainable Tyre Technology, University of Milano-Bicocca, Italy, 2017.

[11]   S. Thomas, R. Stephen, Rubber Nanocomposites: Preparation, Properties, and Applications, John Wiley & Sons, 2010.

[12]   C. Tsenoglou, Macromolecules 22 (1989) 284–289.

[13]   D. Adolf, Macromolecules 21 (1988) 228–230.

[14]   M.G. Brereton, M. Filbrandt, Polymer (Guildf). 26 (1985) 1134–1140.

[15]   H. Warson, in:, Appl. Synth. Resin Latices, 2001, pp. 1–48.

[16]   M. Negahban, Int. J. Solids Struct. 37 (2000) 2811–2824.

[17]   L.E. Nielsen, F.D. Stockton, J. Polym. Sci. Part A Gen. Pap. 1 (1963) 1995–2002.

[18]   A.T. DiBenedetto, J. Polym. Sci. Part B Polym. Phys. 25 (1987) 1949–1969.

[19]   L.H. Sperling, Introduction to Physical Polymer Science: Fourth Edition, John Wiley & Sons, Inc., Hoboken, NJ, USA, 2005.

[20]   Worldwide Rubber Statistics – 2017, Houston, TX, 2017.

[21]   R. Evans, The Composition of a Tyre: Typical Components Creating Markets for Recycled Resources, Oxon, 2006.

[22] An unknown object: the tire - Materials | Michelin The tire digest. http://thetiredigest.michelin.com/an-unknown-object-the-tire-materials.

[23] J.B. van Beilen, Y. Poirier, Trends Biotechnol. 25 (2007) 522–529.

[24] H.M. Nor, J.R. Ebdon, Prog. Polym. Sci. 23 (1998) 143–177.

[25] H. Kang, Y. Soo Kim, G.C. Chung, Plant Physiol. Biochem. 38 (2000) 979–987.

[26] J.E. Puskas, E. Gautriaud, A. Deffieux, J.P. Kennedy, Prog. Polym. Sci. 31 (2006) 533–548.

[27] H. Brown, Rubber : Its Sources, Cultivation, and Preparation, J. Murray, London :, 1914.

[28] Y. Hayashi, Plant Biotechnol. 26 (2009) 67–70.

[29] J.T. Sakdapipanich, J. Biosci. Bioeng. 103 (2007) 287–292.

[30] C.C. Ho, T. Kondo, N. Muramatsu, H. Ohshima, J. Colloid Interface Sci. 178 (1996) 442.

[31] J. Sansatsadeekul, J. Sakdapipanich, P. Rojruthai, J. Biosci. Bioeng. 111 (2011) 628–634.

[32] H. Zhang, A.K. Scholz, Y. Merckel, M. Brieu, D. Berghezan, E.J. Kramer, C. Creton, J. Polym. Sci. Part B Polym. Phys. 51 (2013) 1125–1138.

[33] A. Suzuki, H. Oikawa, K. Murakami, Polymer 26 (1985) 97–100.

[34] S. Toki, T. Fujimaki, M. Okuyama, Polymer 41 (2000) 5423–5429.

[35] J.A. Brydson, Rubber Chemistry, Applied Science Publishers, 1978.

[36] A.N. Gent, Engineering with Rubber : How to Design Rubber Components, Hanser, Munich, 2001.

[37] M. Morton, Rubber World 201 (1989) 55–66.

[38] C.M. Blow, Rubber Technology and Manufacture, Edited by C. M. Blow, Institution of the Rubber Industry, 1971.

[39] B. Rodgers, W.H. Waddell, S. Solis, W. Klingensmith, B. Rodgers, W.H. Waddell, S. Solis, W. Klingensmith, in:, Kirk-Othmer Encycl. Chem. Technol., John Wiley & Sons, Inc., Hoboken, NJ, USA, 2004.

[40] B. Rodgers, Rubber Compounding: Chemistry and Applications, Marcel Dekker, 2004.

[41] M. Rodgers, S. Mezynski, Kautschuk Und Gummy, Kuntstoffe 46 (1993) 718–726.

[42] B.D. Simpson, The Vanderbilt Rubber Handbook, R. T. Vanderbilt Co., 1978.

[43] K.H. Nordsiek, Kautschuk Und Gummi Kunststoffe 38 (1985) 178–185.

[44] B.B. Boonstra, Polymer 20 (1979) 691–704.

[45] J. Fröhlich, W. Niedermeier, H.D. Luginsland, Compos. Part A Appl. Sci. Manuf. 36 (2005) 449–460.

[46] S.J. Park, K.S. Cho, J. Colloid Interface Sci. 267 (2003) 86–91.

[47] J.E. Mark, B. Erman, F.R. Eirich, Science and Technology of Rubber, Elsevier Academic Press, 2005.

[48] W.M. Hess, Rubber Chem. Technol. 64 (1991) 386–449.

[49] C.R. Herd, G.C. McDonald, W.M. Hess, Rubber Chem. Technol. 65 (1992) 107–129.

[50] D. Barnard, C.S.L. Baker, I.R. Wallace, Rubber Chem. Technol. 58 (1985) 740–750.

[51] A.R. Payne, R.E. Whittaker, Rubber Chem. Technol. 44 (1971) 440–478.

[52] M.-J. Wang, Rubber Chem. Technol. 72 (1999) 430–448.

[53] I. Pliskin, N. Tokita, J. Appl. Polym. Sci. 16 (1972) 473–492.

[54] T. a Vilgis, G. Heinrich, M. Kluepell, Reinforcement of Polymer Nano-Composites: Theory, Experiments and Applications, Cambridge University Press, 2009.

[55] J.J. Brennan, T.E. Jermyn, B.B. Boonstra, J. Appl. Polym. Sci. 8 (1964) 2687–2706.

[56] A.R. Payne, W.F. Watson, Rubber Chem. Technol. 36 (1963) 147–155.

[57] Yvonick Chevallier, Jean-Claude Morawski, Precipitated Silica with Morphological Properties, Process for Producing It and Its Application, Especially as a Filler, EP0157703A1, 1985.

[58] L.R. Evans, W.H. Waddell, Kautschuk, Gummi, Kunststoffe 48 (1995) 718–723.

[59] M.-J. Wang, Rubber Chem. Technol. 71 (1998) 520–589.

[60] W. Niedermeier, J. Fro È hlich, H. Luginsland, K. È, Kautschuk Und Gummi Kunststoffe 55 (2002) 356–366.

[61] W.M. Hess, G.C. McDonald, E. Urban, Rubber Chem. Technol. 46 (1973) 204–231.

[62] D.S. Villars, J. Am. Chem. Soc. 69 (1947) 214–217.

[63] E. Papirer, V.T. Nguyen, J.B. Donnet, Carbon N. Y. 16 (1978) 141–144.

[64] D. Rivin, J. Aron, A.I. Medalia, Rubber Chem. Technol. 41 (1968) 330–343.

[65] F. Bueche, J. Appl. Polym. Sci. 4 (1960) 107–114.

[66] ASTM D1765.

[67] J. O'Brien, E. Cashell, G.E. Wardell, V.J. McBrierty, Macromolecules 9 (1976) 653–660.

[68]   A.P. Legrand, N. Lecomte, A. Vidal, B. Haidar, E. Papirer, J. Appl. Polym. Sci. 46 (1992) 2223–2232.

[69]   T.A. Vilgis, G. Heinrich, Macromolecules 27 (1994) 7846–7854.

[70]   A. Voet, J.C. Morawski, J.B. Donnet, Rubber Chem. Technol. 50 (1977) 342–355.

[71]   Roland Rauline, Rubber Compound and Tires Based on Such a Compound, EP0501227A1, 1992.

[72]   A.P. Legrand, The Surface Properties of Silicas, John Wiley, 1998.

[73]   William L. Hergenrother, James Oziomek, William M. Cole, Addition of Salts to Improve the Interaction of Silica with Rubber, US6180710B1, 2001.

[74]   J.W. ten Brinke, S.C. Debnath, L.A.E.M. Reuvekamp, J.W.M. Noordermeer, Compos. Sci. Technol. 63 (2003) 1165–1174.

[75]   U. Goerl, A. Hunsche, A. Mueller, H.G. Koban, Rubber Chem. Technol. 70 (1997) 608–623.

[76]   M.P. Wagner, Rubber Chem. Technol. 49 (1976) 703–774.

[77]   W.H. Waddell, L.R. Evans, Rubber Chem. Technol. 69 (1996) 377–423.

[78]   Charles Goodyear, US3633A, 1844.

[79]   G. Oenslager, Ind. Eng. Chem. 25 (1933) 232–237.

[80]   Zaucker Ewald, Orthner Ludwig, Bogemann Max, Vulcanization Accelerator, US1942790A, 1934.

[81]   Marion W Harman, Process of Vulcanizing Rubber and Product Produced Thereby, US2100692A, 1937.

[82]   A.K. Bhowmick, M.M. Hall, H.A. Benarey, Rubber Products Manufacturing Technology, M. Dekker, CRC Press, New York, 1994.

[83]   R.H. Campbell, R.W. Wise, Rubber Chem. Technol. 37 (1964) 635–649.

[84]   R.H. Campbell, R.W. Wise, Rubber Chem. Technol. 37 (1964) 650–667.

[85]   N.J. Morrison, M. Porter, Rubber Chem. Technol. 57 (1984) 63–85.

[86]   P. Ghosh, S. Katare, P. Patkar, J.M. Caruthers, V. Venkatasubramanian, K.A. Walker, Rubber Chem. Technol. 76 (2003) 592–693.

[87]   W. Hofmann, Vulcanization and Vulcanizing Agents., Maclaren and Sons Ltd., London, 1967.

[88]   S.K. De, J.R. White, Rubber Technologist's Handbook, Rapra Technology Ltd, 2001.

[89]   A.K. Chandra, V. Bhandari, in:, Adv. Elastomers II, Springer, Berlin, Heidelberg, 2013,

pp. 183–203.

[90]   D.J. Schuring, Rubber Chem. Technol. 53 (1980) 600–727.

[91]   Indian Rubber Institute., Rubber Engineering, 1st ed., McGraw-Hil, New York, 1999.

Chapter 3

Biorefinery process for the simultaneous recovery of lignin, hemicelluloses, cellulose nanocrystals and silica from rice husk and *Arundo donax**

Syed Danish Ali, Davide Barana, Anika Salanti, Luca Zoia, Marco Emilio Orlandi

An integrated biorefinery process based on acidic leaching, alkaline treatment, and concentrated sulfuric acid hydrolysis was set up for the simultaneous recovery of lignin, hemicelluloses, silica, and cellulose nanocrystals (CNCs) from *Arundo donax* and rice husk. These fractions can serve as a viable source of biochemicals with potential high-value applications. A spectroscopic and chromatographic characterization demonstrated that a combined acidic-alkaline treatment enhanced the degradation of lignin-carbohydrate complexes releasing lignin and hemicelluloses in higher yield and purity than the sole alkaline treatment. The remaining cellulose-rich solid was bleached through a totally chlorine free process and then hydrolyzed to cellulose nanocrystals isolation. The morphology and dimensions of the prepared CNCs were investigated by Transmission Electron Microscope (TEM) analysis. TEM analysis clearly demonstrated the rod-like morphology of the synthesized CNCs for both samples with a dimension of about 200 nm in length and 5-15 nm in diameter. *Arundo donax* cellulose nanocrystals were extracted and characterized for the first time in literature. Moreover, from rice husk, pure amorphous silica was obtained almost in 90 % yield and 99 % purity, avoiding incineration. In term of mass balance, it was possible to refine the investigated biomasses for the production of lignin, hemicelluloses, silica and CNCs in almost 40 % overall yield.

3.1 Introduction

Due to the increasing concerns generated from fossil resource dependence, the study of alternative sources of bio-based products is highly desirable [1]. In recent years, lignocellulosic biomasses have emerged as potential renewable resources due to their annual renewability and large biomass stock [2]. Nevertheless, in order to take advantage of the various components of the biomass and maximize the added value, the fractionation of lignocellulosic into the three primary components, namely cellulose, hemicelluloses, and lignin must be performed. This process is called biorefinery and consists of an integrate conversion system for the production of fuels, power, heat, and/or value-added chemicals from biomasses [2].

Among agricultural residues and herbaceous crops, rice husk [3], the outer cover of rice grain, and *Arundo donax* [4], a low-maintenance crop growing on marginal land, are extremely interesting. Rice is among the most cultivated crops in the world with a global production of about 740 million tons/year in 2014. Rice husk (RH) accounts for about 20 % w/w of rice, and it is one of the major agro-industrial side-product produced worldwide. With regard to its composition, it is note-worthy the large amount of ash and lignin, which confers rice husk an outstanding recalcitrance toward biological and environmental threats. As a starting biomass, rice husk has many advantages: the small-sized shape (1–2 mm) in which it is naturally produced avoid the need for a mechanical pretreatment, it is easily recovered during the rice processing system without additional cost, it is extremely widespread, and has a high annual availability. *Arundo donax* (AD), or Giant Cane, is a tall perennial cane which grows in damp soils, either fresh or moderately saline. The AD is a strong candidate for use as a renewable biomass source because of its fast growth rate, ability to flourish in different soil types and climatic conditions.

Many studies are focused on the extraction of potentially high-value products from lignocellulosic biomasses, such as lignin [3], cellulose nanocrystals [5,6], silica [7] and fermentable sugar for bioethanol production [8]. But recently the interest of the researchers focused on the opportunity for a simultaneous recovery of all the lignocellulose fractions [9–11] in a unique, comprehensive process. In this study, a convenient biorefinery process was set up for rice husk and *A. donax* for the simultaneous

recovery of lignin, hemicellulose (only from the AD), cellulose nanocrystals, and silica (only from RH) in high yield and purity. Currently, lignin is mainly obtained as a byproduct of the papermaking industry and often directly burned as a combustible for energy generation. Despite the major advances in the use of lignin, especially of Kraft and lignosulphonates, there is a growing interest in the use of sulfur-free lignins (for example from bio-ethanol production or soda pulping). Hemicelluloses are polysaccharides in plant cell walls and include xyloglucans, xylans, mannans, and glucomannans [12]. The detailed structure of hemicelluloses and their abundance vary among different species and cell types. The most important biological role of hemicelluloses is their contribution to strengthening the cell wall by interaction with cellulose and lignin. Cellulose nanocrystals (or nanowhisker) are attracting a great deal of interest due to their properties including nano dimension, high surface area, unique morphology, low density and mechanical strength, as well as large availability, complete renewability, biodegradability and low toxicity [13]. Rice husk is a naturally ash-rich substrate. About 96% of this inorganic fraction is composed by pure silica [14], which represents an economically viable raw material for the production of silica gels and powders [15–18] as well as soluble silicates [19–21].

In this work, an alkaline treatment was selected for the fractionation of the lignocellulosic materials. The use of NaOH solutions is widely employed as a common method to process wood and non-woody lignocellulosic materials to remove lignin [22,23]. It is worth noticing that, besides lignin, the alkaline treatment is also able to solubilize other lignocellulosic components such as hemicelluloses, residual extractives, and ashes [24]. The removal of lignin is usually the first and trickiest step in a biorefinery process. To improve the yield of the extracted lignin it was decided to perform a preliminary acidic treatment before the alkaline extraction. Recently, it was demonstrated the superior efficiency of combined acidic-alkaline treatments in increasing cellulose digestibility for bioethanol production [24–28]. The reported pretreatments were found to induce physical changes, such as decreasing cellulose crystallinity, which is particularly undesired in the isolation of cellulose nanocrystals though. Even so, a mild acidic pretreatment improves the silica fraction purity and many authors concluded that a preliminary leaching of rice husk with different mineral acids is an effective way to remove most of the metallic impurities and produce pure silica completely white in color [29].

3.2 Experimental

3.2.1 Materials

Rice husk and *Arundo donax* were kindly provided by a local farm. All reagents and solvents (ACS grade) were purchased from Sigma-Aldrich and used as received without further purification.

3.2.2 Methods

3.2.2.1 Acid Leaching

Arundo donax (AD) and rice husk (RH) (10 g) were air dried, crushed in a blender for 5 min and passed through a 1 mm screen. The ground materials thus obtained were washed separately in 200 mL of 0.1 M HCl for 2 h at 100 ^{o}C under magnetic stirring. Then the material was recovered by Buchner filtration, washed with 20 mL of fresh water and air-dried overnight.

3.2.2.2 Alkaline Treatment

Both grounded reference and leached rice husk and *A. donax* (10 g) were treated with 200 mL of 0.1 M NaOH for a specific time period (1, 2 h) at 100 ^{o}C under magnetic stirring. The cellulose-rich insoluble material left was separated by filtration and washed with 20 mL of 0.1 M NaOH aqueous solution. The filtrate was acidified with 5 M HCl until pH 1 was reached to allow lignin precipitation. Precipitated lignin was collected by centrifugation (3500 g, 10 min), washed with deionized water, and freeze-dried.

3.2.2.3 Hemicellulose A Recovery

The filtrate collected after the acid leaching of the AD was reduced in volume under vacuum and poured into a ten-fold volume of ethanol (absolute alcohol, 99.8 %) to

precipitate the polysaccharide fraction named Hemicellulose A at 4 ^{o}C for 24 h. Hemicellulose A was recovered by centrifugation (3500 g, 10 min) and air dried.

3.2.2.4 Hemicellulose B Recovery

The aqueous supernatant collected after the alkaline treatment of AD was reduced in volume by rotavapor and poured into a ten-fold volume of ethanol to precipitate hemicelluloses. This polysaccharide fraction, recovered by centrifugation (3500 g, 10 min), was named Hemicellulose B.

3.2.2.5 Silica Recovery

The aqueous supernatant collected after the alkaline treatment of rice husk was stirred at 90 ^{o}C for 4 h at pH 4 to precipitate silica. The solid precipitated material was purified with water for 3 centrifugation cycles (3500 g, 10 min) to remove water-soluble salts formed after neutralization processes. The recovered silica was oven dried at 100 ^{o}C overnight.

3.2.2.6 Total Chlorine Free Bleaching

The procedure applied is a modification of the method optimized by Kuznetsov et al [30] for the delignification of aspen wood. Five grams of cellulose-rich solids, recovered after the alkaline treatment, were treated with 150 mL of an aqueous solution comprising acetic acid (25 wt %), hydrogen peroxide (4 wt %) and sulfuric acid (2 wt %) for 4 h at 100 ^{o}C under vigorous stirring. The bleached cellulose-rich samples were recovered by vacuum assisted filtration, washed with cold water, oven dried at 60 ^{o}C overnight.

3.2.2.7 Cellulose Nanocrystals Isolation

Cellulose nanocrystals (CNCs) were extracted from bleached cellulose-rich materials by treatment with 60 % H_2SO_4 for 1 h at 55 ^{o}C according to an acid/cellulose weight ratio of 9. The product was then poured into a ten-fold volume of ice-cold water and stirred for 10 min. The cellulose sediment was purified by repeated cycles of centrifugation at an

acceleration of 3200 g for 15 min and re-suspension of the solid with distilled water by ultrasonic mixing for 5 min. The turbid supernatant thus obtained was dialyzed against distilled water for 1 week until a pH of 5–6 was reached. CNCs gravimetric yield was measured after drying the suspension in the oven at 100 °C overnight.
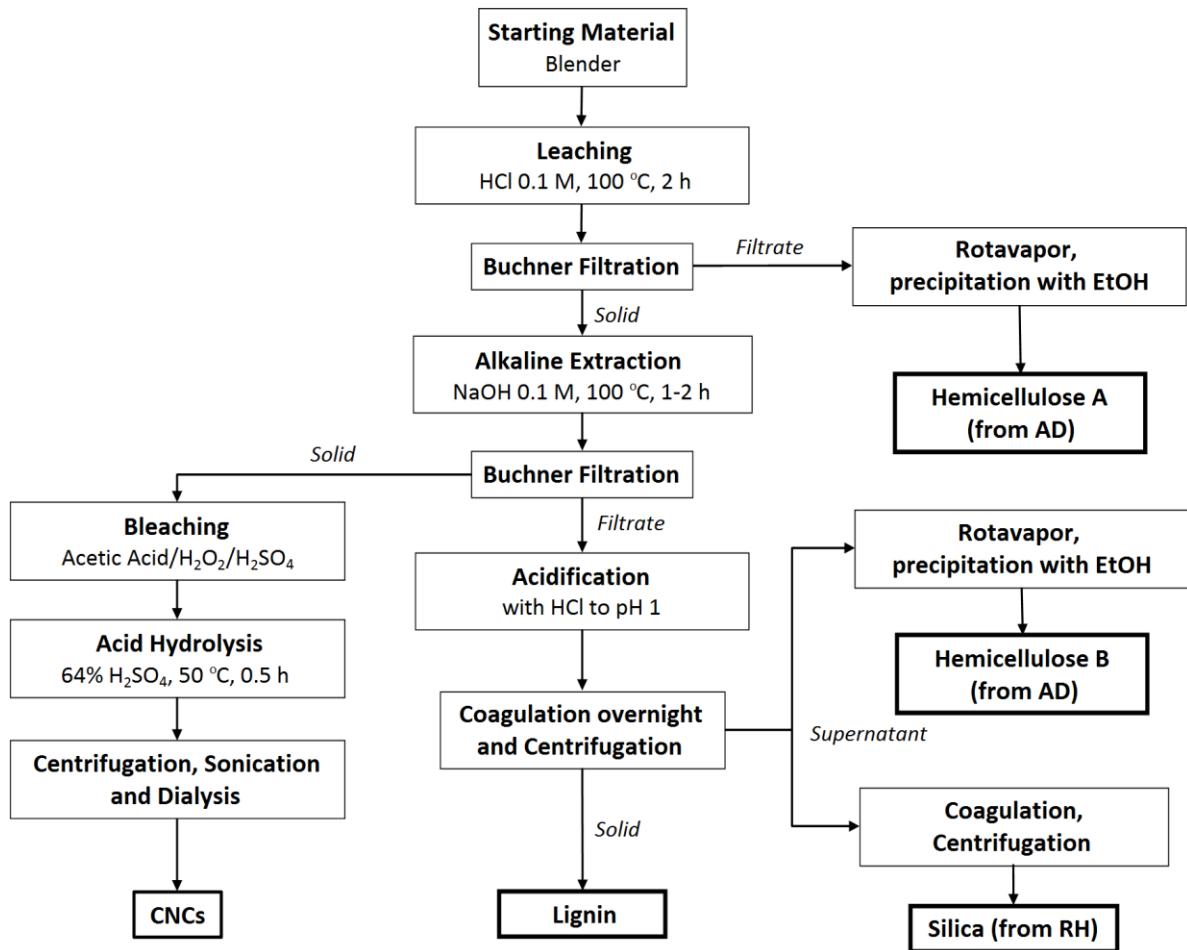
Figure 3.1: Flow sheet diagram of the biorefinery process

3.2.3 Characterizations

3.2.3.1 Lignin Contents

The amount of total lignin was calculated as the sum of the acid-insoluble (Klason lignin) and acid soluble lignin content, measured according to the method reported by Yeh et al

[31]. All the value reported in the text and in the tables (as lignin purity) are the average of three analyses ±1.0 % (P = 0.05, n = 3).

3.2.3.2 Ash Contents

Accurately weighed and dried samples (100 mg) were put in tared, well-desiccated porcelain crucible sand and placed in a muffle furnace set at 550 ^{o}C for 3 h. The crucibles were then stored in a desiccator until room temperature was reached. The ash content was determined gravimetrically. The values reported in the text and in the tables are the average of three analyses ±0.1 % (P = 0.05, n = 3).

3.2.3.3 Acidolytic Lignin Isolation

Lignin extraction was performed according to a method reported by Canevali et al [32].

3.2.3.4 Lignocellulosic Material Acetylation in Ionic Liquid

The acetylation reaction was carried out in 1-allyl-3-methylimidazolium chloride ([amim]Cl), following the procedure reported by Salanti et al [33].

3.2.3.5 Hemicellulose Benzoylation in Ionic Liquid

The benzoylation reaction was carried out in 1-allyl-3-methylimidazolium chloride ([amim]Cl), according to the method described by Salanti et al [33].

3.2.3.6 Lignin Acetylation

A total of 60 mg of extracted lignin was acetylated in a pyridine-acetic anhydride solution (1:1 v/v, 4 mL) and kept overnight at 40 ^{o}C. After stripping with ethanol, toluene, and chloroform (25 mL × 3 each solvent), the sample was dried in vacuum. The acetylated lignin has been solubilized in THF for GPC analysis.

3.2.3.7 GPC Analysis

Gel Permeation Chromatography (GPC) analyses were performed on a Waters 600 E liquid chromatography connected to an HP1040 ultraviolet detector set at 280 nm. The injection port was a Rheodyne loop valve equipped with a 20 μL loop. The GP-column system was composed by a sequence of an Agilent PL gel 5 μm, 500 Å, and an Agilent PL gel 5 μm, 104 Å. The solvent used was tetrahydrofuran (Fluka 99.8%). PL Polymer Standards of Polystyrene from Polymer Laboratories were used for calibration. Evaluation of the number-average molecular weight (Mn), the weight-average molecular weight (Mw), and the peak molecular weight (Mp) of the extracted lignin was accomplished. Moreover, the ratio I = Mw/Mn, defined as Polydispersity Index was also calculated. The Mn, Mw, and Mp values reported are the average of three analyses (Mw: 1000 g/mol; Mn, Mp: 100 g/mol, P = 0.05, n = 3).

3.2.3.8 FTIR Analysis

Fourier Transform Infrared Spectroscopy (FTIR) was used for sample characterization. The analyses were performed with a Nicolet iS10 spectrometer (Thermo Scientific) equipped with an iTR Smart device (total scan 32, range 4000–800 cm^{-1}, resolution 1 cm^{-1}).

3.2.3.9 SEM Analysis

Scanning Electron Microscopy (SEM) investigations of silica powder were performed in high vacuum conditions by a Tescan Vega TS5136XM, equipped with an energy dispersion electronic microprobe EDAX Genesis 4000 XMS Imaging 60 SEM (accelerating voltage 20 kV; current 190 pA; working distance 23 mm; spot size 250 nm).

3.2.3.10 TEM Analysis

Transmission Electron Microscopy (TEM) was used to investigate the structure of the isolated cellulose nanocrystals. 10 μL of the nanocrystals preparation was dropped onto Formvar-coated 300 mesh copper grids and after 5 min the solution was gently removed.

Samples were counterstained for 5 min with a saturated solution of uranyl acetate, washed with MilliQ water to eliminate excess uranyl acetate, and allowed to air dry. TEM analyses were performed on a Zeiss LEO 912ab Energy Filtering TEM operating at 120 kV, and images were collected using a CCD-BM/1K system. Digital images were taken at a magnification of 15k and 30k.

3.3   Results and Discussion

Lignin and ash content in *A. donax* and rice husk were assessed through gravimetric techniques after acidolytic extraction and mineralization, respectively. The holocellulose content was then evaluated by mass difference, according to the equation [100 % − (lignin content + ash content)]. *A. donax* was found to be characterized by 65.4 % holocellulose, 29.9 % lignin and 4.7 % ashes, whereas rice husk was composed by 62.2 % holocellulose, 21.8 % lignin and 16.0 % ashes. The composition of *A. donax* is in good agreement with recent literature data [34]. Relative amounts of rice husk constituents were also found to be in line with the compositions proposed by previous studies [35].

3.3.1 Alkaline Pretreatment vs Acidic-Alkaline Pretreatment

The alkaline lignin extraction was accomplished by treating grounded *A. donax* with 0.1 M aqueous NaOH at 100 ^{o}C. Table 3.1 reports lignin yield (assessed gravimetrically with reference to the total lignin content) and purity (measured by Klason methodology) after 1 h and 2 h treatment, respectively. The purity achieved was very low for both the treatments and this was also experimentally confirmed by FTIR characterization. The FTIR spectra of AD lignin samples obtained according to different extraction conditions: 0.1 M NaOH, 100 ^{o}C, 1 h (1 h NaOH); 0.1 M NaOH, 100 ^{o}C, 2 h (2 h NaOH); combined acidic-alkaline treatment 0.1 M HCl, 100 ^{o}C, 2 h/0.1 M NaOH, 100 ^{o}C, 2 h (2 h HCl + 2 h NaOH); and acidolytic lignin reference sample, are shown in Fig. 3.2. FTIR spectra of 1 h NaOH and 2 h NaOH exhibited a strong peak at 1100–1000 cm^{-1}, related to the stretching vibration of the C-O bond, typical of polysaccharides. On the other hand, a preliminary acidic leaching was performed on the starting materials, which was then subjected to alkaline treatment.

Table 3.1: Purity and yield of *Arundo donax* lignin samples obtained according to different extraction conditions

	1 h NaOH	2 h NaOH	2 h HCl + 2 h NaOH	Acidolytic lignin
Purity (%)	45	55	90	95
Lignin Yield (%)	43	53	45	48

The effect of the combined acidic-alkaline treatment (0.1 M HCl, 100°C, 2 h/0.1M NaOH, 100°C, 2 h) on lignin yield and purity was then evaluated through gravimetric, spectroscopic, and chromatographic techniques. According to Table 3.1, a significant increase in purity was observed. The FTIR analysis demonstrated that the peak related to C-O stretching vibrations strongly decreased in the combined process and overall the spectrum became similar to the acidolytic reference one.
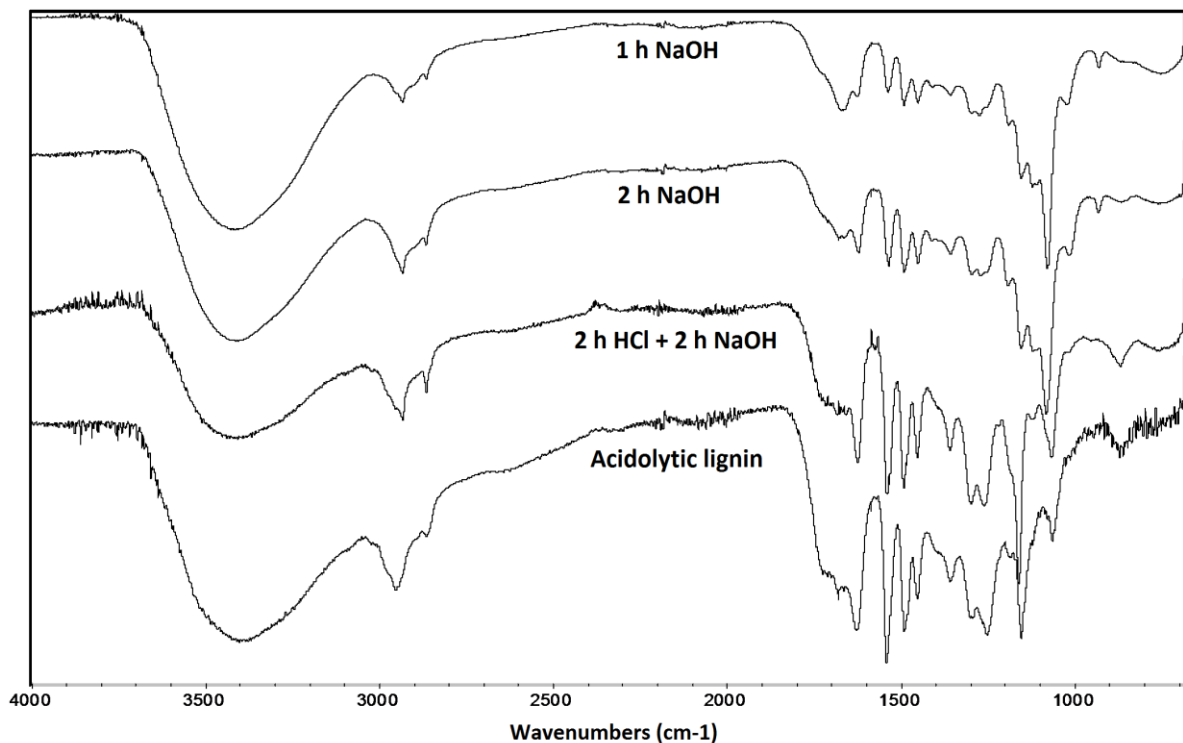
Figure 3.2: FTIR spectra of *Arundo donax* lignin samples obtained according to different extraction conditions
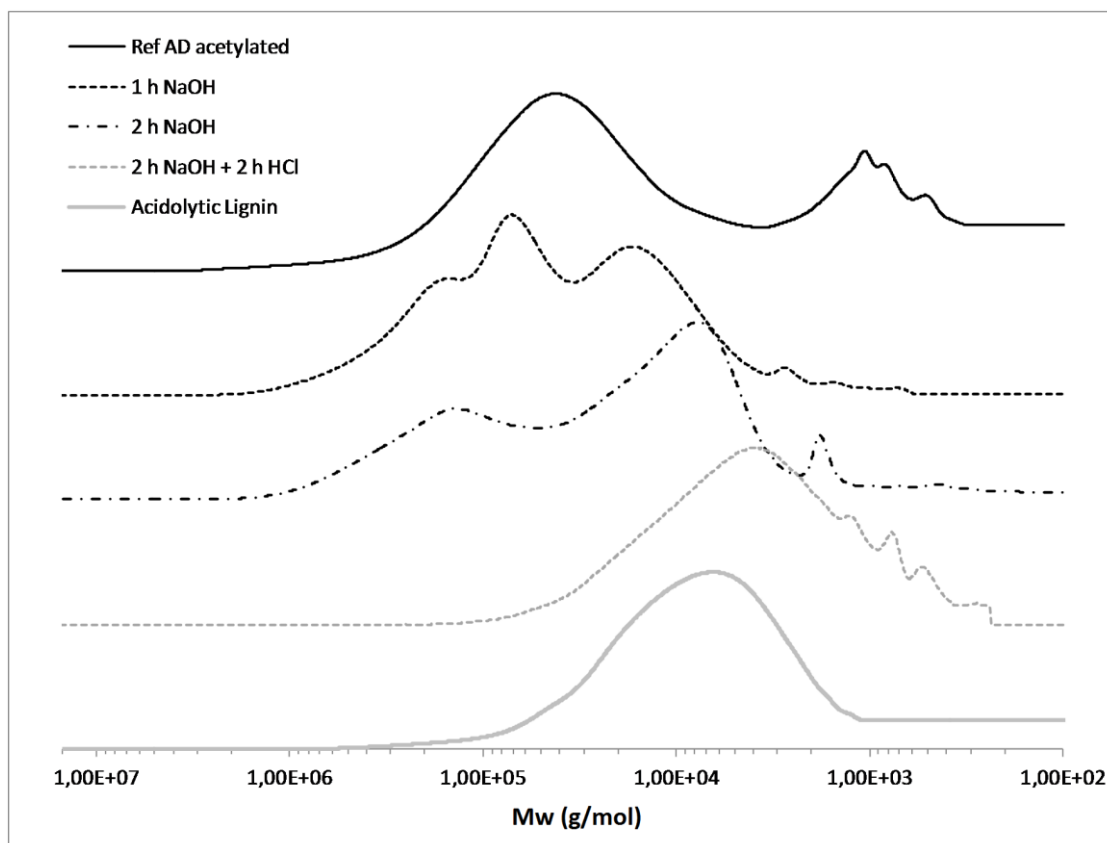
Figure 3.3: Gel permeation chromatography of *Arundo donax* lignin samples

Fig. 3.3 depicts the GPC chromatograms acquired for different lignin samples of *A. donax* after acetylation in the ionic liquid. The use of ionic liquids allows for the obtainment of fully derivatized samples, with enhanced solubility in tetrahydrofuran, the chromatographic solvent of choice [36], avoiding possible misinterpretations of the analysis due to insoluble fractions. In particular, the chromatographic profile of the ionic liquid acetylated samples of the untreated *A. donax* (black line), the material recovered after alkaline extraction at 1 h and 2 h of treatment (black dotted and point-dotted line respectively), the material recovered after combined acidic and alkaline treatment (gray dotted line) and acidolytic lignin reference sample (gray line) are compared in Fig. 3.3. As already reported by Salanti et al. [33] the chromatographic profile of acetylated native *A. donax* seems to be characterized by the presence of hemicellulose in some way connect to aromatic compounds, i.e. phenolic compounds and/or lignin (Lignin-Carbohydrate Complexes, LCCs). The extracted materials were characterized by different GPC profile: the peak associated to the unrefined acetylated lignocellulosic substrate at about 100,000

g/mol became roughly bimodal as a consequence of the alkaline treatments, revealing a partial hydrolysis of the lignin-carbohydrate complexes and, thus, the liberation of lignin. This trend seems to be clearly time-dependent: protracting the alkaline extraction from 1 to 2 h, a change in the chromatographic peak assigned to the released lignin (approximately 10,000 g/mol), that becomes the predominant one, was induced. In conclusion, in agreement with previous considerations about the combined acidic-alkaline pretreatment, a rather pure lignin was recovered when the alkaline treatment was combined with the leaching stage. In this last case the peak associated to lignin-carbohydrate complexes completely disappeared, and the chromatogram became similar to the reference acidolytic lignin. Overall, the analyses collected indicated that a certain amount of polysaccharides are covalently bonded with lignin and that a combined acidic-alkaline treatment seems to improve the degradation of LCCs resulting in the isolation of a pure lignin fraction.

In light of the positive results obtained for *A. donax*, the combined acidic-alkaline treatment was also applied for the fractionation of rice husk. Purity, yield and and GPC data of rice husk lignin samples obtained according to different extraction conditions: 0.3 M NaOH, 90 $^{\circ}$C, 4 h (Ref [3]); combined acidic-alkaline treatment 0.1 M HCl, 100 $^{\circ}$C, 2 h/0.1 M NaOH, 100 $^{\circ}$C, 2 h (HCl + NaOH); acidolytic lignin reference sample, are reported in Table 3.2. The results on lignin yield, purity, and average molecular weight indexes are compared with the same results obtained by Salantiet et al. [3], where the authors optimized the lignin extraction exploiting the alkaline treatment; acidolytic lignin is reported as a reference. Even if the alkaline treatment there described is performed under harsher reaction conditions than the presented process, the outcome in purity and yield is lower (78 % and 29 % vs 95 % and 46 %, respectively). The GPC analysis pointed out the higher purity in term of residual polysaccharides of the lignin recovered after the combined acidic-alkaline treatment. The calculated average molecular indexes are lower, demonstrating a minor content of covalently linked polysaccharides. Similar considerations could be done from the FTIR analysis. FTIR spectra of rice husk lignin samples recovered according to different extraction conditions are shown in Fig 3.4. The peak associated to polysaccharides appeared at 1100-1000 cm^{-1} related to C-O stretching vibrations strongly decreased in the combined acidic-alkaline process and overall the spectrum became

similar to the acidolytic reference one. Resuming the data, by using the combined acidic-alkaline process, it was possible to recover 45 % of the lignin from the AD and 46 % from the RH, with purity of 90 % and 96 % respectively.

Table 3.2: Purity, yield, and GPC data of rice husk lignin samples obtained according to different extraction conditions

	Ref [3]	HCl + NaOH	Acidolytic lignin
Purity (%)	78	95	90
Lignin Yield (%)	29	46	51
GCP (g/mol)			
M_p	4500	3900	5100
M_n	13600	8800	10200
M_w	115000	32500	41000
PD	8.4	3.7	4.0
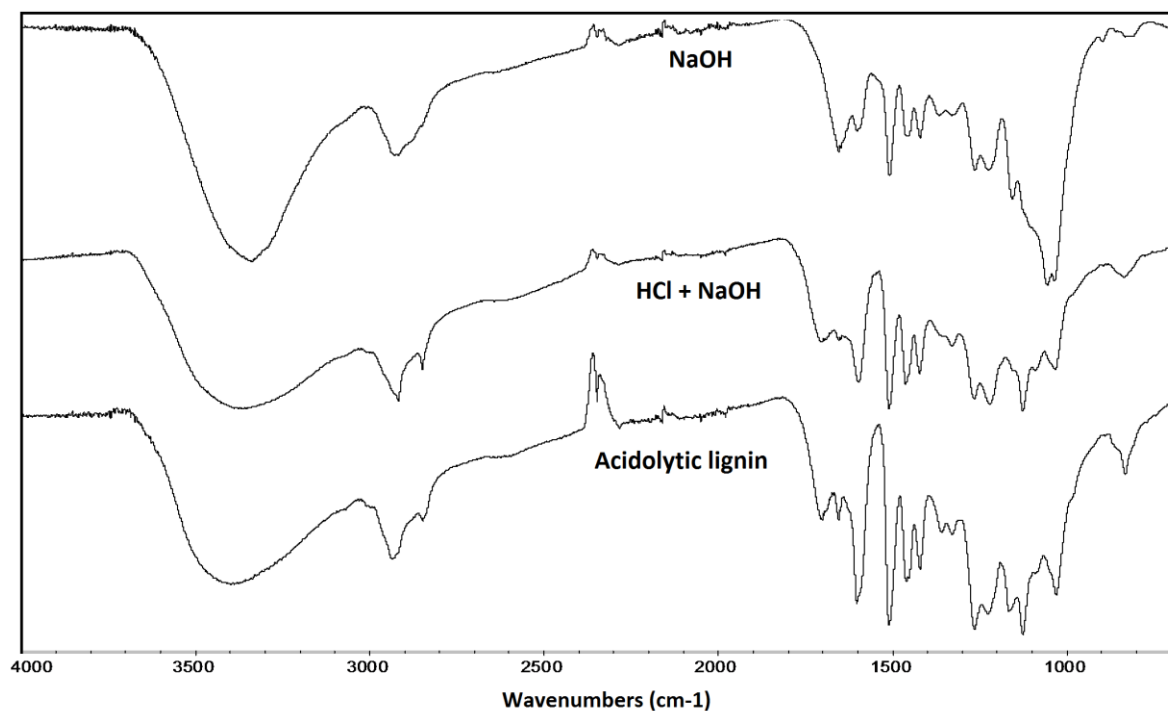
Figure 3.4: FTIR spectra of rice husk lignin samples recovered according to different extraction conditions

3.3.2 Hemicellulose Recovery

During the combined acidic-alkaline treatment of AD, a fraction of the hemicellulose was solubilized during the acid leaching, while the following alkaline treatment also extracted a second fraction of the hemicellulose. Therefore, hemicellulose from *A. donax* was recovered from the aqueous supernatant obtained after acidic leaching (Hemicellulose A) and alkaline extraction (Hemicellulose B) by ethanol precipitation, as described in the experimental section. The FTIR spectra and GPC chromatogram of the hemicellulose A and B are shown in Fig 3.5. According to the FTIR analysis, both hemicellulose A and B showed the typical spectra of a polysaccharide. Fraction A featured the typical peaks of xylans, [37] while fraction B seemed to be partly contaminated by cellulose, that was probably solubilized during the alkaline treatment. GPC profiles also supported this interpretation: fraction A had a molecular weight distribution centered around 20,000 g/mol, while the chromatogram of fraction B was shifted to higher molecular weights. Moreover, the white solid recovered did not show the characteristic peaks of lignin corresponding to the aromatic skeleton vibrations, revealing an overall good purity. In terms of yield, 7 g of hemicellulose A and 8 g of fraction B from 100 g of starting material were collected. Assuming a hemicellulose content in *A. donax* of about 28 % w/w, approximately 55 % of the original hemicellulose was recovered.
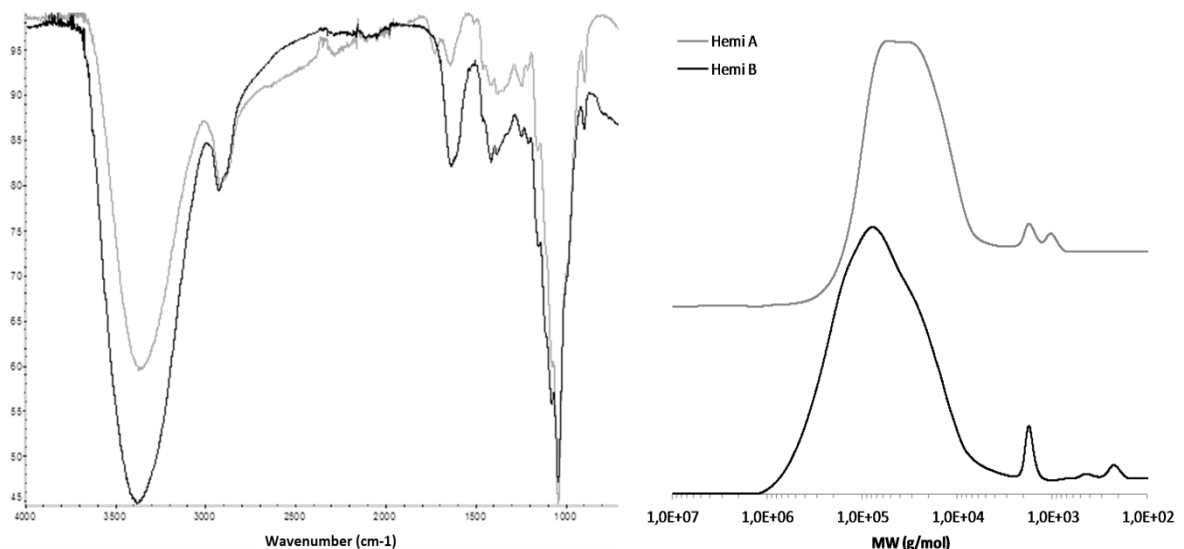
Figure 3.5: FTIR and GPC characterization of hemicellulose (fraction A and B) from AD

3.3.3 Silica Recovery

Silica was extracted from rice husk which is consisting of about 16 % of ashes, among which more than 95% is composed of silica. The ashes get solubilized in the highly alkaline reaction medium during the alkaline treatment of rice hush. The supernatant obtained after the alkaline treatment is rich in lignin and silica contents. After lignin coagulation, the silica was precipitated and purified from the supernatant as reported in the Methods section. The collected silica was characterized morphologically by SEM and elemental composition of the precipitated solid was investigated by EDX analysis. Fig 3.6 shows the SEM image and EDX data of the precipitated silica. It can be clearly seen that the silica had an amorphous and coarse morphology, but the purity in silicon dioxide reached 98.5 %. The recovery of silica in well-defined morphology and dimension lies outside the scope of this work, which was instead focused on the possibility to refine silica in high yield and purity. In term of yield, the procedure allowed to obtain 88 % of total ash content (16 %)

Oxide	wt %
Na_2O	0,61
MgO	0,19
Al_2O_3	0,36
SiO_2	98,56
K_2O	0,08
CaO	0,21

500 um
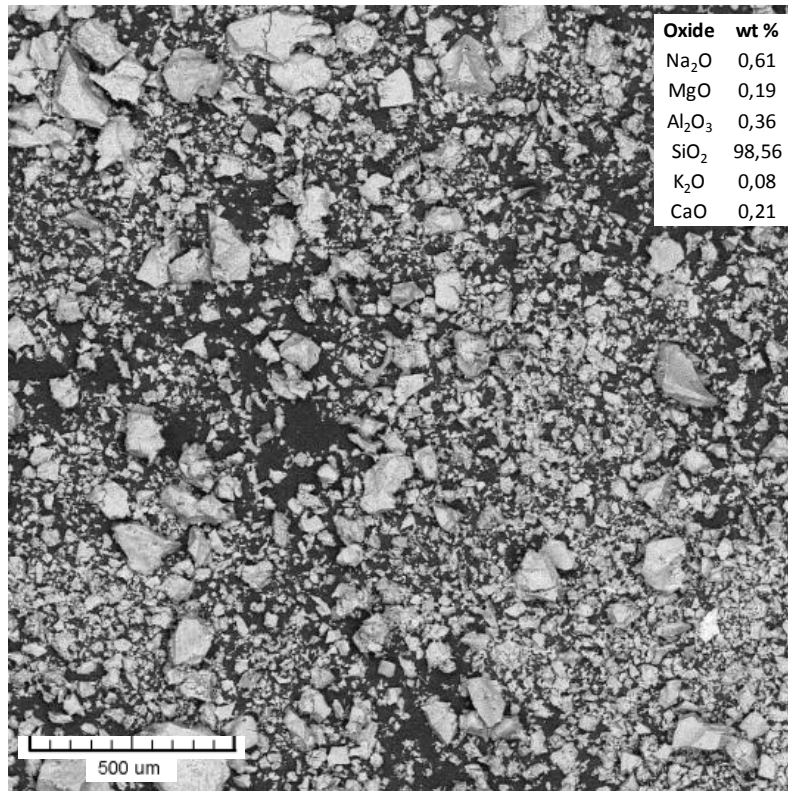
Figure 3.6: SEM and EDX results of amorphous silica recovered from RH

from the starting material (i.e., 14 g from 100 g of RH). Since about 96 % of the total ash content of RH is composed of silica, the procedure succeeded in the recovery of silica with a yield higher than 90 %. It is to note that this material could be a potential source of soluble silicates and it could be produced avoiding incineration.

3.3.4 CNCs Recovery

CNCs were extracted from the cellulose-rich material obtained after acidic and alkaline treatment. The isolation method is based on acidic hydrolysis with concentrated sulfuric acid. It is worth noticing that before nanocrystals isolation the materials were submitted to bleaching to remove residual lignin. The solid material obtained after the alkaline treatment is rich in cellulose contents but still contain a minute fraction of lignin. To remove this residual lignin, the cellulose-rich materials were subjected to bleaching process as described in the experimental section. In this work, a TCF (total chlorine free) treatment based on the use of hydrogen peroxide as oxidant was applied [6,22]. Sulfuric
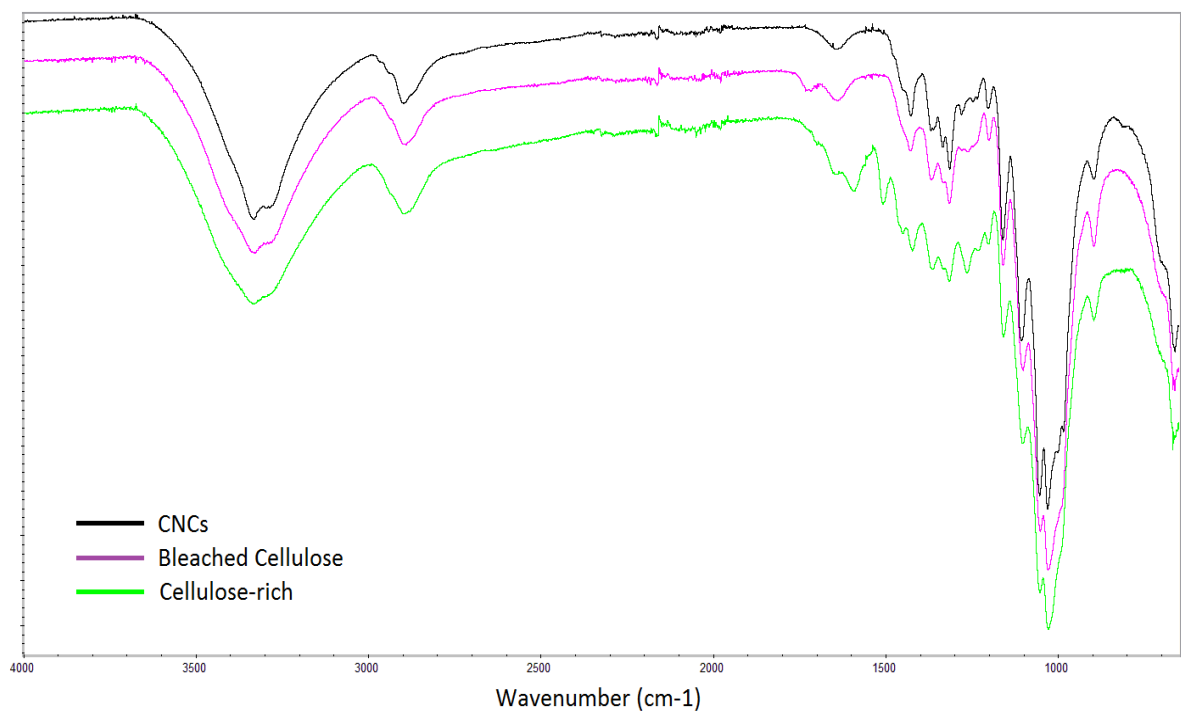
Figure 3.7: FTIR spectra of cellulose-rich material, cellulose after bleaching and CNCs from rice husk

acid used in the bleaching process catalyzed the delignification. Acetic acid was used in the reaction mixture to facilitate the dissolution of the products of lignin oxidative depolymerization [30]. The removal of residual lignin after the bleaching process was confirmed by the FTIR analysis. FTIR spectra of cellulose-rich materials before and after bleaching and CNCs are shown in Fig 3.7. Two peaks observed in the FTIR spectrum of the cellulose-rich material at 1520-1510 cm^{-1} and 1250 cm^{-1} are associated with the aromatic ring and C-O out of plane stretching vibration of aryl group in the lignin, respectively [38]. After the bleaching process, these peaks were disappeared and spectrum of the bleached cellulose material became similar to the spectrum of CNCs. The cellulose-rich materials were bleached with a yield of 62.7 % for RH and 61.0 % for *A. donax* (based on the weight of the starting materials), respectively.

The white cellulose-rich materials, obtained after the bleaching, were treated with concentrated sulfuric acid. Concerning RH, the optimum conditions were 60 % H_2SO_4 for 1 h at 55 ^oC according to an acid/cellulose weight ratio of 9 [5], whereas for the AD these were 60 % H_2SO_4 for 2 h at 55 ^oC at an acid/cellulose weight ratio of 9. After hydrolysis, the turbid supernatant was purified by centrifugation, and the concentration of CNCs was measured by drying the suspension in the oven at 100 ^oC overnight. Starting from 100 g of rice husk, it was attained a 0.8 % suspension containing 12 g of CNCs. From 100 g of *A. donax*, it was obtained a 0.5 % suspension containing 11 g of CNCs. During the optimization of the isolation procedure, the presence of CNCs was at first simply confirmed by observing the distinctive texture of the suspension under polarized light source. The FTIR spectrum of the CNCs shows the characteristic bands for cellulose. A broad peak appeared at 3500-3100 cm-1 corresponds to the stretching vibrations of the hydrogen-bonded O-H groups. Some other peaks appeared at 2980-2850 cm^{-1}, 1640 cm^{-1}, 1430 cm^{-1}, 1370 cm^{-1}, and 1317 cm^{-1} are associated with C-H stretching, O-H bending due to adsorbed water, CH_2 scissoring motion, C-H bending, and CH_2 wagging vibrations, respectively. The sharp characteristic peaks appeared at 1155 cm^{-1}, 1105 cm^{-1}, 1060-990 cm^{-1} and 905-890 cm^{-1} corresponds to the C-C ring stretching band, C-O-C glycosidic ether band, C-O-C pyranose ring stretching vibrations and cellulosic β-glycosidic linkage, respectively [38]. The morphology and dimensions of the prepared CNCs were investigated by TEM. The TEM images at of the CNCs prepared from RH and AD are shown in Fig 3.8. It

is clearly possible to observe the rod-like structure for both samples and a length of the crystal of about 200 nm and 5-15 nm in diameter. It is worth mentioning that this is the first isolation and morphological characterization of cellulose nanocrystals extracted from *A. donax*.
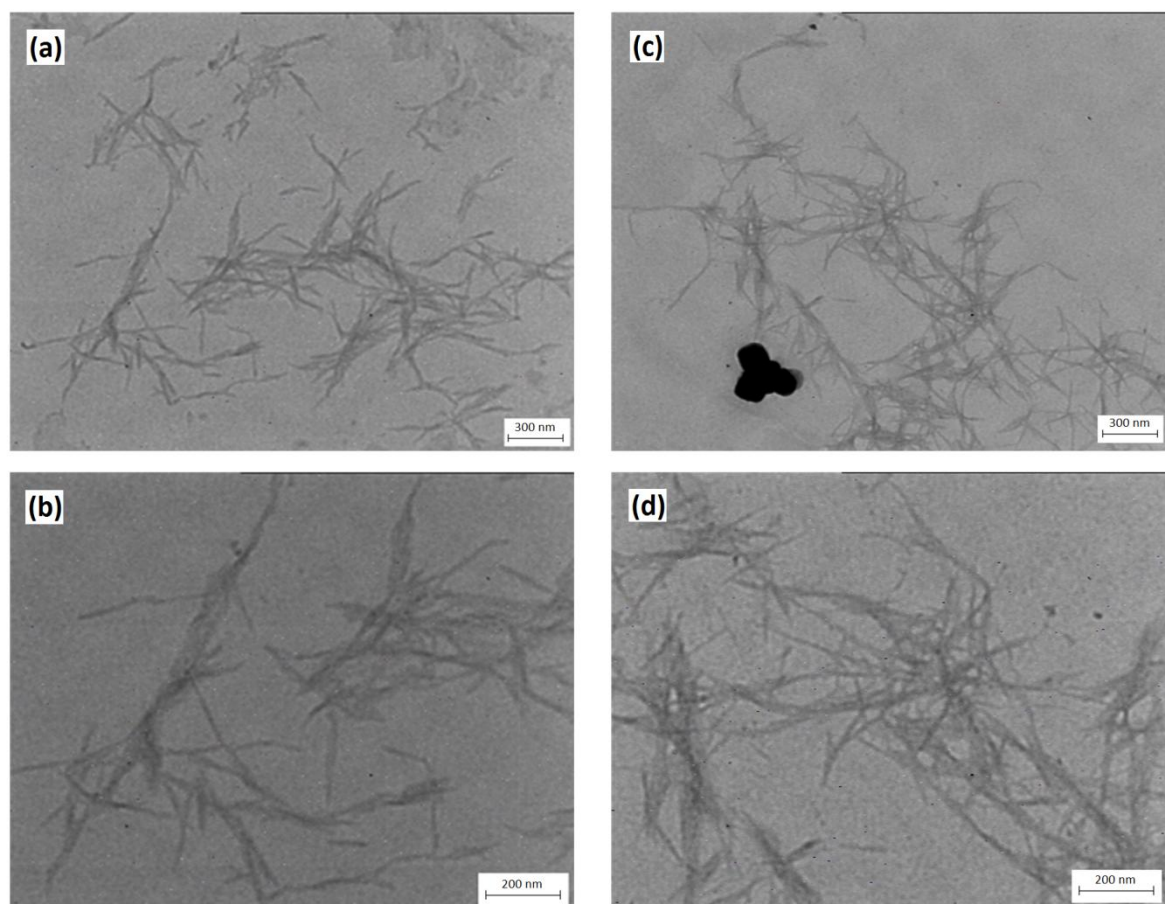
Figure 3.8: TEM images of CNCs isolated from AD (a, b) and RH (c, d)

3.3.5 Overview of Proposed Biorefinery Process

The presented process allows to concurrently recover the main components of the lignocellulosic substrates examined. Table 3.3 summarizes partial and total yield of cellulose (as CNCs), hemicelluloses, lignin and silica after fractionation of RH and AD. The partial yield is calculated on the relative content of each fraction in the starting material

(content in cellulose and hemicellulose reported by Salanti et al. [33] and Lemons e Silva et al. [8] respectively for RH and AD). The overall yield is calculated on the amount of starting

Table 3.3: Overall extraction yield (%) of lignin, hemicellulose, cellulose as CNCs, and silica from RH and AD

(%)	Rice Husk			Arundo donax		
	Starting	Partial yield	Overall yield	Starting	Partial yield	Overall yield
Cellulose	40[a]	30	12	35[a]	31	11
Hemicellulose	21[a]	-	-	28[a]	55	15
Lignin	22	46	10	29	45	13
Silica (Ashes)	16	90	14	4	-	-
			36			**39**

[a] The contents of cellulose and hemicellulose reported are from ref [8,33]

material. In terms of mass balance, it was possible to refine the investigated bio-masses at almost 40 % overall yield. In more detail, about 30 % of the original cellulose was successfully converted into cellulose nanocrystals. Considering that approximately 2/3 of the pristine cellulose is found in the crystalline form [6], it means that almost half the cellulose was recovered in the form of nanocrystals. The missing fraction was hydrolyzed during the refining process, mainly during the acid hydrolysis step or in second place discarded as a solid residue generated during the purification of cellulose nanocrystals by means of centrifugation. For *A. donax*, about 55 % of the starting hemicellulose was recovered. A small fraction may remain soluble after the addition of the anti-solvent but the most abundant part of the missing hemicellulosic fraction could still be bound to cellulose and consequently being depolymerized during bleaching and acid hydrolysis. Similarly, roughly half of the starting lignin content in both biomasses was successfully extracted during the alkaline treatment and recovered. A small amount of lignin could be cleaved and lost in the form of small soluble fragments during different steps of the process. However, the preponderant part of the unrecovered portion remains trapped into the cellulose-rich substrate and subsequently degraded during the bleaching process. The recovery of silicon dioxide is particularly interesting in terms of yield as it exceeds 90 %.

It is important to mention that peculiar characteristics and purity of the isolated fractions acquire an essential role to confer high added value to the recovered products. For this reason, their safeguard along the process can overcome a boost in the yield. According to recent literature reports, the majority of the endeavors are mainly directed toward the valorization of a single biomass component and, in many cases, the described processes are based on procedures that compromise the effective separation of other fractions. The simultaneous recovery of cellulose, hemicellulose, and lignin from *A. donax* by means of a multistage fractionation method is already reported by Shatalov and Pereira [39] with an overall yield that approaches 70 %. The lower over-all yield of the process proposed in this work might be justified by the milder conditions applied. In fact, the main advantage of the reported fractionation system lies in the possibility to simultaneously recover products characterized by a higher added value (in particular CNCs) as harsher treatments can easily compromise the crystalline domains and hinder the production of nanocrystals. Concerning rice husk, at the best of our knowledge, this is the first time that a process able to valorize three major components at the same time is reported. Furthermore, the yields of pure silica and cellulose nanocrystals are appealing while the lower efficiency of the process towards the refinement of lignin is compensated by its purity. In fact, at present times, a refinement of technical lignins similar to that of crude oil is considered unavoidable in order to actualize their full potential [40].

Additionally, it is worth noticing that the leaching treatment introduced as a preliminary step seems to offer numerous advantages: i) removal of water-soluble hemicelluloses and other extractives; ii) partial hydrolysis of lignin-carbohydrate complexes; iii) extraction of metal impurities that could negatively affect the silica fraction purity; iv) extraction of metal impurities that could negatively affect the cellulose nanocrystals isolation. Analogously, the alkaline extraction could be beneficial for other fruitful applications based on the exploitation of the cellulose-rich portion of the material, such as the production of carbon anodes from rice husk via hydrothermal carbonization [41].

3.4   Conclusions

The biorefinery process reported represents a viable method to fractionate lignocellulosic biomasses into lignin, hemicelluloses, silica and CNCs for the preparation of high-value products. The major appeal of the proposed process lies in the relative simplicity of the refining procedures that still enable to recover all the desired products with high purity and valid overall yield. When compared to already reported methods, the presented process emerges for the relatively mild conditions applied and the use of inexpensive, largely available and environmentally secure reactants. In addition, all the steps are carried out using exclusively water as a solvent and operating at atmospheric pressure. In an industrial scale-up perspective this could enable the avoidance of expensive and energy consuming machinery and a simplified safety management. Furthermore, to the best of our knowledge, it is the first time that a process focuses on the simultaneous recovery of three major fractions of rice husk avoiding combustion and embodying the production of cellulose nanocrystals. It is also the first time that extraction of CNCs from *A. donax* is reported.

References

[1]   F. Cherubini, Energy Convers. Manag. 51 (2010) 1412–1421.

[2]   V. Menon, M. Rao, Prog. Energy Combust. Sci. 38 (2012) 522–550.

[3]   A. Salanti, L. Zoia, M. Orlandi, F. Zanini, G. Elegir, J. Agric. Food Chem. 58 (2010)
        10049–10055.

[4]   R. Saikia, R.S. Chutia, R. Kataki, K.K. Pant, Bioresour. Technol. 188 (2015) 265–272.

[5]   N. Johar, I. Ahmad, A. Dufresne, Ind. Crops Prod. 37 (2012) 93–99.

[6]   S.M.L. Rosa, N. Rehman, M.I.G. De Miranda, S.M.B. Nachtigall, C.I.D. Bica,
        Carbohydr. Polym. 87 (2012) 1131–1138.

[7]   T.H. Liou, Mater. Sci. Eng. A 364 (2004) 313–323.

[8]   C.F.L. e Silva, M.A. Schirmer, R.N. Maeda, C.A. Barcelos, N. Pereira, Electron. J.
        Biotechnol. 18 (2015) 10–15.

[9]   P. Kaparaju, M. Serrano, A.B. Thomsen, P. Kongjan, I. Angelidaki, Bioresour. Technol.
        100 (2009) 2562–2568.

[10]   F.-W. Liu, J. Am. Folk. 125 (2012) 204–225.

[11]   S.L. Sun, J.L. Wen, M.G. Ma, R.C. Sun, J. Agric. Food Chem. 62 (2014) 8120–8128.

[12]   H.V. Scheller, P. Ulvskov, Annu. Rev. Plant Biol. 61 (2010) 263–289.

[13]   Y. Habibi, L.A. Lucia, O.J. Rojas, Chem. Rev. 110 (2010) 3479–3500.

[14]   B.D. Park, S. Gon Wi, K. Ho Lee, A.P. Singh, T.H. Yoon, Y. Soo Kim, Biomass and
        Bioenergy 25 (2003) 319–327.

[15]   U. Kalapathy, A. Proctor, J. Shultz, Bioresour. Technol. 85 (2002) 285–289.

[16]   U. Kalapathy, A. Proctor, J. Shultz, Bioresour. Technol. 73 (2000) 257–262.

[17]   D. An, Y. Guo, B. Zou, Y. Zhu, Z. Wang, Biomass and Bioenergy 35 (2011) 1227–1234.

[18]   R. Ghosh, J. Chem. Eng. Process Technol. 4 (2013).

[19]   N. Yalçin, V. Sevinç, Ceram. Int. 27 (2001) 219–224.

[20]   T.H. Liou, C.C. Yang, Mater. Sci. Eng. B Solid-State Mater. Adv. Technol. 176 (2011)
        521–529.

[21]   V.P. Della, I. Kühn, D. Hotza, Mater. Lett. 57 (2002) 818–821.

[22]   Y.C. Park, J.S. Kim, Energy 47 (2012) 31–35.

[23]   R.J. Stoklosa, D.B. Hodge, Bioenergy Res. 8 (2015) 1224–1234.

[24]   D.P. Singh, R.K. Trivedi, Int. J. ChemTech Res. 5 (2013) 727–734.

[25]   S. Kim, J.M. Park, J.W. Seo, C.H. Kim, Bioresour. Technol. 109 (2012) 229–233.

[26]   B. Guo, Y. Zhang, G. Yu, W.H. Lee, Y.S. Jin, E. Morgenroth, Appl. Biochem. Biotechnol. 169 (2013) 1069–1087.

[27]   C. Wan, Y. Zhou, Y. Li, Bioresour. Technol. 102 (2011) 6254–6259.

[28]   A. Salanti, L. Zoia, P. Frigerio, M. Orlandi, Bioresour. Technol. 128 (2013) 330–336.

[29]   A. Chakraverty, P. Mishra, H.D. Banerjee, J. Mater. Sci. 23 (1988) 21–24.

[30]   B.N. Kuznetsov, I.G. Sudakova, N. V. Garyntseva, L. Djakovitch, C. Pinel, React. Kinet. Mech. Catal. 110 (2013) 271–280.

[31]   T.F. Yeh, T. Yamada, E. Capanema, H.M. Chang, V. Chiang, J.F. Kadla, J. Agric. Food Chem. 53 (2005) 3328–3332.

[32]   C. Canevali, M. Orlandi, L. Zoia, R. Scotti, E.L. Tolppa, J. Sipila, F. Agnoli, F. Morazzoni, Biomacromolecules 6 (2005) 1592–1601.

[33]   A. Salanti, L. Zoia, E.L. Tolppa, M. Orlandi, Biomacromolecules 13 (2012) 445–454.

[34]   T. Komolwanich, P. Tatijarern, S. Prasertwasu, D. Khumsupan, T. Chaisuwan, A. Luengnaruemitchai, S. Wongkasemjit, Cellulose 21 (2014) 1327–1340.

[35]   A. Abbas, S. Ansumali, Bioenergy Res. 3 (2010) 328–334.

[36]   L. Zoia, A.W.T. King, D.S. Argyropoulos, J. Agric. Food Chem. 59 (2011) 829–838.

[37]   M. Kacuráková, P. Capek, V. Sasinková, N. Wellner, A. Ebringerová, Carbohydr. Polym. 43 (2000) 195–203.

[38]   A. Kumar, Y.S. Negi, V. Choudhary, N.K. Bhardwaj, J. Mater. Phys. Chem. 2 (2014) 1–8.

[39]   A.A. Shatalov, H. Pereira, Ind. Crops Prod. 43 (2013) 623–630.

[40]   D. S Argyropoulos, J. Biotechnol. Biomater. S6 (2014).

[41]   L. Wang, Z. Schnepp, M.M. Titirici, J. Mater. Chem. A 1 (2013) 5269.

Chapter 4

Partial replacement of silica with cellulose nanocrystals in natural rubber compounds

Syed Danish Ali, Luca Zoia, Luca Castellani, Marco Emilio Orlandi

This chapter describes the use of cellulose nanocrystals (CNCs) as reinforcing filler to partially substitute the silica in natural rubber (NR) compounds. The CNC/Silica/NR compounds were prepared with increasing contents of CNCs (from 0 to 15 phr) and decreasing contents of silica (from 30 to 15 phr), with total filler contents of 30 parts per 100 parts of rubber (phr), by physical mixing in Brabender internal mixer. Bound rubber, vulcanization characteristics, dynamic mechanical properties, and tensile mechanical properties of the prepared compounds were investigated. The partial replacement of silica with CNCs improved the vulcanization characteristics and processability of the prepared compounds. However, dynamic mechanical and tensile mechanical properties, such as tensile strength, elongation at break, and modulus at 300 % elongation were reduced with the increase in CNCs contents.

4.1   Introduction

Reinforcing fillers are the main component of rubber compounds which are added to improve the properties of elastomers. Carbon black and silica are the most commonly used reinforcing fillers in the tire industry due to their outstanding reinforcing effects [1–5]. The introduction of carbon black in tire compounds improves the strength, modulus, tear strength, and abrasion resistance [6,7]. Silica is also used in tire compounds to reduce the rolling resistance and heat build-up in-addition to high strength, modulus, and abrasion resistance [8–11]. Despite the high reinforcing effects of these fillers, there are some limitations of these fillers. Carbon blacks are mainly produced from non-renewable fossil fuels. Due to depletion and negative effects of fossil resources on the environment, there

is a great demand for the development of materials from renewable resources. Moreover, the high densities of both carbon black (1.8 g/cm^3) and silica (2.0 g/cm^3) as compared to polymers (0.92 g/cm^3 for natural rubber) make the density of filled-rubber relatively high. Consequently, these fillers reverse the important property of the polymer materials, which is their low density. Furthermore, high energy and a long time are required for processing of silica. Considering these shortcomings, it is necessary to develop some alternative fillers with low density, eco-friendly, and renewable in nature to replace the traditional fillers used in the tire industry.

Cellulose nanocrystals (CNCs), an emerging class of extremely interesting bio-based nano-materials, have gained tremendous level of attention in both academic and industrial communities due to its fascinating physiochemical properties such as renewability, biodegradability, biocompatibility, environmental friendly, low density, high aspect ratio, high surface area, easy to process, and high mechanical properties [12–16]. Additionally, the axial Young's modulus of CNCs is equal to that of Kevlar but higher than steel. A theoretical study showed that a perfect crystal of cellulose has Young's modulus value of 167.5 GPa [17]. CNCs can be prepared from low-value lignocellulosic feedstocks such as rice husk, Arundo donax, wheat straw, bagasse, etc, as discussed in previous chapters. The idea of reinforcing polymer matrices using CNCs as filler has acquired significant interest and advancement. A lot of studies have been reported on the use of CNCs as reinforcing filler in various polymer matrices [18–24]. This work describes the use of CNCs to partially or fully replace the silica in natural rubber compounds while focusing on the use of these compounds for tire application. The silica used in the tire industry is very high-performance silica and replacement of it with other fillers is really challenging. Therefore, this work was carried out to study the possibility to use CNCs instead of or along with the silica in the tire industry. As the CNCs were required in large quantity to prepare the compounds, the CNCs used in the study were prepared from Whatman No. 1 filter paper as model CNCs to represent the CNCs extracted from biomasses. Whatman No. 1 filter paper has high crystalline-cellulose contents, so a high yield of CNCs was obtained. Different quantities of CNCs were added to equally replace silica in CNC/silica/NR compounds and the effect of incorporating CNCs on vulcanization characteristics, dynamic mechanical, and tensile mechanical properties of the rubber compounds was studied.

4.2   Experimental

4.2.1 Materials

The following chemicals were used in the preparation of CNC/Silica/NR compounds. Natural rubber (SIR-20 grade) was purchased from Astlett, high dispersible silica Ultrasil VN3, which is commonly used in the tire industry, was from Evonik, bis[3-(triethoxysilyl)propyl] Tetrasulfide (TESPT) was obtained from Sigma-Aldrich, soluble sulfur was from Zolfoindustria, zinc oxide was from Zincolossidi, stearic acid was from Sogis, N-cyclohexyl-2-benzothiazylsulfenamide (CBS) was from Zolfoindustria, 2,2,4-trimethyl-1,2-dihydroquinoline (TMQ) was from Sovchem, and N-(1,3-Dimethylbutyl)-N'-phenyl-p-phenylenediamine (6PPD) was obtained from Eastman. Sulfuric acid used in the hydrolysis reaction was obtained from Sigma-Aldrich.

4.2.2 Methods

4.2.2.1   Cellulose Nanocrystals Preparation

Cellulose nanocrystals (CNCs) used in this work were prepared by acid hydrolysis of Whatman No. 1 filter paper using sulfuric acid. First, the filter paper was cut into small pieces of less than 1 cm in size. These small pieces of filter paper were soaked into the ice-cold sulfuric acid solution (64 % w/w). For every gram of filter paper, 8 ml of sulfuric acid solution was used. After homogenizing the filter paper in acid solution, the reaction mixture was transferred to pre-heated oil bath set at 50 $^\circ$C. The reaction mixture was constantly stirred using a glass rod for 60 min. Then, the reaction was stopped by adding a ten-fold volume of ice-cold water. The cellulose sediments were purified by repeated cycles of centrifugation at an acceleration of 3200g for 15 min and re-suspension of the solid in distilled water by ultrasonic mixing for 5 min. The turbid supernatant thus obtained was dialyzed against distilled water for one week until a pH of 5–6 was reached. The CNCs suspension was freeze-dried for further use in rubber compounds. CNCs gravimetric yield was measured after drying the suspension in the oven at 100 $^\circ$C overnight.

4.2.2.2   CNC/Silica/NR Compounds Preparation

The CNC/Silica/NR compounds were prepared by physically mixing the natural rubber with other ingredients (filler system, vulcanization system, and antioxidants) using Brabender internal mixer with a total volume of 50 ml and fill factor of 0.9. The compounds were prepared by increasing the contents of CNCs (0, 5, 10, and 15 phr) and decreasing contents of silica (30, 25, 20, and 15 phr), the total fillers contents were 30 phr. The prepared compounds were labeled as CNC_x-$Silica_y$, where "x" represents the CNCs loading in phr and "y" is the silica loading in phr. The formulation in phr of the prepared compounds is shown in Table 4.1.

Table 4.1: Formulation (phr) of the prepared CNC/Silica/NR compounds

Ingredients	CNC_0-$Silica_{30}$	CNC_5-$Silica_{25}$	CNC_{10}-$Silica_{20}$	CNC_{15}-$Silica_{15}$
Polymer				
NR	100	100	100	100
Filler System				
Silica	30	25	20	15
CNC	0	5	10	15
TESPT	2.4	2.4	2.4	2.4
Vulcanization System				
Soluble Sulfur	2	2	2	2
Zinc Oxide	5	5	5	5
Stearic Acid	2	2	2	2
CBS	2	2	2	2
Antioxidants				
TMQ	1	1	1	1
6PPD	1.5	1.5	1.5	1.5

The CNCs/Silica/NR compounds were prepared in two steps. The first step was performed in 10 min. The internal mixer temperature was set at 60 ^{o}C and rotor speed at 60 rpm. During the first three minutes, the natural rubber was added into the mixer, and then filler

system was added and mixed for next 5 min. The temperature of the mixer was raised to 140 ^{o}C at 7 min. Stearic acid and zinc oxide were added at 8 min, mixed for next two min and at 10 min the mixing was stopped. The second step was performed at 60 ^{o}C for 9 min at a rotor speed of 60 rpm. The masterbatch from the first step was added during the first four minutes. Then, antioxidants, soluble sulfur, and CBS were added at 4 min and mixed for the next 5 min. The mixing was stopped at 9 min. At the end of both steps, the prepared compounds were passed three times through a two-roll mill at 40 ^{o}C for further homogenization.

4.2.3 Characterizations

4.2.3.1   TEM and AFM Analyses of CNCs

Dimensions and morphology of the prepared CNCs were characterized by transmission electron microscope (TEM) and atomic field microscope (AFM) analyses. TEM analysis was carried out using the same procedure as described in section-3.2.3.11. For AFM analysis, the sample was prepared by placing a drop of CNCs suspension on the pre-cleaned silicon substrate. The analysis was performed on a multimodal AFM (DI, Veeco, USA) operating in a tapping mode.

4.2.3.2   Swelling and Extraction Measurements

The bound rubber (the fraction of the polymers chains adsorbed on the filler surface) of the prepared compounds was measured by swelling and extraction experiments. Samples of about 0.20 g with a dimension of around 10 × 10 × 2 mm^3 were immersed in 10 ml of toluene at room temperature for three days in closed vessels. The compounds were swollen and rubber chains which were not bound by the fillers were solubilized by the toluene. The solvent was replaced every day to remove the extractable rubber chains. At the end of the third day, the swollen mass was dried in vacuum at 70 ^{o}C until constant weight. Neat NR without any filler got completely dissolved in toluene under the same conditions. The extractable fraction (*f%*) of the compounds was calculated by using the Equation 4.1 [25].

$$f\% = \frac{m_o\text{-}m_d}{m_o} \times 100 \qquad (4.1)$$

Where, m_o and m_d are the weight of the samples before and after swelling experiments, respectively. The bound rubber ($B_r\%$) was calculated by using the Equation 4.2 [26].

$$B_r\% = \frac{[m_d\text{-}m_o\left(\frac{m_f}{m_f\text{+}m_r}\right)}{m_o\left(\frac{m_f}{m_f\text{+}m_r}\right)} \times 100 \qquad (4.2)$$

Where m_o and m_d are the same as in Equation 4.1, m_r and m_f are the fractions of the rubber and filler in the compounds, respectively.

4.2.3.3   Vulcanization of CNC/Silica/NR Compounds

The vulcanization curves of the prepared CNC/Silica/NR compounds were recorded using a Moving Die Rheometer (RPA 2000, Alpha Technologies). The measurements were performed at a temperature of 150 ^{o}C, 4.3 bar pressure, running time of 30 min, and rotor frequency of 1 Hz. Vulcanization parameters, such as maximum torque (M_H), minimum torque (M_L), scorch time (Ts2), and optimum cure time (T_{90}) were obtained from the vulcanization curves.

4.2.3.4   Dynamic Mechanical Analysis

Dynamic mechanical analysis of both unvulcanized and vulcanized CNC/Silica/NR compounds were performed by using Rubber Process Analyzer (RPA 2000, Alpha Technologies) working in a shear stress mode. The strain sweep measurements were performed from 1 to 100 % strain at 70 ^{o}C and frequency of 1Hz.

4.2.3.5   Tensile Mechanical Analysis

Tensile mechanical properties, such as tensile strength, elongation at break, and stress at 300% elongation were measured by tensile mechanical analyses. Before performing the analysis, the samples were pressed in 2 mm thick sheets by a two-roll mill and vulcanized

in a hydraulic press under the pressure of 4.3 bar at 150 $^{\circ}$C for 30 min. The vulcanized samples were conditioned in the measuring environment for 24 h. Samples for analysis were prepared by die-cutting the vulcanized sheets in five dumbbell-shaped specimens of standard dimensions. Tensile mechanical analyses of the prepared dumbbell-shaped specimens were performed by using a Zwick/Roell tensile testing machine. The measurements were performed according to ISO 37 and UNI 6065 standards. The stress-strain curves were recorded by progressive straining of samples. For each sample, five measurements were performed and the average value was reported.

4.3   Results and Discussion

4.3.1 CNCs Isolation

The CNCs used in this work were isolated from the Whatman No. 1 filter paper by controlled acid hydrolysis using sulfuric acid. During the hydrolysis process, the amorphous or paracrystalline regions in cellulose fibers are more available to acid attack and preferentially hydrolyzed, on the other hand, crystalline regions show high resistance to acid attack and isolated in the form to cellulose nanocrystals. The acid molecules preferentially attack the amorphous regions of the cellulose fibers and get diffused into the cellulose microfibrils, causing the breakage of glycosidic bonds within cellulose chains. This process leads to the destruction of the hierarchical structure of microfibrils into the CNCs. The selective acid cleavage of cellulose chains takes place due to the difference in kinetics of hydrolysis between the crystalline and amorphous regions. The crystallinity and morphology of the isolated CNCs are similar to the original cellulose fibers [19,27,28]. The Whatman filter paper has high contents of crystalline cellulose which resulted in the high yield of the CNCs. Starting from the 10 g of the filter paper, the process resulted in a CNC suspension of 1.2 % (w/v), containing about 7 g of the CNCs. The synthesis of CNCs at first was confirmed by the distinctive texture of the CNCs suspension in polarized light.

The TEM and AFM images of the prepared CNCs are shown in Fig. 4.1. Highly crystalline rod-like morphology of the prepared CNCs is clearly seen in both TEM and AFM images.

The images show the size and size distribution of the prepared CNCs. The length of the crystals ranges from 300 to 400 nm and width between 10 to 20 nm.
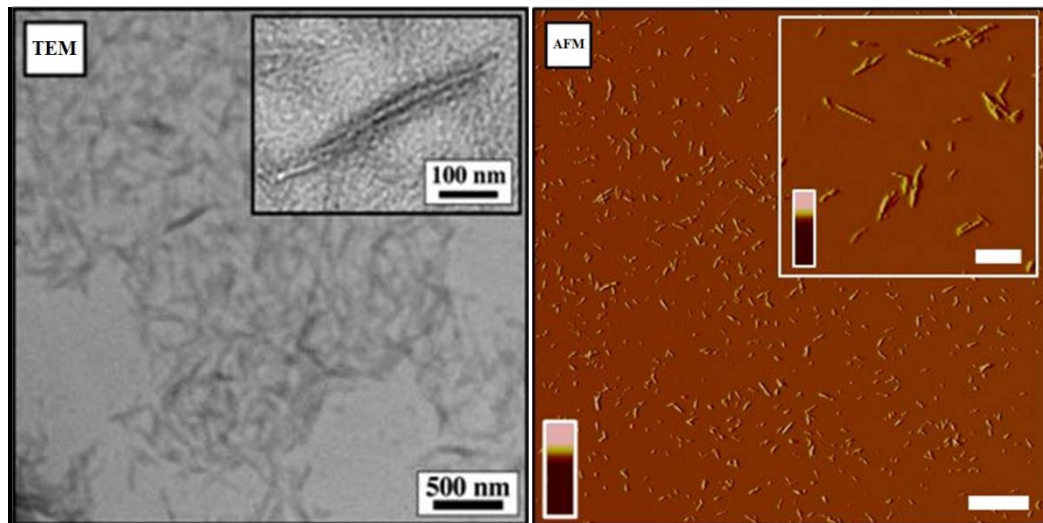
Figure 4.1: TEM and AFM images of the prepared cellulose nanocrystals

4.3.2 Natural Rubber Compounds

The natural rubber compounds were prepared by increasing contents of CNCs, that were 0, 5, 10 and 15 phr, and decreasing contents of silica, that were 30, 25, 20 and 15 phr, while the total contents of both fillers were maintained at constant value (30 phr) in all the prepared compounds. The compounds were prepared in two steps and high shear and long mixing time were applied to evenly disperse all the ingredients in the rubber matrix. The temperature was raised to 140 ^{o}C during the first step to create a chemical bond between the filler and silane coupling agent. The vulcanizing agents were added in the second step which was performed at low temperature to avoid the pre-vulcanization of the rubber compounds as the high temperature was used in the first step.

4.3.2.1   Swelling and Extraction Measurements

Swelling and extraction experiments were performed on unvulcanized rubber compounds to measure the amount of rubber bound on the filler surface and also trapped within the

filler. The values of the extractable fractions ($f\%$) and bound rubber ($B_r\%$), calculated using the equation (4.1) and (4.2), are reported in Table 4.2. The effect of CNC/Silica loading on bound rubber is shown in Fig. 4.2. The percentage of bound rubber represents the extent of interaction between the filler and polymer and is associated with the level of reinforcement [29]. Results show that a high fraction of polymer chains are immobilized around the filler particles and extractable with a solvent and this amount increases with increasing the CNCs contents. This is due to the poor compatibility of CNCs with rubber as compared to silica.
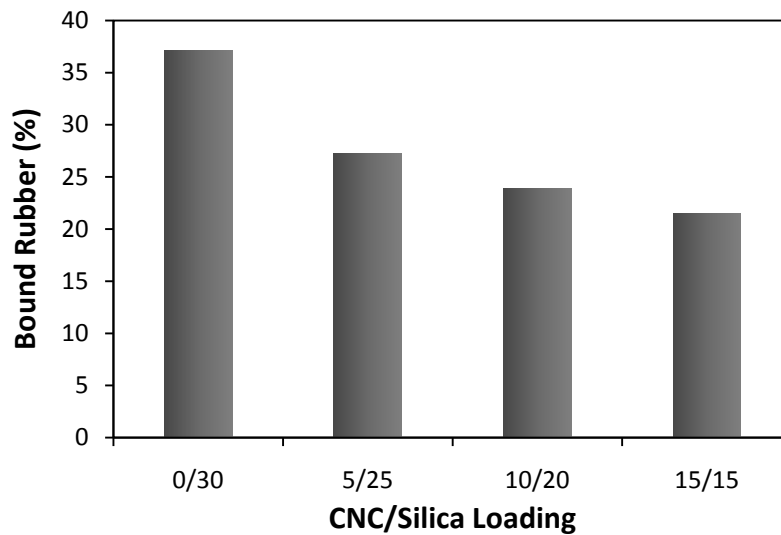
Figure 4.2: Effect of CNC/Silica loading on bound rubber in unvulcanized compounds

Table 4.2: Extractable fraction ($f\%$) and bound rubber ($B_r\%$) of unvulcanized compounds

Property	CNC_0-$Silica_{30}$	CNC_5-$Silica_{25}$	CNC_{10}-$Silica_{20}$	CNC_{15}-$Silica_{15}$
$f\%$	49.14	55.99	58.59	60.39
$B_r\%$	36.11	27.22	23.84	21.50

4.3.2.2   Vulcanization Characteristics

The prepared CNC/Silica/NR compounds were vulcanized for 30 min and change in torque was recorded versus time. The vulcanization curves give a complete picture of the overall

kinetics of vulcanization. The vulcanization curves of the compounds are shown in Fig. 4.3. The vulcanization parameters, such as scorch time (T_S2), optimum curing time (T_{90}), minimum (M_L) and maximum (M_H) value of torques are shown in Table 4.3.
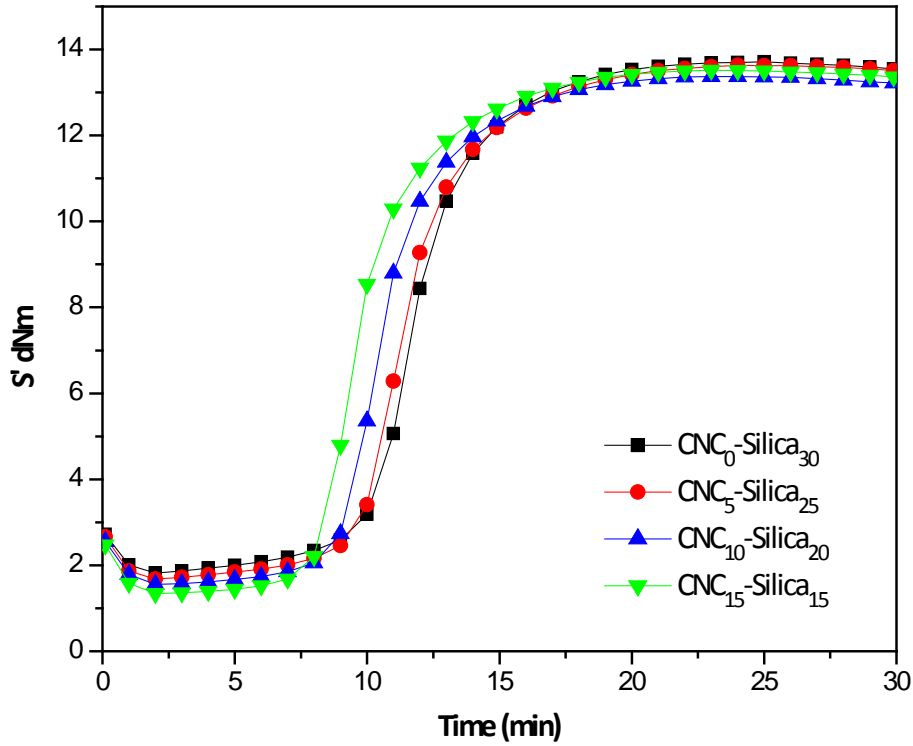
Figure 4.3: Vulcanization curves of the prepared CNC/Silica/NR compounds

Table 4.3: Vulcanization parameters of the prepared CNC/Silica/NR compounds

Parameter	CNC$_0$-Silica$_{30}$	CNC$_5$-Silica$_{25}$	CNC$_{10}$-Silica$_{20}$	CNC$_{15}$-Silica$_{15}$
T_S2 (min)	10.36	10.11	9.28	8.44
T_{90} (min)	15.57	15.48	14.50	13.99
M_L (dNm)	1.82	1.68	1.55	1.34
M_H (dNm)	13.71	13.63	13.38	13.52
ΔM (M_H-M_L)	11.89	11.95	11.83	12.18

The vulcanization curves were obtained by plotting the graph between time and torque. The torque is proportional to the elastic modulus at low strains. As the vulcanization is

carried out at high temperature, so the effect of viscous modulus on torque is negligible. The increase in torques is representative of vulcanization and proportional to the number of crosslinks formed. The time elapsed before vulcanization, the rate of vulcanization once it starts and extent of crosslinking are the important parameters of the vulcanization process. Scorch time represents the start of vulcanization reactions as evident by a sudden increase in torque and must be sufficient to allow the mixing, flowing, and shaping of the rubber products before vulcanization. Once the crosslinking starts, the process must be fast with a controlled crosslinking degree [30]. It can be seen from the results, the scorch time of the prepared compounds shows a decreasing trend with the increase of CNCs contents. Similarly T_{90} i.e., the time required to reach the optimum value of crosslinking, also shows the decreasing trend with the increase of CNCs contents in prepared compounds. Although the differences are small, these results show that the addition of CNCs is somehow affecting the crosslinking; reduce the time for initiation of vulcanization and curing time, however, the rate of vulcanization was almost same for all the compounds. The decrease in scorch time and curing time is due to the fact that the CNCs assist the better dispersion of silica. Some CNCs might get inserted between the silica particles during compounding and prevent them to aggregate. This high dispersion of silica resulted in the higher availability of silane-coated silica surfaces, facilitating the early start of vulcanization process, therefore a reduction in scorch time and optimum curing time was observed [31,32]. Moreover, silica could adsorb curatives which slow down the vulcanization process [33,34]. Results show that the value of both minimum torque (M_L) and maximum torque (M_H) also decrease with the increase of CNCs contents. Before the start of vulcanization reactions, the value of torque drops due to the low viscosity of the un-vulcanized compound at a high temperature and reaches a minimum value (M_L). As the M_L is indicative of the effective viscosity of un-vulcanized compounds, results show that the addition of CNCs increased the processing performance of compounds and acted as plasticizers. The difference between the maximum and minimum torque ($\Delta M = M_H - M_L$) represents the degree of crosslinking. The results show that there is no significant difference between the crosslinking degrees of all prepared compounds. Hence, CNCs do not have a significant effect on the crosslinking degree of the compounds.

4.3.2.3　　　Dynamic Mechanical Analysis

Dynamic mechanical analyses of both unvulcanized and vulcanized compounds were performed in shear stress mode to study the effect of silica replacement with CNCs on dynamic mechanical properties, such as storage modulus and tan delta. The change in storage modulus (G') as a function of strain for both unvulcanized and vulcanized compounds is shown in Fig. 4.4. It can be seen from the results that the storage modulus decreases with the increase of strain in all the compounds either unvulcanized or vulcanized. The modulus at low strains (G'_0) is quite high as compared to modulus at high strain (G'_∞) and shows a typical non-linear dependence of G' on the applied dynamic strain, which is commonly known as the Payne effect ($\Delta G = G'_0 - G'_\infty$). It is well known that in filled rubber compounds the behavior of complex shear modulus ($G^* = G' + iG''$) as a function of shear strain is idealized by four contributions; three strain independent and one strain dependent. Polymer network, hydrodynamic effect, and in-rubber structure contribute as strain independent and filler network as the strain-dependent part of the modulus. The contribution of modulus due to polymer network depends on nature and crosslink density of the polymer. The hydrodynamic effect is the effect of strain amplification due to the undeformable rigid filler phase. The in-rubber structure is the combination of filler structure in the polymer and the degree of filler-polymer interactions. The nature of the interaction between the filler and polymer could be physical or chemical. The filler network represents the extent of filler-filler interactions; the breakdown of these interactions with increasing strain is responsible for stress softening and plays a significant role in understanding the reinforcement mechanism of filled rubber compounds [35,36]. Hence, moduli of rubber compounds at low (G'_0) and high strains (G'_∞) are the representative of filler-filler and filler-polymer interactions, respectively.

It is clearly seen from the results that both low strain and high strain moduli of unvulcanized and vulcanized compounds is decreasing with the increase of CNCs contents with the exception of CNC_{10}-$Silica_{20}$ in vulcanized compounds which showed a higher modulus than CNC_5-$Silica_{25}$ and CNC_{15}-$Silica_{15}$ at high strains. It was also observed that the Payne effect also decreases with the increase of the CNCs contents in both unvulcanized and vulcanized compounds as shown in Table 4.4. This is due to the fact that the silica as a
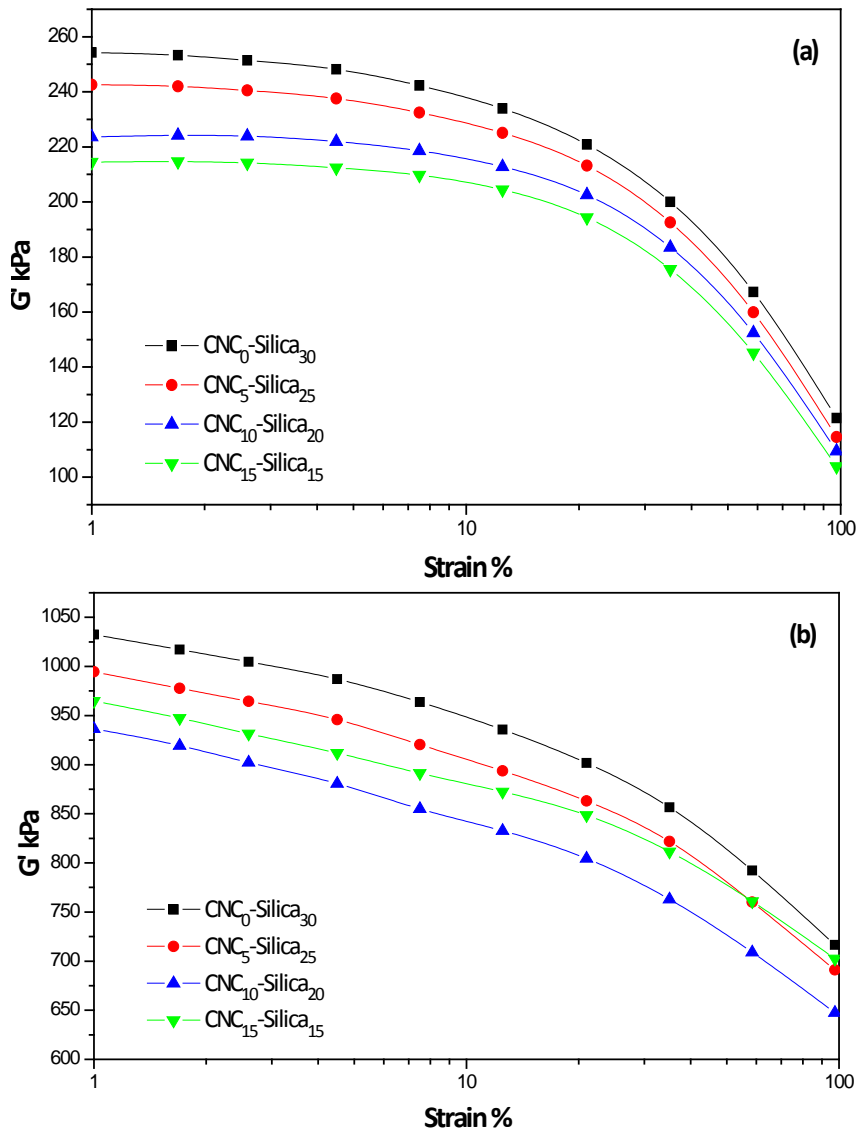
Figure 4.4: Storage modulus (G') as a function of strain for (a) unvulcanized and (b) vulcanized compounds

Table 4.4: Payne effect of unvulcanized and vulcanized compounds

Compounds	CNC_0-$Silica_{30}$	CNC_5-$Silica_{25}$	CNC_{10}-$Silica_{20}$	CNC_{15}-$Silica_{15}$
Unvulcanized	132.81	128.02	114.08	110.58
Vulcanized	316.10	303.34	289.03	262.40

filler forms a very strong filler network and high filler-filler interactions are present between the silica particles which resulted in a high value of modulus at low strains. The rubber trapped between the filler particles also behaves like filler, so, filler networking

increases the effective volume of filler in the rubber compounds. On the other hand, with the addition of CNC, the silica networking is weakened which resulted in lowering the modulus and decrease in Payne effect. Also, due to the well established silica-silane technology, silica showed higher filler-polymer interactions than CNCs and resulted in decreasing modulus at high strains with the increase of CNCs contents. It was also observed that for the same loading of CNCs, the Payne effect increases after vulcanization. It is due to the flocculation of the filler during the vulcanization process, as the viscosity of the polymer matrix is low at high temperature.
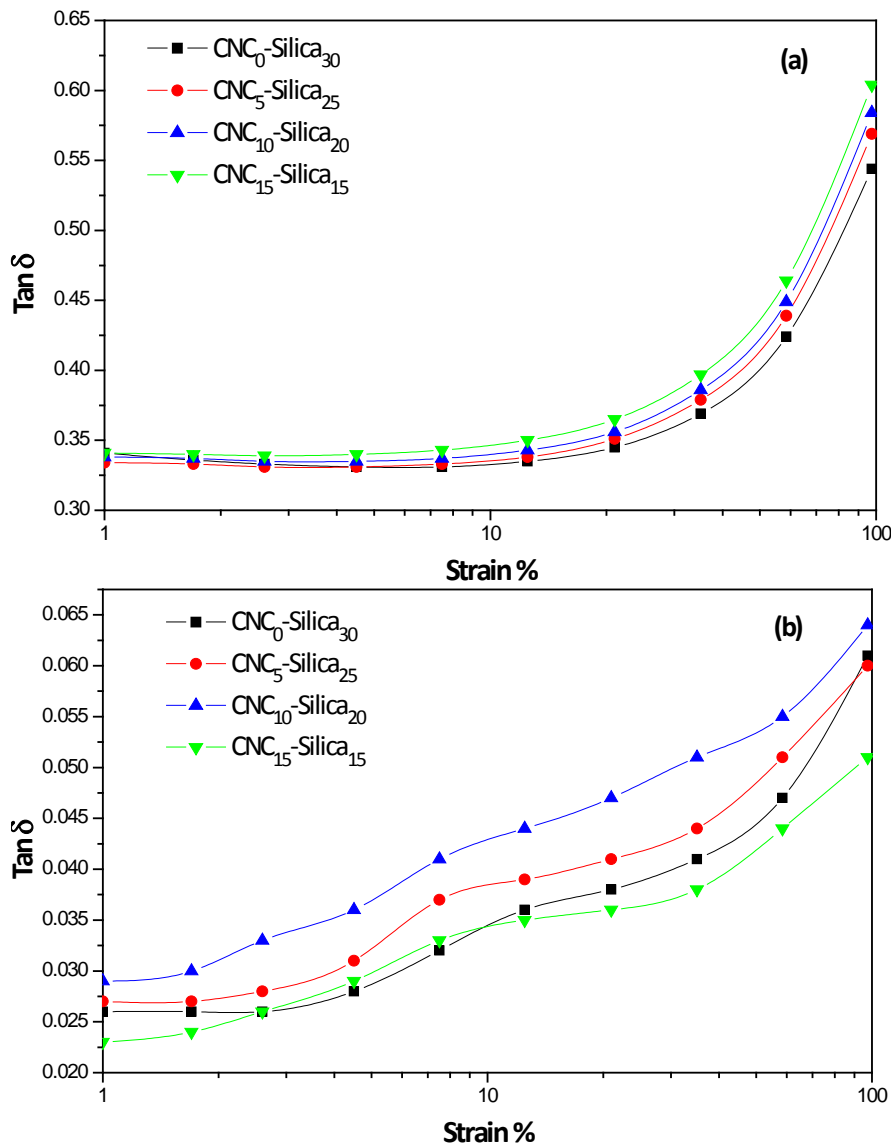
Figure 4.5: Tan δ as a function of strain for (a) unvulcanized and (b) vulcanized compounds

Tan δ–curves of both unvulcanized and vulcanized compounds are shown in Fig. 4.5. It can be clearly seen from the results that hysteresis increases with the increase of strain for both unvulcanized and vulcanized compounds. This is due to the fact that the filler network stabilizes the viscous polymer chains and shows lower hysteresis at low strains but at high strain, the filler network is broken down, polymer chains are no more stabilized by the filler and show more viscous behavior, which resulted in higher hysteresis. It was also observed that the hysteresis shows an increasing trend with the increase of CNCs contents in unvulcanized compounds. This is due to the fact that CNCs act as plasticizers and increase the viscosity of the unvulcanized compounds. For a given loading of filler, the tan δ drastically reduced after the vulcanization which is due to the lower viscous nature of the crosslinked polymer matrix. The vulcanized CNC_{15}-$Silica_{15}$ compounds showed the lowest hysteresis which is due to the higher degree of crosslinking than other compounds.

4.3.2.4   Tensile Mechanical Analysis

Tensile mechanical analyses of the prepared CNC/Silica/NR compounds were performed to study the effect of partial replacement of silica with CNCs on the tensile mechanical properties, such as tensile strength (TS), elongation at break (Eb), and tensile modulus at progressive elongations. Typical stress-strain curves obtained from the tensile test for the prepared CNC/Silica/NR compounds are shown in Fig. 4.6. Tensile mechanical properties derived from these curves, such as tensile strength, elongation at break and modulus at different strains, are shown in Table 4.5. It can be clearly seen from the results that the stress increases with the increase of strains. The value of modulus increases with the increase of CNCs contents at low strains until 100 % elongation as shown in the inset of Fig. 4.6. While at high strains the modulus decreases with the increase of CNCs contents. The improvement in modulus until 100 % can be justified by the high stiffness and rod-like structure of the CNCs. Results show that the tensile strength, elongation at break, and modulus at 300 % elongation decreased when the CNCs contents increased from 0 to 15 phr. The decrease of these properties with increasing the CNCs contents might be due to the poor compatibility of the CNCs with natural rubber and uneven dispersion of the CNCs and formation of CNCs agglomerates in rubber matrix. A high dispersion of the filler enhances the interaction between the filler and rubber matrix, which is an important
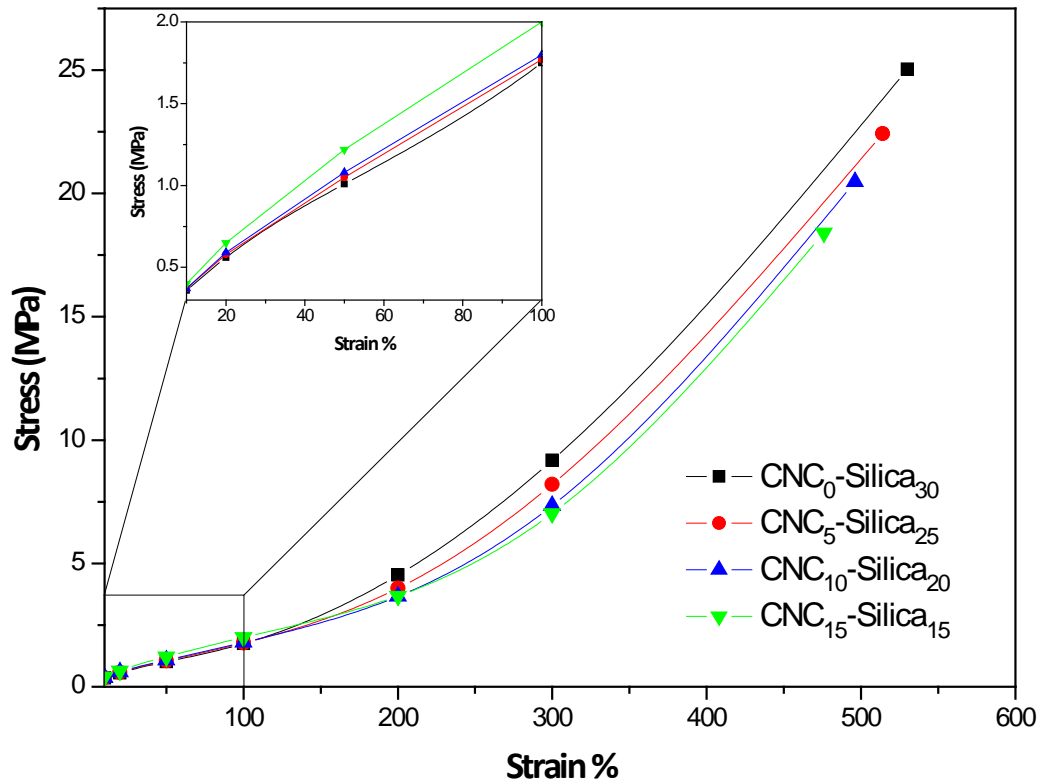
Figure 4.6: Stress-strain curves of prepared compounds obtained from tensile tests

Table 4.5: Tensile mechanical properties of the prepared CNC/Silica/NR compounds

Property	CNC_0-$Silica_{30}$	CNC_5-$Silica_{25}$	CNC_{10}-$Silica_{20}$	CNC_{15}-$Silica_{15}$
Stress 10% (MPa)	0.36	0.37	0.37	0.40
Stress 50% (MPa)	1.01	1.05	1.08	1.22
Stress 100% (MPa)	1.75	1.77	1.8	2.0
Stress 200% (MPa)	4.53	3.99	3.66	3.68
Stress 300% (MPa)	9.18	8.21	7.34	7.03
Elongation at break (%)	530.1	514.1	496.2	475.9
Tensile Strength (MPa)	25.04	22.42	20.47	18.4

parameter to obtain better tensile properties [37,38]. Due to poor compatibility of the CNCs with rubber, higher contents of CNCs increase the tendency of CNCs to form the agglomerates which resulted in reduced tensile mechanical properties. On the other hand, silica has very high interfacial interactions with rubber matrix, which allowed it to evenly

disperse in the rubber matrix, thus compounds with higher contents of silica have better tensile mechanical properties.

4.4 Conclusions

Natural rubber compounds were prepared by partially replacing the silica with CNCs. The CNCs contents were increased from 0 to 15 phr and silica contents were reduced from 30 to 15 phr, while the total amount of filler was 30 phr. The effect of incorporation of CNCs on bound rubber, vulcanization characteristics, dynamic mechanical properties and tensile mechanical properties was investigated. Vulcanization curves of the compounds showed that the partial replacement of silica with CNCs does not show a significant change in the degree of crosslinking, however, scorch time and curing time was improved. Moreover, the addition of CNC improved the processability of the compounds. The storage modulus of the compounds decreased when CNCs contents were increased, due to lower CNCs-polymer interactions than silica. Partially replacing the silica with CNCs enhanced the tensile modulus at low strain up to 100 % elongation due to high stiffness and rod-like structure of the CNCs. On the other hand, tensile strength, elongation at break and modulus at 300 % elongation was reduced with the increase of CNCs contents which is due to the poor compatibility of the CNCs with rubber matrix. The use of CNCs to partially replace the silica in natural rubber compounds improves some properties while reducing the others. Hence, silica cannot be completely replaced by the CNCs, however, improved tensile mechanical properties can be obtained by modifying the CNCs surface with some functional groups to enhance the interactions with the polymer.

References

[1]   H. Angellier, S. Molina-Boisseau, A. Dufresne, Macromolecules 38 (2005) 9161–9170.

[2]   M. Arroyo, M.A. López-Manchado, B. Herrero, Polymer 44 (2003) 2447–2453.

[3]   M. Castellano, L. Conzatti, G. Costa, L. Falqui, A. Turturro, B. Valenti, F. Negroni, Polymer 46 (2005) 695–703.

[4]   L. Bokobza, J.P. Chauvin, Polymer 46 (2005) 4144–4151.

[5]   A. Ansarifar, L. Wang, R.J. Ellis, Y. Haile-Meskel, J. Appl. Polym. Sci. 119 (2011) 922–928.

[6]   T.A. Vilgis, G. Heinrich, Macromolecules 27 (1994) 7846–7854.

[7]   W.M. Hess, W.K. Klamp, Rubber Chem. Technol. 56 (1983) 390–417.

[8]   R.R. Heinz Esch, Udo Görl, Robert Kuhlmann, Precipitated Silicas, European Patent 0647591, 1995.

[9]   N. Rattanasom, S. Prasertsri, T. Ruangritnumchai, Polym. Test. 28 (2009) 8–12.

[10]   H. Peng, L. Liu, Y. Luo, X. Wang, D. Jia, Polym. Compos. 30 (2009) 955–961.

[11]   K.W. Stöckelhuber, A. Das, R. Jurk, G. Heinrich, Polymer 51 (2010) 1954–1963.

[12]   J.P.F. Lagerwall, C. Schütz, M. Salajkova, J. Noh, J. Hyun Park, G. Scalia, L. Bergström, NPG Asia Mater. 6 (2014) e80.

[13]   N. Lin, J. Huang, A. Dufresne, Nanoscale 4 (2012) 3274.

[14]   V. Favier, H. Chanzy, J.Y. Cavaille, Macromolecules 28 (1995) 6365–6367.

[15]   K. Gopalan Nair, A. Dufresne, N.M. Behavior, Biomacromolecules 4 (2003) 666–674.

[16]   A. Bendahou, H. Kaddami, A. Dufresne, Eur. Polym. J. 46 (2010) 609–620.

[17]   K. Tashiro, M. Kobayashi, Polymer 32 (1991) 1516–1526.

[18]   A. Junior de Menezes, G. Siqueira, A.A.S. Curvelo, A. Dufresne, Polymer 50 (2009) 4552–4563.

[19]   M.M. Ruiz, J.Y. Cavaillé, A. Dufresne, J.F. Gérard, C. Graillat, Compos. Interfaces 7 (2000) 117–131.

[20]   L. Chazeau, J.Y. Cavaill??, J. Perez, J. Polym. Sci. Part B Polym. Phys. 38 (2000) 383–392.

[21]   M. Paillet, A. Dufresne, Macromolecules 34 (2001) 6527–6530.

[22]   M.A.S. Azizi Samir, F. Alloin, J.Y. Sanchez, A. Dufresne, Polymer 45 (2004) 4149–

4157.

[23]   S. Noorani, J. Simonsen, S. Atre, in:, ACS Symposium Series 938, 2006, pp. 209–220.

[24]   M. Grunert, W.T. Winter, Polym. Mater. Sci. Eng. 82 (2000) 232. Spring.

[25]   N. Suzuki, F. Yatsuyanagi, M. Ito, H. Kaidou, J. Appl. Polym. Sci. 86 (2002) 1622–1629.

[26]   L. Conzatti, G. Costa, L. Falqui, A. Turturro, in:, Rubber Technol. Handb., Smithers Rapra Publishing, 2001, pp. 1–27.

[27]   M. Mariano, N. El Kissi, A. Dufresne, J. Polym. Sci. Part B Polym. Phys. 52 (2014) 791–806.

[28]   A. Dufresne, Nanocellulose: From Nature to High Performance Tailored Materials, 2012.

[29]   B.B. Boonstra, Polymer . 20 (1979) 691–704.

[30]   D.R. Tobergte, S. Curtis, in:, Elsevier Academic Press, 2013, pp. 1689–1699.

[31]   S.H. Xu, J. Gu, Y.F. Luo, D.M. Jia, Express Polym. Lett. 6 (2012) 14–25.

[32]   W. Bai, K. Li, Compos. Part A Appl. Sci. Manuf. 40 (2009) 1597–1605.

[33]   S.-S. Choi, Elastomers Compos. 36 (2001) 37–43.

[34]   A.S. Hashim, B. Azahari, Y. Ikeda, S. Kohjiya, Rubber Chem. Technol. 71 (1998) 289–299.

[35]   A.R. Payne, J. Appl. Polym. Sci. 6 (1962) 57–63.

[36]   A.I. Medalia, Rubber Chem. Technol. 51 (1978) 437–523.

[37]   M. Haghighat, A. Zadhoush, S. Nouri Khorasani, J. Appl. Polym. Sci. 96 (2005) 2203–2211.

[38]   U.S. Ishiaku, C.S. Chong, H. Ismail, Polym. Test. 19 (2000) 507–521.

Chapter 5

Surface functionalization of cellulose nanocrystals with silanes and their compounds with natural rubber

Syed Danish Ali, Luca Zoia, Luca Castellani, Marco Emilio Orlandi

To enhance the dispersion and compatibility of CNCs in polymer matrix, the surface of cellulose nanocrystals (CNCs) was functionalization with organofunctional silane coupling agents by; pre-functionalization and post-functionalization methods, using six different silanes: bis[3-(triethoxysilyl)propyl]tetrasulfide (TESPT), bis[3-(triethoxysilyl)propyl]-disulfide (TESPD), 3-methacryloxypropyltriethoxysilane (MPS), 3-mercaptopropyl-trimethoxysilane (MRPS), 3-aminopropyltriethoxysilane (APS), and vinyltriethoxysilane (VTES). The pre-functionalization was carried out in ethanol/water mixture. The silanes were adsorbed on the surface of CNCs through hydrogen bonding and a heat treatment at 115-120 ^{o}C after adsorption experiments created a covalent bond between the CNCs surface and the silane. The surface functionalization was confirmed by Fourier-transform infrared (FTIR) spectroscopy and silicon content measurements by Inductively coupled plasma-optical emission spectroscopy (ICP-OES). The change in the crystallinity of the CNCs after the surface functionalization was studied by powder X-ray diffraction (XRD). The contact angle measurements showed the change in the surface character of the pre-functionalized CNCs from hydrophilic to hydrophobic. The pre-functionalized CNCs were then successfully incorporated in natural rubber. The post-functionalization was carried out by incorporating the unfunctionalized CNCs in natural rubber then silane coupling agents were added during the compounding in the internal mixer. The effect of these two functionalization methods of CNCs on the vulcanization characteristics, dynamic mechanical properties and tensile mechanical properties of the filled rubber compounds were investigated and these properties were compared with the compounds filled with untreated CNCs and silica.

5.1 Introduction

As demonstrated in the previous chapter, the silica was partially replaced with CNCs in natural rubber compounds and the effect of CNCs incorporation on vulcanization characteristics, dynamic and tensile mechanical properties of final compounds was discussed. The highly hydrophilic character of the CNCs lowers the compatibility with the hydrophobic polymer matrix. From results, it was concluded that the silica cannot be replaced with CNCs due to poor compatibility of CNCs with natural rubber. In order to obtain better dispersion and enhanced compatibility of CNCs with natural rubber, it is necessary to modify the surface of CNCs.

The presence of numerous hydroxyl groups on the surface of CNCs provides active sites for chemical modification. The surface modification of CNCs has been widely studied using different chemical modification methods, such as etherification, esterification, silylation, oxidation, cationization, polymer grafting, etc [1–7]. This research work involves the chemical modification of CNCs using organofunctional silane coupling agents. Functional triethoxysilane are commonly used as coupling agents in many industrial applications, especially in the tire industry to compatibilize silica with polymer matrices to improve the mechanical properties of the rubber compounds [8–17]. Two types of reactive moieties are present in the structure of silanes which facilitate the interaction between the hydrophilic filler and hydrophobic polymer. The alkoxy groups of silane react with the hydroxyl group of the CNCs while on the other hand, the organic functionalities, such as vinyl, sulfide, mercapto, methacryl, amine, etc, interact with polymer matrices [18–20].

In this work, six silane coupling agents with different organic functionality (polysulfide, methacryl, mercapto, amine, and vinyl) were used to modify the surface of the CNCs. The purpose of this surface functionalization was to increase the hydrophobic character of the CNCs, to improve the interfacial adhesion between the CNCs and hydrophobic polymer and get better dispersion of CNCs in the polymer matrix. The pre-functionalized CNCs were incorporated as a filler in natural rubber compounds through the co-precipitation method. Co-precipitation method further helps in better dispersion of the CNCs in the polymer matrix. The CNCs were also post-functionalized by incorporating the pristine CNCs in natural rubber and the silane coupling agents were added during the compounding in an

internal mixer. The effect of these two functionalization methods on the final properties of the CNCs-filled rubber compounds was investigated.

5.2 Experimental

5.2.1 Materials

CNCs used in this work were obtained in the form of aqueous suspension (11.5-12.5 wt%) from Cellulose Lab, Canada. The length of the CNCs ranges between 150 to 200 nm, width from 5 to 20 nm and the density of dried CNCs powder was 1.5 g/cm^3. Six silane coupling agents bis[3-(triethoxysilyl)propyl]tetrasulfide (TESPT), bis[3-(triethoxysilyl)propyl]disulfide (TESPD), 3-methacryloxypropyltriethoxysilane (MPS), 3-mercaptopropyltrimethoxysilane (MRPS), 3-aminopropyltriethoxysilane (APS), and vinyltriethoxysilane (VTES), were obtained from Sigma-Aldrich. Analytical grade ethanol and acetic acid were also obtained from Sigma-Aldrich. Natural rubber latex was supplied by Von Bundit, Thailand with solid contents of 60 % (w/w). The chemical used during the preparation of rubber compounds, such as silica, vulcanizers, and antioxidants were the same as mentioned in section 4.2.1.

5.2.2 Methods

5.2.2.1 Surface Functionalization of CNCs

The surface functionalization of CNCs was performed in ethanol-water solution at room temperature. The procedure applied is the modification of the method used for the surface modification of cellulose fibers with silane coupling agents [21,22]. Initially, the silanes were pre-hydrolyzed by adding 25 mmol/g of CNCs of bifunctional silanes (TESPT and TESPD), and 50 mmol/g of CNCs of monofunctional silanes (MPS, MRPS, APS, and VTES) in ethanol/water mixture 80/20 (w/w). This reaction mixture was stirred for 2 h at room temperature. In another round bottom flask, 2 % (w/w) CNCs suspension was prepared by adding dried CNCs in a mixture of ethanol and water 80/20 (w/w), sonicated for 15 minutes and stirred for 1 h at room temperature. Then, initially prepared pre-

hydrolyzed silane solution was added to CNCs suspension and stirred for 2 h at room temperature. At the end of the reaction, the CNCs were isolated by centrifugation at 10,000 rpm for 15 min, re-dispersed in water and freeze-dried. The dried CNCs were heat treated at 120 °C for 2h. All the heat treated functionalized CNCs were subjected to Soxhlet extraction for 12 h using ethanol to remove the unreacted silane. The CNCs functionalized with this method were termed as pre-functionalized CNCs (F-CNCs). Schematic representation of CNCs functionalization and the chemical structure of the silanes are shown in Fig. 5.1.
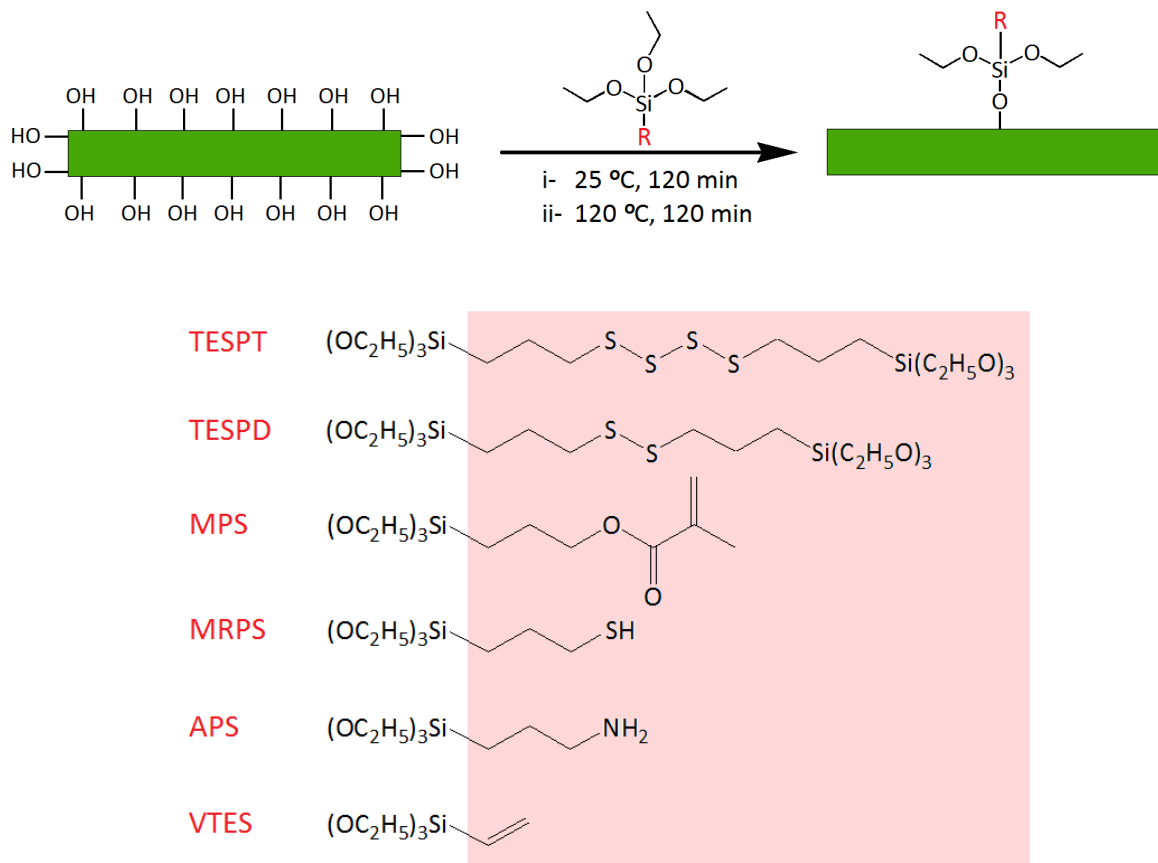
Figure 5.1: Schematic representation of CNCs functionalization with different silane coupling agents

5.2.2.2 Rubber Compounding

Natural rubber compounds were prepared by co-precipitation method. Two reference compounds of silica and untreated CNCs were prepared. Initially, masterbatches of pre-

functionalized CNCs (F-CNCs) with natural rubber were prepared. To prepare the masterbatch, desired quantity of the F-CNCs (3.64 g of F-CNC for 10 phr of filler contents) were dispersed in 100 ml of a mixture of ethanol and water 70/30 (v/v). This suspension of the F-CNCs was added to 60.77g of natural rubber latex and stirred for 1 h. Then, the emulsion was coagulated by progressive addition of the acetic acid. The coagulated rubber was reduced to a thin sheet using a two-roll mill and washed with distilled water until neutral pH was reached. The thin sheets of masterbatches were dried under vacuum at 40 ^{o}C until constant weight. The obtained masterbatches were mixed with other ingredients (vulcanizers, and antioxidants) using Brabender internal mixer using the procedure as given in Table 5.1. These compounds, prepared with pre-functionalized CNCs, were labeled as "Pre-Silane", where Silane represents the silane coupling agent used for functionalization. Six other compounds were also prepared by preparing the masterbatches of pristine CNCs with natural rubber using the same procedure as for F-CNCs. These masterbatches were mixed with silane coupling agents, vulcanizers, and antioxidants using Brabender internal mixer using the procedure as described in Table 5.1. These compounds were labeled as "Post-Silane", where Silane represents the silane coupling agent used. The formulation of all the prepared compounds is summarized in Table 5.2.

Table 5.1: Mixing procedure of rubber compounds

Time (min)	RPM	Temp (^{o}C)	Operation
		Step-1	
0	60	60	Loaded the masterbatch or NR
3	60	60	Added silane and filler
7	60	60 -> 140	Raised the temperature
8	60	140	Added stearic acid and zinc oxide
10	60	140	Unloading
		Step-2	
0	60	60	Loaded compound from step-1
4	60	60	Added vulcanizers and antioxidants
9	60	60	Unloading the compound

Table 5.2: Formulation of the prepared rubber compounds in phr

Ingredients	Silica	CNC	Pre-TESTP	Pre-TESPD	Pre-MPS	Pre-MRPS	Pre-APS	Pre-VTES	Post-TESTP	Post-TESPD	Post-MPS	Post-MRPS	Post-APS	Post-VTES
NR	100	-	-	-	-	-	-	-	-	-	-	-	-	-
Silica	10	-	-	-	-	-	-	-	-	-	-	-	-	-
CNCs	-	-	-	-	-	-	-	-	-	-	-	-	-	-
Masterbatch NR (100 phr) + F-CNCs (10phr)	-	-	110	110	110	110	110	110	-	-	-	-	-	-
Masterbatch NR (100 phr) + CNCs (10phr)	-	110	-	-	-	-	-	-	110	110	110	110	110	110
TESPT	0.8	-	-	-	-	-	-	-	0.8	-	-	-	-	-
TESPD	-	-	-	-	-	-	-	-	-	0.8	-	-	-	-
MPS	-	-	-	-	-	-	-	-	-	-	0.8	-	-	-
MRPS	-	-	-	-	-	-	-	-	-	-	-	0.8	-	-
APS	-	-	-	-	-	-	-	-	-	-	-	-	0.8	-
VTES	-	-	-	-	-	-	-	-	-	-	-	-	-	0.8

Other ingredients were same for all compounds; sulfur 2 phr, zinc oxide 5 phr, stearic acid 2, CBS 2 phr, TMQ 1phr and 6PPD 1.5 phr.

5.2.3 Characterization of Functionalized CNCs

5.2.3.1   FTIR Analysis

The FTIR spectra of pristine and functionalized CNCs were recorded to confirm the functionalization of CNCs. The analysis was performed using the same procedure and instruments as mentioned in Chapter-3, section 3.2.3.8.

5.2.3.2   Contact Angle Measurement

Contact angle measurements were performed to evaluate the surface character of the F-CNCs. The measurements were carried out on films of F-CNCs prepared by film casting method. A calibrated drop of water (3 μL) was placed onto the film. The contact angle was measured at room temperature using the OCA20 contact angle system (Data Physics Instruments) equipped with a CDD camera working at up to 200 images per second. The contact angle was determined by measuring the angle between the film surface and the tangent at the drop of the solid-liquid air point.

5.2.3.3   Silicon Contents Measurements

Silicon contents of the F-CNCs were measured to determine the amount of silane coupling agents grafted on the surface of CNCs. The silicon contents were measured by Inductively coupled plasma-optical emission spectroscopy (ICP-OES) using ICP-OES Optima 7000 DV PerkinElmer. The samples were prepared by digesting few milligrams of the F-CNCs in a mixture of 4ml HNO_3, 3 ml HCl and 1 ml HF. After digestion, the samples were diluted four times with *Milli-Q* water and analyzed.

5.2.3.4   X-Ray Diffraction Analysis

Powder X-ray diffraction (XRD) analysis of CNCs and F-CNCs was performed at ambient temperature using the X'Pert PRO diffractometer from PANalytical Company, using Cu Kα

(1.54 Å) as an X-ray source. The operating voltage and current were kept at 45 kV and 40 mA respectively. The data were collected in the range $2\theta = 5$ to 60°.

5.2.4 Characterization of Rubber Compounds

Vulcanization, dynamic mechanical analysis and tensile mechanical analysis of the prepared rubber compounds were performed using the same procedure as described in section 4.2.3.

5.3 Results and Discussion

5.3.1 Surface Functionalization of CNCs

The CNCs were functionalized with six different silane coupling agents. These silanes have two types of reactive functionalities in their structure; the alkoxy groups were same for all the silanes used in this work that react with the hydroxyl group of the CNCs, while the organofunctional groups that react with the polymer matrix were different for all the silanes. The functionalization reactions were carried out in a mixture of ethanol and water. This reaction medium readily solubilized the silanes and the presence of water facilitates the hydrolysis of the silanes to corresponding silanol derivatives R-Si(OH)$_3$ [10,23]. The reaction mechanism of the silanization of the CNCs is shown in Fig. 5.2. The ethoxy groups of the silane undergo hydrolysis in the presence of water and form the silanol-containing species. The hydrolyzed silane in the aqueous medium is highly reactive and may undergo condensation of silanol with each other and also with alkoxy groups to form the dimeric and oligomeric structures. The structure of the organic moiety of the silanes influences both hydrolysis and condensation reactions of the silanol groups [24–26]. The oligomers form the hydrogen bonding with the hydroxyl group of the CNCs and get adsorbed on the surface of CNCs. Finally, during the heat treatment, the hydrogen-bonded hydroxyl groups undergo further condensation reaction and a covalent bond is formed between the CNCs and the silanes. At the interface, there is only one bond from each silicon of organosilane to the CNCs surface. At the CNCs surface, each silicon of the silane forms only
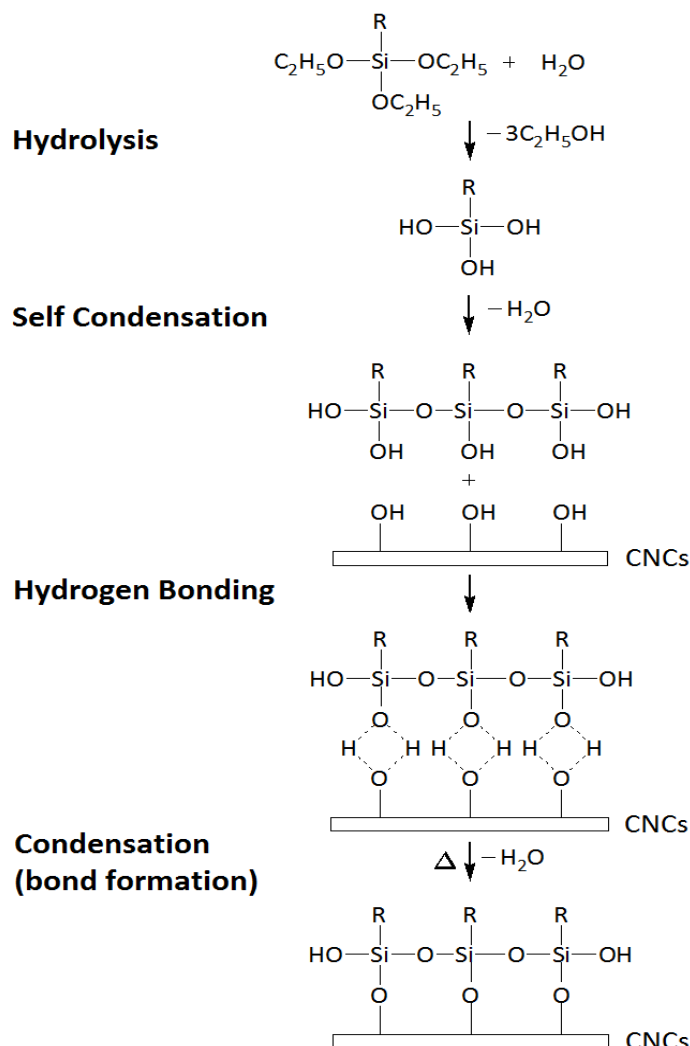
Figure 5.2: Reaction mechanism of CNCs functionalization with silane

one bond with CNCs through one silanol group. The two remaining silanol groups are present either in free or condensed form. The organic functionality of the silane remains available for the chemical or physical interaction with the polymer matrix.

To investigate the nature of the interaction between the CNCs and silanes, the surface functionalized CNCs were subjected to Soxhlet extraction for 12 h with ethanol before and after thermal treatment at 120 ^{o}C. Soxhlet extraction before thermal treatment showed a complete desorption of the silanes, which illustrated that the silane was only physically adsorbed on the surface of CNCs. This adsorption was due to the hydrogen bonding between the CNCs and silanol groups of silane. After thermal treatment at 120 ^{o}C, a chemical bond was formed between the CNCs and silane through the condensation of

hydrogen-bonded hydroxyl groups of the CNCs and silanes. Soxhlet extraction after thermal treatment showed that the silane remained attached on the CNCs surface and silanes were chemically grafted on the CNCs surface.

5.3.1.1   FTIR Analysis

FTIR analysis was used as a fast and efficient method to confirm the functionalization of the CNCs. FTIR spectra of the pristine CNCs and CNCs functionalized with different silane coupling agents after heat treatment and soxhlet extraction are shown in Fig. 5.3. The
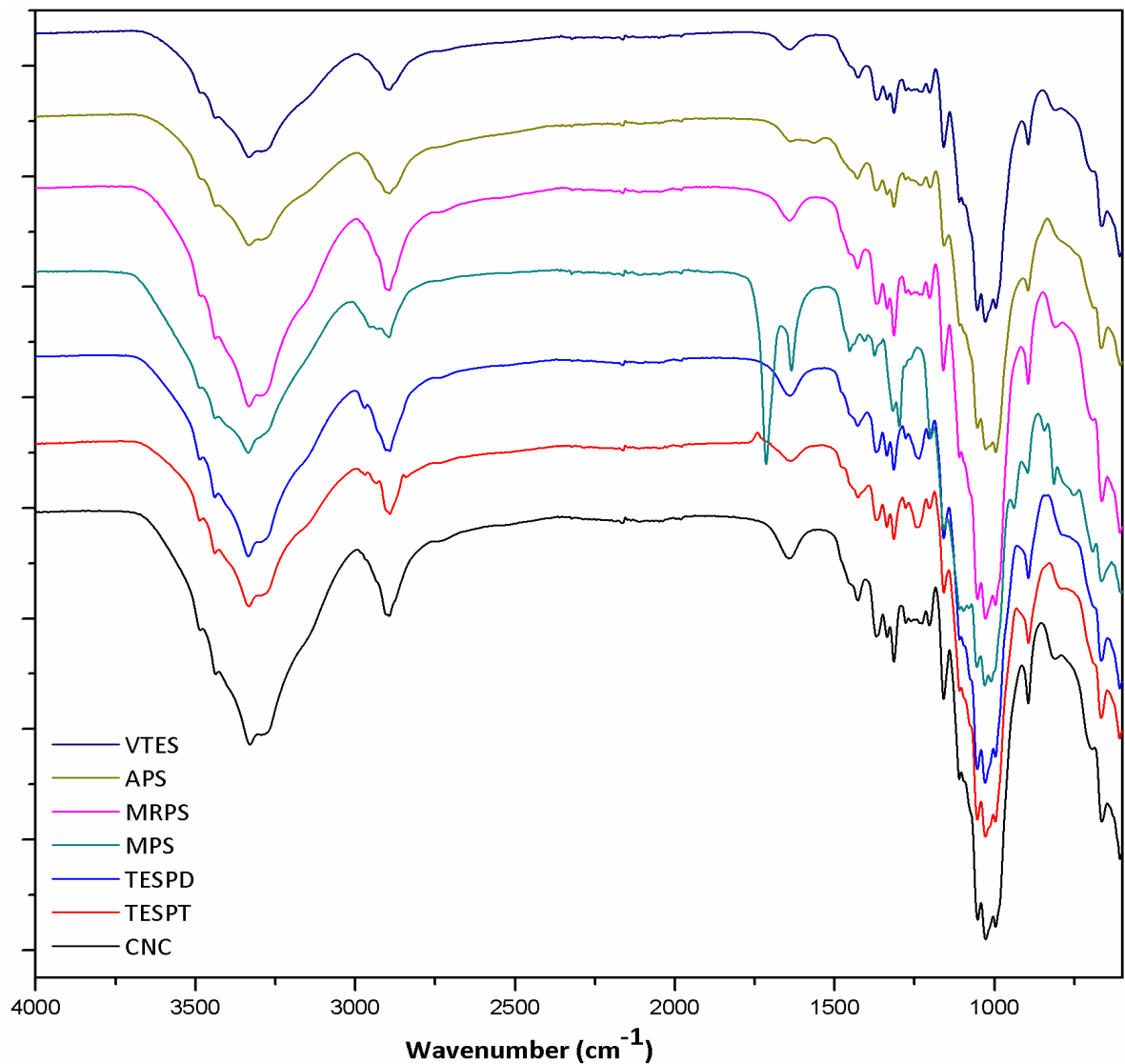
Figure 5.3: FTIR spectra of the pristine CNCs and surface functionalized CNCs

grafting of silane on the CNCs surface took place through the formation of -Si-O-C$_{cellulose}$ bond between the silane and the CNCs. The intense bands observed in all the spectra at 1000-1200 cm^{-1} correspond to stretching vibrations of the C-O-C, Si-O-C$_{cellulose}$ and Si-O-Si bonds [27–29]. Due to overlapping of these bands, it is difficult to completely assign these bands to Si-O-C$_{cellulose}$ or Si-O-Si, however, an increase in the intensity of the peaks after the functionalization provided the evidence that the silanes have been grafted on the CNCs surface. The FTIR spectrum of the CNCs functionalized with MPS showed two intense peaks at 1715 cm^{-1} and 1636 cm^{-1} corresponding respectively to the stretching vibrations of the C=O and C=C groups of the acrylic moiety. The presence of a peak at 1563 cm^{-1} in the spectrum of APS functionalized CNCs is associated to the bending vibration of N-H bond of the primary amine groups.

5.3.1.2   Silicon Contents Measurement

The amount of silane coupling agents grafted on the CNCs surface was quantified by measuring the silicon contents of functionalized CNCs. Since all the silane coupling agents have one of two atoms of silicon so the quantification of the silicon contents is proportional to the amount of silane. The moles of the silane coupling agents grafted on the CNCs calculated from the silicon contents are summarized in Table 5.3. Results showed that high contents of the silanes coupling agents were grafted on the CNCs surface. Different silanes showed different affinity toward the CNCs surface. As the silanes grafting on CNCs surface takes place through the hydrolysis and condensation reactions, the hydrolysis and condensation reactions of the silanol groups are affected by the structure of the organic moiety of the silanes [24–26]. It was observed that MRPS and VTES displayed the lowest adsorption affinity toward the CNCs. Bifunctional silanes (TESPT and TESPD) showed high contents of silanes adsorbed on the CNCs surface. It is proposed that the adsorption of silane takes place through the formation of multilayers. One silane moiety of the TESPT and TESPD is considered to be linked to the CNCs surface through one bond, while the other silane moiety undergoes hydrolysis and polycondensation reactions with vicinal silane molecules, leading to the formation of multilayers [21,30–32]. Both MPS and APS also showed high adsorption affinity toward the CNCs surface. This is attributed to the

presence of acrylic moiety in MPS and amine group in APS, which favored the interaction between the silanes and CNCs surface due to the establishment of hydrogen bonds.

Table 5.3: Amount of silane coupling agents grafted on the CNCs

Silane Contents	TESPT	TESPD	MPS	MRPS	APS	VTES
Amount grafted (mmol/$g_{cellulose}$)	0.598	0.794	0.785	0.102	0.384	0.069

5.3.1.3   Contact Angle Measurement

The change in the surface character of the CNCs after the surface functionalization was evaluated by measuring the contact angle values of a drop of water onto the films of pristine and functionalized CNCs. Fig. 5.4 shows the shape of the water drop on the film of pristine CNCs and CNCs functionalized with a silane coupling agent. The change in contact angle values of a drop of water on pristine and functionalized CNCs films with time are shown in Fig. 5.5. A high hydrophilic character was observed for pristine CNCs film which showed a contact angle value of 31°, which is attributed to the presence of numerous hydroxyl groups in their structure. The surface functionalization of CNCs with silanes significantly changed their surface character from hydrophilic to hydrophobic and increased contact angle to 75°, 76°, 76°, 73°, 71°, and 81° was obtained for TESPT, TESPD, MPS, MRPS, APS, and VTES, respectively. The contact angle values for all the functionalized CNCs were almost the same and remained unchanged with measurement time. APS

(a)   **(b)**

Figure 5.4: Shape of the water drop on film of (a) pristine CNC and (b) functionalized CNC
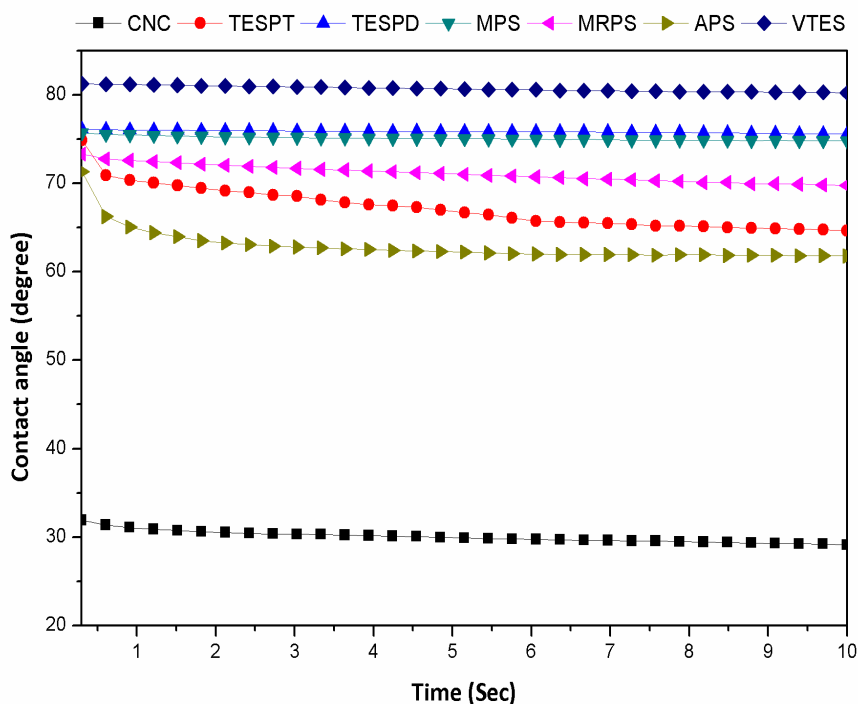
Figure 5.5: Water contact angle changes for pristine and surface functionalized CNCs

showed the lowest value of contact angle, which could be due to the presence of high polar amine group in their structure which can involve in hydrogen bonding. VTES demonstrated the highest value of contact angle however the content of silane-grafted on CNCs was lowest for VTES. It is interesting to note, despite the fact that the loading of silane-grafted on the CNCs surface was different for different silane coupling agents, the surface character was almost the same for all the functionalized CNCs and there is no significant difference between the contact angle values of these functionalized CNCs. It can be explained by considering the fact that, initially a monolayer of silanes is formed on the CNCs surface, then the excess concentration of silane undergo poly-condensation reactions leading to the formation of multilayers [30]. Therefore, functionalized CNCs with a low amount of grafted silane demonstrate the same surface character as CNCs functionalized with a high amount of grafted silane.

5.3.1.4   X-ray Diffraction Analysis

X-ray diffraction analysis was performed to evaluate the effect of surface functionalization on the crystalline structure of the CNCs. The XRD patterns of the pristine CNCs and

functionalized with different silane coupling agents are shown in Fig. 5.6. All pristine and functionalized CNCs displayed the typical diffraction pattern of cellulose Iβ and cellulose II Peaks observed at $2\theta=14.8^{o}$, 16.5^{o}, 22.5^{o}, and 34.6^{o} correspond to the cellulose Iβ and two other peaks at 12.2^{o} and 20.2^{o} correspond to the cellulose II. All the functionalized CNCs showed high crystalline structure as of pristine CNCs. Furthermore, to estimate the crystallinity of all the samples, the crystallinity index (CrI) was calculated using the equation 5.1 [33].

$$\text{CrI (\%)} = \left(1 - \frac{I_1}{I_2}\right) \times 100 \qquad (5.1)$$
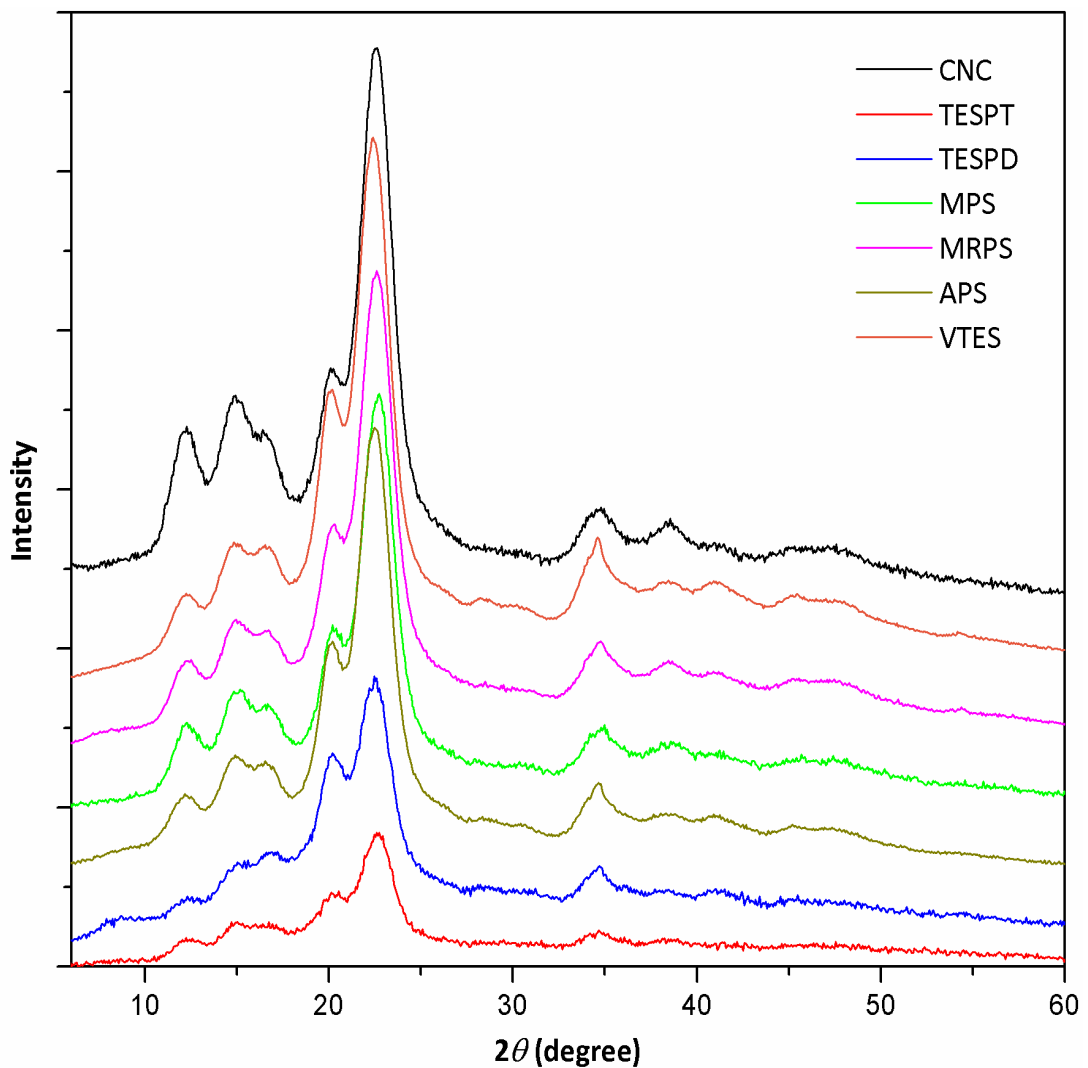
Figure 5.6: XRD patterns of the pristine and functionalized CNCs

Where, I_1 is the intensity of the minimum at the position of about $2\theta = 18^o$ and I_2 is the intensity of the crystalline peak at the maximum at about $2\theta = 22^o$. The crystallinity indices of the pristine and functionalized CNCs are reported in Table 5.4. It was found that the crystallinity index of the CNCs was slightly decreased after the functionalization, suggesting that the crystalline structure of the CNCs was basically preserved. A slight decrease in the crystallinity index is due to the fact that surface of CNCs is covered with non-crystalline silane coupling agents and the decrease is higher for the silanes with a bigger molecular structure e.g. TESPT and TESPD.

Table 5.4: Crystallinity indices of the pristine and functionalized CNCs

	CNCs	TESPT	TESPD	MSP	MRPS	APS	VTES
Crystallinity Index (CrI)	86.4	78.3	76.8	82.7	83.1	84.4	82.4

5.3.2 Natural Rubber Compounds

The surface functionalized CNCs were incorporated into the natural rubber to prepare the rubber compounds as described in experimental section. To study the effect of pre-functionalization (functionalization of CNCs before adding into the rubber matrix), the rubber compounds with post-functionalized CNCs (adding the silane coupling agents and functionalizing the CNCs during the rubber compounding) were also prepared. All the prepared compounds were compared with reference silica compounds because it was the main objective of this work to study the possibility of replacing the silica with CNCs. Six silane coupling agents with different organic functionality (polysulfide, methacryl, mercapto, amine, and vinyl) were used to compatibilize CNCs with natural rubber matrix. The interactions of the silanes with polymer matrix depend on the compatibility or reactivity of the organic functionality toward the polymer, which in turn affects the resulting properties of the composite material. The effect of different silane coupling agents and the effect of mode of functionalization of the CNCs on the vulcanization characteristics and dynamic mechanical properties of the prepared natural rubber compounds are summarized in Table 5.5. It can be seen that pristine CNCs have similar

scorch time (T_S2) as of reference silica; however, the optimum curing time (T_{90}) was significantly reduced. This shows that CNCs accelerate the vulcanization process which is evident from the higher value of curing rate index (CRI) [CRI = $100/(T_{90}-T_S2)$] for CNCs. The adsorption of curatives by silica may explain the lower vulcanization rate of silica-filled compound [34,35]. The adsorbed curatives cannot take part in the crosslinking reactions at the start of the curing process, while as the process elapse the adsorbed materials start desorbing slowly and participate in the curing process, hence the curing rate was slow for silica compound. T_S2, T_{90}, and CRI were improved for the functionalized CNCs. The kinetics of vulcanization of sulfur cure system is dependent on the structure of silane used. TESPT and TESPD showed lower values than untreated CNCs. Among these two sulfidic silanes, the T_S2 and T_{90} decreased with the increase of sulfur atoms in the sulfidic group. Higher T_S2 and T_{90} and lower CRI for TESPT and TESPD could be due to their bulky size which causes steric hindrance for cross-linking. Also, the sulfides must be cleaved before the reaction with the polymer [36,37]. In the case of MRPS and APS functionalized CNCs, T_S2 and T_{90} were significantly reduced and vulcanization rate was increased. The presence of thiol and amine groups in the structure of MRPS and APS, respectively, play an important role in accelerating the curing process of natural rubber [36,38]. It was observed that the curing rate of Post-Silane compounds was higher than the Pre-Silane compounds. In Post-Silane compounds, the silane was added during the compounding which was not only distributed on the interface of CNCs and matrix but also throughout the compounds which may explain this increase in curing rate. Two other important parameters of curing process are minimum (M_L) and maximum (M_H) torque values. The difference of the two correlates closely with the crosslinking density ($\Delta M = M_H - M_L$). The M_L value represents the viscosity of the rubber compounds in unvulcanized state at the test temperature. It was observed that the prepared compounds did not show a significant change in the M_L value. The M_H value and degree of crosslinking of the CNCs-filled compounds were slightly lower than the reference silica compound.

The dynamic mechanical properties data of the vulcanized rubber compounds are summarized in Table 5.5. The storage modulus (G') at low strain [G'_o (at 1 % strain)] is much higher than the storage modulus at high strain [G'_∞ (at 100 % strain)] and typical non-linear behavior of G' with respect to applied strain was observed for all the

Table 5.5: Vulcanization characteristics and dynamic mechanical properties of the prepared rubber compounds

Parameter	Silica	CNC	Pre-TESTP	Pre-TESPD	Pre-MPS	Pre-MRPS	Pre-APS	Pre-VTES	Post-TESTP	Post-TESPD	Post-MPS	Post-MRPS	Post-APS	Post-VTES
Vulcanization Characteristics														
T_S2 (min)	6.74	6.70	7.34	7.58	8.01	6.09	6.22	6.70	6.29	6.68	6.98	4.11	5.47	6.76
T_{90} (min)	13.15	11.1	12.88	13.52	13.10	10.35	10.58	10.66	10.71	11.15	11.16	7.45	9.25	10.52
CRI (min^{-1})	15.60	22.73	18.05	16.84	19.65	23.47	22.94	25.25	22.62	22.37	23.92	29.94	26.46	26.60
M_L (dNm)	1.1	1.0	0.98	0.89	1.0	1.04	1.08	1.09	1.09	1.01	0.99	0.97	1.16	0.93
M_H (dNm)	11.06	10.17	10.09	10.08	9.81	9.56	9.74	9.80	10.11	10.09	9.84	9.97	10.70	9.33
ΔM (dNm)	9.96	9.17	9.11	9.19	8.81	8.52	8.66	8.71	9.02	9.08	8.85	9	9.54	8.4
Dynamic Mechanical Properties														
G'_o (kPa)	763.81	724.9	668.14	661.45	660.91	657.4	668.86	712.3	736.57	738.55	725.17	712.97	775.52	681.48
G'_∞ (kPa)	607.75	538.93	551.46	557.35	546.23	529.49	534.97	524.72	546	554.84	539.66	538.6	562.87	504.42
ΔG (kPa)	156.06	185.97	116.68	104.1	114.68	127.91	133.89	187.58	190.57	183.71	185.51	174.37	212.65	177.06
Tan δ_o	0.023	0.031	0.02	0.022	0.022	0.021	0.014	0.025	0.023	0.024	0.028	0.023	0.02	0.028
Tan δ_∞	0.029	0.041	0.028	0.026	0.028	0.029	0.033	0.044	0.045	0.04	0.043	0.041	0.044	0.042

compounds, which is commonly known as Payne effect ($\Delta G = G'_o - G'_\infty$). The Payne effect is linked to the extent of filler network in the polymer matrix. The modulus of the filled rubber compound at low strain (G'_o) is due to three strain independent contributions (polymer network, hydrodynamic effect, in-rubber structure) and one strain dependent contribution (filler network). At high strain, the filler network is broken down and the modulus represents the filler-rubber interactions, as the filler particles are supposed to be not mutually interacting. It can be seen from the results that, silica showed the higher values of G'_o and G'_∞ than CNCs, representing very high filler-filler and filler-polymer interactions. However, untreated CNCs also showed very strong filler networking as evident from the high Payne effect. This is due to the fact that the untreated CNCs were not compatibilized by the silane coupling agent, hence the ability of polar hydroxyl group of the CNCs to form the hydrogen bonding resulted in strong filler-filler interactions. The Pre-Silane compounds with pre-functionalized CNCs showed a considerable decrease in Payne effect and G'_o values. Surface treatment of the CNCs changed the surface character of the CNCs from hydrophilic to hydrophobic, and this hydrophobization of CNCs strongly decrease the filler network while increasing the filler-polymer interactions. Payne effect of the Pre-Silane compound was relative to the contents of silane-grafted on CNCs. TESPT, TESPD and MPS compounds showed the lowest Payne effect due to the highest contents of grafted silane which reduced the filler-filler interactions. On the other hand, the Pre-VTES compound showed the quite similar behavior as of untreated CNCs, due to lowest contents of VTES grafted on CNCs. In the case of Post-Silane compounds, the Payne effect was quite higher than Pre-Silane compounds and showing much higher filler networking. However, high G'_∞ values show high filler-polymer interactions too. The Payne effect of Post-Silane compounds was more or less same, however, Post-APS compound showed higher Payne effect and storage modulus than other compounds, which could be due to a high degree of crosslinking. High crosslinking density increased the modulus not only at low strain but also at high strain, in other words crosslinking increase the strain independent contribution of the modulus i.e. polymer network.

Tan δ values of the prepared compounds are given in Table 5.5. Tan δ represents the amount of energy dissipation and depends on the rate of filler network breakdown and reformation due to the strain amplitude. For all the compounds, the Tan δ at low strain

(Tan δ_o at 1 % strain) is lower than Tan δ at high strain (Tan δ_∞ at 100 % strain). At low strains, the filler network was capable to reform after deformation and the viscous polymer was stabilized by the filler network, hence a low Tan δ was observed. While at high strain, filler network was broken down and not able to reform in the time frame of dynamic measurement, so polymer chains were no more stabilized by the filler and showed more viscous behavior, hence a high hysteresis was observed. It was observed that untreated CNCs compound showed higher Tan δ than silica compound, which is due to the strong filler network formed by the CNCs in the unfunctionalized state. As the hysteresis is resulted due to the breakdown of filler network, so the disruption of a strong filler network during straining dissipates more energy. The compounds prepared with pre-functionalized CNCs showed lower hysteresis than untreated CNCs and silica due to lower filler networking and the results are in agreement with the results of storage modulus and Payne effect. The Post-Silane compounds showed the higher value of Tan δ than Pre-Silane compounds due to the strong filler networking.

The effect of surface functionalization of CNCs (pre-functionalization and post-functionalization) in comparison with reference silica and untreated CNCs on the tensile mechanical properties, such as tensile modulus at different strain amplitudes, tensile strength, and elongation at break are summarized in Table 5.6. Tensile measurements were performed on vulcanized samples at room temperature. It can be seen from the results that silica showed higher reinforcement (300 % modulus) than untreated CNCs however the difference was not so significant. High aspect ratio and high stiffness of the CNCs formed a rigid filler network which resulted in comparable tensile properties. Since the CNCs were not treated with a silane coupling agent, a poor interfacial adhesion between the CNCs and polymer matrix resulted in lower reinforcement than the silica-filled compound. Adequate interfacial interactions are required for effective transfer of stress between the filler and polymer matrix [39,40]. It was surprising to note that the Pre-Silane compounds filled with pre-functionalized CNCs showed quite lower tensile properties than reference untreated CNCs. Although, the dynamic mechanical analysis showed improved filler-polymer interactions and lower Payne effect for Pre-Silane compounds. The only possible reason for this lowering of tensile properties could be due to poor dispersion and uneven distribution of these functionalized CNCs, since the rubber

Table 5.6: Tensile mechanical properties of the prepared rubber compounds

Parameter	Silica	CNC	Pre-TESTP	Pre-TESPD	Pre-MPS	Pre-MRPS	Pre-APS	Pre-VTES	Post-TESTP	Post-TESPD	Post-MPS	Post-MRPS	Post-APS	Post-VTES
Stress at 10% (MPa)	0.3	0.31	0.3	0.29	0.28	0.27	0.26	0.3	0.31	0.31	0.31	0.31	0.31	0.3
Stress at 50% (MPa)	0.87	0.84	0.85	0.8	0.78	0.74	0.73	0.83	0.88	0.86	0.84	0.86	0.89	0.79
Stress at 100% (MPa)	1.39	1.37	1.4	1.28	1.26	1.17	1.14	1.34	1.48	1.42	1.38	1.44	1.5	1.3
Stress at 200% (MPa)	2.88	2.89	2.71	2.27	2.35	2.24	1.99	2.82	3.35	3.13	3.19	2.99	3.54	2.80
Stress at 300% (MPa)	5.78	5.32	4.43	3.57	3.98	3.79	3.27	5.1	6.31	5.88	5.53	5.92	6.97	5.16
Tensile Strength (MPa)	24.06	22.24	16.96	15.37	19.19	19.84	11.55	22.39	22.67	22.44	22.76	21.77	20.05	21.22
Elongation at break (%)	510.56	544.41	502.52	486.06	537.45	542.53	460.16	553.7	532.25	546.28	540.05	533.12	487.32	554.96

compounds were prepared by initially preparing the masterbatches of F-CNCs and natural rubber latex. The dispersion of F-CNCs in ethanol/water mixture was added to natural rubber latex to prepare the masterbatch, as the latex is an aqueous suspension of the natural rubber, so the hydrophobized CNCs were not properly distributed in the rubber matrix, which may explain this reduction of tensile mechanical properties. However, untreated hydrophilic CNCs were homogeneously dispersed in the aqueous latex and formed a strong percolating filler network in the resulting matrix, which resulted in higher tensile properties than Pre-Silane compounds. On the other hand, the Post-Silane compounds showed very high reinforcement as compared to untreated CNCs and silica compounds. The Post-Silane compounds were also prepared by initially prepared the masterbatches. A homogeneous dispersion of CNCs in rubber matrix was obtained by dispersing the pristine hydrophilic CNCs in aqueous natural rubber latex and coagulating it. Then silane coupling agents were added during the compounding in the internal mixer which enhanced the interfacial interactions between the CNCs and rubber matrix. Hence, high dispersion and enhanced filler-polymer interactions allowed achieving the improved tensile properties and high reinforcement of the Post-Silane compounds. Furthermore, this higher reinforcing effect of Post-Silane compounds than silica-filled compounds can be assigned to well-known percolation phenomenon of the high aspect ratio of CNCs, which formed a stiffer continuous network of these rod-like CNCs nanoparticles. Among the Post-Silane compounds, the CNCs functionalized with different silane coupling agents showed different reinforcing effect, depending on the reactivity of the organic functionality of the silane coupling agent toward the natural rubber. The chemical bonding between the silane and natural rubber was created during the sulfur curing process. The silane bearing sulfur in their organic functionality (polysulfide in TESPT and TESPD, and thiol is MRPS) showed high reinforcement as the sulfur contributed to the creation of additional crosslinks [36,37]. The presence of amine group in APS played a catalytic role in accelerating the curing process and high crosslinking density was observed [38]. Hence, Post-APS compound showed the higher reinforcement than other compounds which is due to its high degree of crosslinking. While tensile strength and elongation at break of Post-APS were reduced as the high crosslinking density increases the brittleness of the compound. The Post-VTES showed the lowest tensile properties which could be due to the less reactivity of vinyl moiety and less crosslinking density of the compound. In general, it was

summarized from the obtained results that the post-functionalization is very simple and efficient way to compatibilize the CNCs with natural rubber, while pre-functionalization of CNCs not only required excessive chemical treatment but also resulted in a reduction of mechanical properties of the rubber compound. Hence, the rubber compounds filled with CNCs prepared through post-functionalization method showed the much higher reinforcing capability of the CNCs than silica and can be used to replace the silica in tire compounds.

5.4   Conclusions

The natural rubber compounds filled with functionalized CNCs were prepared. The CNCs were functionalized with six different silane coupling agent having different organic functionality (polysulfide, acrylic, mercapto, amine, and vinyl). The functionalization was carried out by two different methods; pre-functionalization of CNCs in ethanol/water mixture before preparing the compound and post-functionalization of CNCs by adding silane coupling agents during the compounding process in an internal mixer. FTIR analysis and silicon content measurements confirmed the grafting of silane coupling agents on the CNCs by the pre-functionalization method. The change in the surface character of the CNCs from hydrophilic to hydrophobic was confirmed by contact angle measurement. XRD analysis showed that the crystalline structure of the CNCs was preserved after the functionalization. The effect of the functionalization mode on the final properties of the natural rubber compounds was investigated and compared with compounds filled with silica and untreated CNCs. It was observed from the obtained results that mechanical properties of the compounds filled with pre-functionalized CNCs were inferior to silica and untreated CNCs which could be their poor dispersion during the preparation of masterbatches. However, the compounds with post-functionalized CNCs showed much higher reinforcement than the silica-filled compound. Hence, it was concluded that the post-functionalization is a simple and efficient way to compatibilize the CNCs with natural rubber and the rubber compounds of CNCs prepared through post-functionalization method showed the much higher reinforcing capability of the CNCs than silica and can be used to replace the silica in tire compounds.

References

[1] B. Sun, Q. Hou, Z. Liu, Y. Ni, Cellulose 22 (2015) 1135–1146.

[2] A. Salam, L.A. Lucia, H. Jameel, Cellulose 22 (2015) 397–406.

[3] B. Sun, Q. Hou, Z. Liu, Z. He, Y. Ni, Cellulose 21 (2014) 2879–2887.

[4] U.D. Hemraz, K.A. Campbell, J.S. Burdick, K. Ckless, Y. Boluk, R. Sunasee, Biomacromolecules 16 (2015) 319–325.

[5] J.-L. Huang, C.-J. Li, D.G. Gray, RSC Adv. 4 (2014) 6965.

[6] J. Yang, C.-R. Han, J.-F. Duan, M.-G. Ma, X.-M. Zhang, F. Xu, R.-C. Sun, X.-M. Xie, J. Mater. Chem. 22 (2012) 22467.

[7] A. Villares, C. Moreau, A. Dammak, I. Capron, B. Cathala, Soft Matter 11 (2015) 6472–6481.

[8] E.P. Plueddemann, Silane Coupling Agents, 2nd ed., Plenum Press, New York, 1991.

[9] K.D. Weaver, J.O. Stoffer, D.E. Day, Polym. Compos. 16 (1995) 161–169.

[10] D.P.K. and P.D.M. C. W. CHU, J. Adhes. Sci. Technol. 7 (1993) 417–433.

[11] L. Basilissi, G. Di Silvestro, H. Farina, M.A. Ortenzi, J. Appl. Polym. Sci. 128 (2012) n/a-n/a.

[12] P. Wei, X. Qu, H. Dong, L. Zhang, H. Chen, C. Gao, J. Appl. Polym. Sci. 128 (2013) 3390–3397.

[13] W. Kaewsakul, K. Sahakaro, W.K. Dierkes, J.W.M. Noordermeer, Rubber Chem. Technol. 85 (2012) 277–294.

[14] M.A. Brook, Silicon in Organic, Organometallic, and Polymer Chemistry, John Wiley & Sons, Ltd, New York, 2000.

[15] L. Chazeau, C. Gauthier, J.M. Chenal, in:, Rubber Nanocomposites Prep. Prop. Appl., John Wiley & Sons, Ltd, New York, 2010, pp. 291–330.

[16] W.K. Dierkes, L.A.E.M. Reuvekamp, A.J.W. Ten Brinke, J.W.M. Noordermeer, Silanes and Other Coupling Agents 3 (2004) 89–103.

[17] J.W. ten Brinke, S.C. Debnath, L.A.E.M. Reuvekamp, J.W.M. Noordermeer, Compos. Sci. Technol. 63 (2003) 1165–1174.

[18] M.A. Rodriguez, M.J. Liso, F. Rubio, J. Rubio, J.L. Oteo, J. Mater. Sci. 34 (1999) 3867–3873.

[19] H. Ishida, J.L. Koenig, J. Colloid Interface Sci. 64 (1978) 565–576.

[20] S. Naviroj, S.R. Culler, J.L. Koenig, H. Ishida, J. Colloid Interface Sci. 97 (1984) 308–317.

[21] M.C. Brochier Salon, M. Abdelmouleh, S. Boufi, M.N. Belgacem, A. Gandini, J. Colloid Interface Sci. 289 (2005) 249–261.

[22] M. Abdelmouleh, S. Boufi, M.N. Belgacem, A.P. Duarte, A. Ben Salah, A. Gandini, Int. J. Adhes. Adhes. 24 (2004) 43–54.

[23] H. Ishida, J.L. Koenig, Appl. Spectrosc. 32 (1978) 469–479.

[24] J.K. Crandall, C. Morel-Fourrier, J. Organomet. Chem. 489 (1995) 5–13.

[25] H. Kang, W. Meesiri, F. Blum, Mater. Sci. Eng. A 126 (1990) 265–270.

[26] F.D. Osterholtz, E.R. Pohl, J. Adhes. Sci. Technol. 6 (1992) 127–149.

[27] C.H. Chiang, H. Ishida, J.L. Koenig, J. Colloid Interface Sci. 74 (1980) 396–404.

[28] L.G. Britcher, D.C. Kehoe, J.G. Malisons, A.G. Swincer, Macromolecules 28 (1995) 3110–3118.

[29] M. Kacuráková, A.C. Smith, M.J. Gidley, R.H. Wilson, Carbohydr. Res. 337 (2002) 1145–53.

[30] M. Abdelmouleh, S. Boufi, A. Ben Salah, M.N. Belgacem, A. Gandini, Langmuir 18 (2002) 3203–3208.

[31] A. Jokinen, P. Mikkola, J. Matisons, J. Rosenholm, J. Colloid Interface Sci. 196 (1997) 207–214.

[32] U. Goerl, A. Hunsche, A. Mueller, H.G. Koban, Rubber Chem. Technol. 70 (1997) 608–623.

[33] G.A.F. Roberts, in:, Pap. Chem., Springer Netherlands, Dordrecht, 1991, pp. 9–24.

[34] S.-S. Choi, Elastomers Compos. 36 (2001) 37–43.

[35] A.S. Hashim, B. Azahari, Y. Ikeda, S. Kohjiya, Rubber Chem. Technol. 71 (1998) 289–299.

[36] B.T. Poha, C.C. Nga, Eur. Polym. J. 34 (1998) 975–979.

[37] P. Vondracek, M. Hradec, V. Chvalovsky, H.D. Khanh, Rubber Chem. Technol. 57 (1984) 675–685.

[38] C. Hayichelaeh, L.A.E.M. Reuvekamp, W.K. Dierkes, A. Blume, J.W.M. Noordermeer, K. Sahakaro, Rubber Chem. Technol. (2017) rct.82.83708.

[39] L.M. Matuana, C.B. Park, J.J. Balatinecz, J. Vinyl Addit. Technol. 3 (1997) 265–273.

[40] N.G. McCrum, C.P. Buckley, C.B. Bucknall, Principles of Polymer Engineering, Oxford University Press, New York, 1988.

Chapter 6

Novel CNC/Silica Hybrid as potential reinforcing filler for natural rubber compounds

Syed Danish Ali, Luca Zoia, Luca Castellani, Marco Emilio Orlandi

This chapter describes the synthesis of CNC/Silica hybrid by decorating the surface of cellulose nanocrystals (CNCs) with silica. The CNC/Silica hybrid was prepared by a simple, efficient, and cost-effective co-precipitation method. The morphology, structure, and CNC to silica contents of the hybrid were investigated by Field emission scanning electron microscopy (FESEM), Fourier-transform infrared spectroscopy (FTIR), X-ray diffraction (XRD) and Thermal gravimetric analysis (TGA). The surface area of the hybrid was measured by nitrogen physisorption measurements. Rod-like morphology of the hybrid was observed with a surface area 99 m^2/g. The prepared hybrid was used as reinforcing filler in natural rubber compounds and compared with standard high reinforcing silica that is commonly used in the tire industry. The compounds were prepared by two methods; dry mixing and co-precipitation. The effect of the preparation method on the properties of the prepared compounds was studied. The co-precipitation method was found more effective than dry mixing. Density, vulcanization characteristics, dynamic mechanical properties and tensile mechanical properties of the compounds were investigated and compared with reference silica compounds. Results demonstrated that rod-like CNC/Silica hybrid provided higher reinforcement to rubber than reference silica along with the much lower density of the final compounds and can be used as potential reinforcing filler in tire tread compounds.

6.1   Introduction

The hybrid organic/inorganic materials produced by combining organic and inorganic phases at the nanoscale have attracted huge attention in the last few decades owing to

their distinctive properties acquired by the synergistic combination of organic and inorganic components, with complementary properties [1–3]. The properties of these hybrid materials are not only the sum of the properties of their individual counterparts but the inner interface could also play an important role. Improved and unique properties of the hybrid materials allow the use of these materials in high-tech industrial applications [4].

Based on the interesting properties of CNCs, the potential of CNCs to replace silica in rubber compounds was additionally explored by preparing a CNC/Silica hybrid. Cellulose-based hybrid materials have been reported in the literature using cellulose or modified cellulose with different inorganic counterparts [5–19]. The presence of numerous hydroxyl groups on the surface of CNCs offers the possibility to chemically modify the surface and allow the use of CNCs as a template for loading the inorganic materials. Silica is the most commonly used reinforcing filler in the tire industry and used in tire compounds to reduce the rolling resistance and heat build-up in-addition to high strength, modulus and abrasion resistance [20–22]. The CNC/Silica hybrid will combine the properties of both CNCs and silica and could be ideal reinforcing filler for tire tread compounds. The CNC/silica hybrid in this study was prepared by using the CNCs as template and CNCs were decorated with a layer of silica nanoparticles. The resulting hybrid material will have a rod-like structure with high aspect ratio and lower density than silica. The silica layer on the surface of CNCs could show better compatibility with polymer matrix due to well-developed silica-silane technology. The hybrid could act like high aspect ratio silica particles and higher reinforcement could be obtained for rubber compounds than reference silica-filled compounds.

6.2 Experimental

6.2.1 Materials

The following chemicals were used for the synthesis of CNC/Silica hybrid. Sodium hydroxide (NaOH), sulfuric acid (H_2SO_4), acetic acid, and cetyltrimethylammonium bromide (CTAB) were purchased from Sigma-Aldrich. CNCs, silica, natural rubber latex, and the

materials used in the rubber compounding, such as silane, vulcanizers, and antioxidants were the same as mentioned in section 5.2.1.

6.2.2 Methods

6.2.2.1   CNC/Silica Hybrid Synthesis

The CNC/Silica hybrid (CSH) was synthesized by co-precipitation method. The procedure used here is the modification of method used for the precipitation of silica by Dokter and Tijburg [23]. Initially, a sodium silicate solution was prepared by adding 7g of silica and 2.8g NaOH in 90 ml of distilled water in a round bottom flask and reaction mixture was stirred at 300 rpm for 1 h at 80 ^{o}C. A clear solution was obtained at the end. In another three neck round bottom flask, about 5g (42 g CNC suspension 12% w/w) of CNC and 0.8g of CTAB was added in 450 ml of distilled water. This reaction mixture was stirred for 30 min and the temperature was maintained at 75-85 ^{o}C. This temperature was maintained throughout the reaction. The initially prepared sodium silicate solution was added to the above CNCs solution at a rate of 0.67 ml/min for about 90 min. During the addition of sodium silicate solution, the sulfuric acid (15 % w/w) was added simultaneously to maintain the pH of the reaction mixture at 9.2 – 9.4. After 90 min of reaction, the dosing of sodium silicate solution and sulfuric acid were stopped and the reaction mixture was allowed to stirring for 15 min. Then, sulfuric acid was added again in 10 min so that the pH was lowered to 7.5. The sodium silicate solution was dosed again at a rate of 0.67 ml/min for next 45 min and the pH was maintained at 7.3-7.6 by simultaneous addition of sulfuric acid (15 % w/w). After 45 min of reaction, sulfuric acid (15 % w/w) was dosed again in 20 min so that the pH was lowered to 4. After that, the resulting precipitated-CSH was obtained after centrifugation at an acceleration of 3200g for 10 min, repeatedly washing with distilled water until all CTAB was removed and freeze dried. The flow sheet diagram of the CNC/Hybrid synthesis is shown in Fig. 6.1.
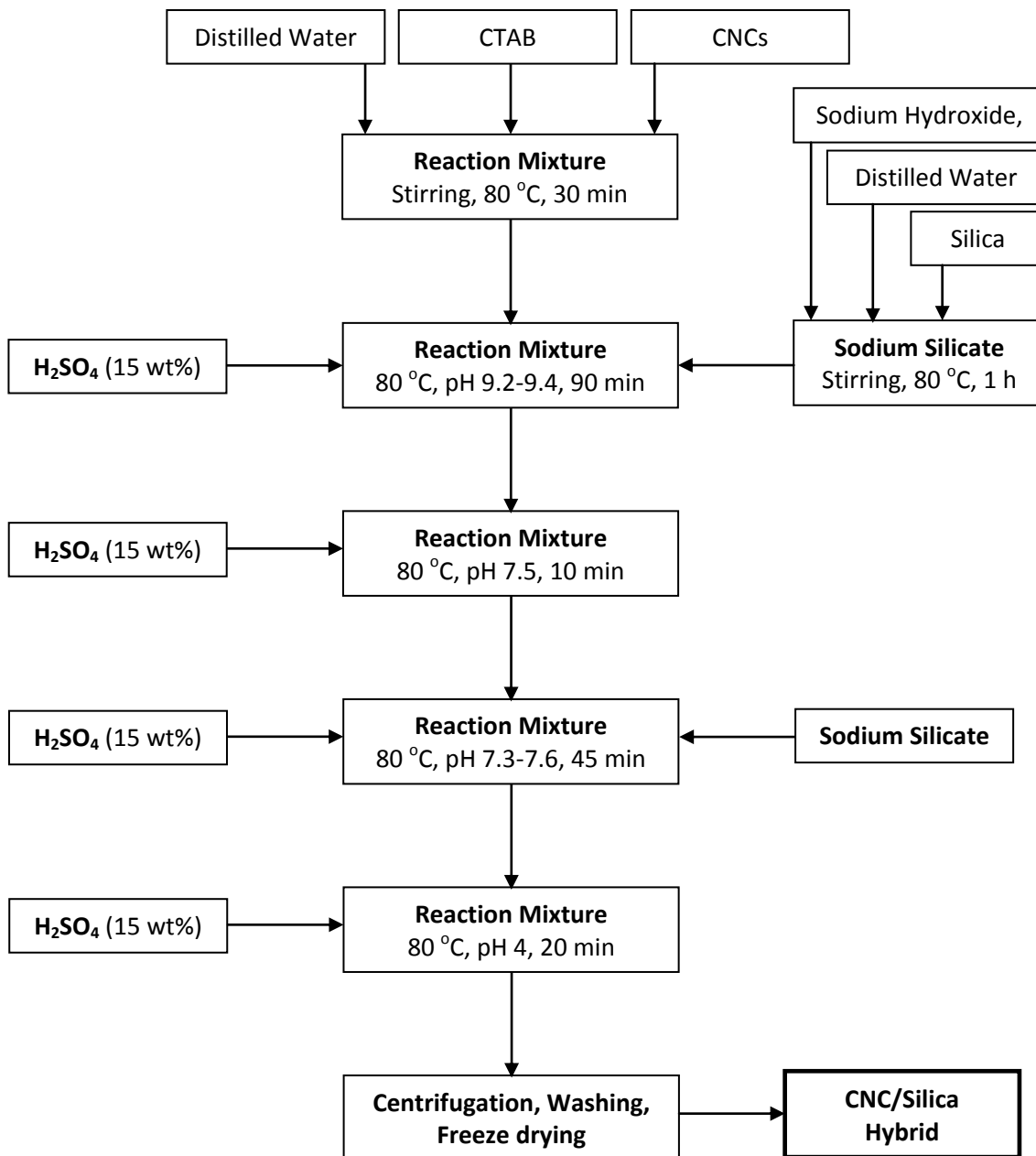
Figure 6.1: Flow sheet diagram of CNC/Silica hybrid synthesis

6.2.2.2   Rubber Compounding

The natural rubber (NR) compounds of CSH and reference silica were prepared by two methods; dry mixing and co-precipitation. The effect of these methods on the dispersion of the filler in the rubber matrix and final properties of the rubber compounds was investigated. Formulation of the prepared compounds in phr is shown in Table 6.1. For each method, a reference silica compound was prepared. The Dry-CSH and Dry-Silica

represent the CSH compound and reference silica compound, respectively, prepared by dry mixing. The Co-CSH and Co-Silica represent the CSH compound and reference silica compound, respectively, prepared by co-precipitation method. The compounds were prepared with 30 phr of filler contents.

Table 6.1: Formulation of the prepared rubber compounds in PHR

Ingredients	Dry-Silica	Dry-CSH	Co-Silica	Co-CSH
NR	100	100	-	-
Silica	30	-	-	-
CSH	-	30	-	-
Masterbatch NR(100phr)+Silica(30phr)	-	-	130	-
Masterbatch NR(100phr)+CSH(30phr)	-	-	-	130
Carbon Black (N375)	4	4	4	4
TESPT	2.4	2.4	2.4	2.4
Soluble Sulfur	2	2	2	2
Zinc Oxide	5	5	5	5
Stearic Acid	2	2	2	2
CBS	2	2	2	2
TMQ	1	1	1	1
6PPD	1.5	1.5	1.5	1.5

In the dry mixing, the rubber compounds were prepared by mixing all the ingredients using the Brabender internal mixer. The ingredients were mixed using the same procedure as described in Chapter 5, Table 5.1.

In co-precipitation method, the masterbatches of NR with fillers were initially prepared. The CSH was not dried and the hybrid suspension was used as such for the preparation of masterbatch. To prepare the masterbatch the calculated amount of the filler based on the phr used (9.76 g of hybrid for 30 phr of filler contents) was added to the calculated

quantity of natural rubber latex (32.53 g for 100 phr). The emulsion was stirred for 1 h at room temperature. Then, the emulsion was coagulated by progressive addition of the acetic acid solution (10 % v/v). The coagulated rubber was reduced to a thin sheet using a two-roll mill and washed with distilled water until neutral pH was reached. The thin sheets of masterbatch were dried under vacuum at 40 $^{\circ}$C until constant weight. The obtained masterbatches were mixed with other ingredients (silane, vulcanizers, and antioxidants) using internal mixer using the procedure given in Chapter 5, Table 5.1.

To study the effect of filler contents on the properties of the natural rubber compounds, the compounds were prepared with 20, 30 and 40 phr of filler contents using the formulation shown in Table 6.2. The compounds were labeled as CSH-X for hybrid compounds and Silica-X for reference silica compounds, where X represents the phr of fillers.

Table 6.2: Formulation in phr of the prepared compounds with different filler contents

Ingredients	Silica-20	Silica-30	Silica-40	CSH-20	CSH-30	CSH-40
NR	100	100	100	-	-	-
Silica	20	30	40	-	-	-
Masterbatch NR(100phr)+CSH(20phr)	-	-	-	120	-	-
Masterbatch NR(100phr)+CSH(30phr)	-	-	-	-	130	-
Masterbatch NR(100phr)+CSH(40phr)	-	-	-	-	-	140
TESPT	1.6	2.4	3.2	1.6	2.4	3.2
Soluble Sulfur	2	2	2	2	2	2
Zinc Oxide	5	5	5	5	5	5
Stearic Acid	2	2	2	2	2	2
CBS	2	2	2	2	2	2
TMQ	1	1	1	1	1	1
6PPD	1.5	1.5	1.5	1.5	1.5	1.5

6.2.3 Characterization of CNC/Silica Hybrid

6.2.3.1   FTIR Analysis

The FTIR spectra of CNC, Silica and CNC/Silica hybrid were recorded to confirm the synthesis of the hybrid. The analysis was performed using the same procedure and instruments as mentioned in Chapter-3, section 3.2.3.8.

6.2.3.2   FESEM Analysis

The surface morphology and dimensions of the prepared hybrid were investigated by Field Emission Scanning Electron Microscopy (FESEM). The sample for analysis was prepared by dispersing a very small amount of prepared hybrid in ethanol and sonicated for 15 min. A drop of the suspension was placed on a silicon substrate and dried in air. The sample was not coated with gold and analyzed as such. The FESEM analysis was performed using Zeiss UltraPlus FESEM operating at 7.0 kV and the working distance between 3.5 and 4 mm. The images were recorded at different magnifications.

6.2.3.3   Nitrogen Physisorption Measurements

Total surface area, micropores area, and micropore volume were measured by nitrogen physisorption using a Quantachrome Autosorb-1 apparatus according to BET and t-plot methods. The samples were evacuated at 200 ^{o}C for 16 h before the analysis.

6.2.3.4   Thermal Gravimetric Analysis

Thermal Gravimetric analysis (TGA) of the prepared hybrid was performed to quantify the percentage of CNCs and silica in the CNC/Silica hybrid. The analysis was performed using Mettler Toledo TGA1 instrument. Few milligrams of the sample were placed in an open crucible pan and heated from 30 ^{o}C to 800 ^{o}C in a nitrogen atmosphere with nitrogen flow rate of 60 ml/min. The temperature was increased in three steps; from 30 to 80 ^{o}C at a heating rate of 20 ^{o}C/min and held at 80 ^{o}C for 15 min, then from 80 to 170 ^{o}C at a heating

rate of 30 ^oC/min and held at 170 ^oC for 15 min, and from 170 to 800 ^oC at a heating rate of 30 ^oC/min and held at 800 ^oC for 10 min in air (60 ml/min).

6.2.3.5 XRD Analysis

Powder XRD analysis of CNCs, silica, and the hybrid was performed using the X'Pert PRO diffractometer from PANalytical Company, using Cu Kα (1.54 Ǻ) as an X-ray source. The operating voltage and current were kept at 40 kV and 30 mA respectively.

6.2.4 Characterization of Rubber Compounds

The density of the rubber compounds was measured on few grams of the rubber compounds using Micromeritics Accupy C 1330 helium pycnometer. The dispersion of the filler in the rubber matrix was analyzed by Optical microscope. The analysis was performed on a freshly cut sample of vulcanized rubber compounds. The sample was freezed in liquid nitrogen and test sample to 1 micron was cut by Leica RM2165 microtome. The analysis was performed using Leica DM4000 M microscope with a 10x objective. Images of the surface of the samples were recorded. The images were analyzed by automatic image analysis technique using the Image-Pro Plus image analysis software. The dimensions, number of agglomerates, and percentage of undispersed filler in the rubber matrix were calculated. Vulcanization process, dynamic mechanical analysis and tensile mechanical analysis of the prepared rubber compounds were performed using the same instrumentation and procedures as described in section 4.2.3.

6.3 Results and Discussion

6.3.1 CNC/Silica Hybrid Synthesis

The CNC/Silica hybrid was synthesized by decorating the surface of CNCs with the layer of silica nanoparticles. The presence of numerous hydroxyl groups on the surface of CNCs act as nucleation centers and offer the possibility to decorate the surface with different organic and inorganic materials. However, CNCs obtained through sulfuric acid hydrolysis

process carry negative charges due to the attachment of sulfate groups on the surface of CNCs. Hence, cetyltrimethylammonium bromide (CTAB) was added during the synthesis of the hybrid. Since CTAB is a cationic surfactant, it can be adsorbed or aligned on the surface of CNCs and could act as a bridge of electrostatic attractions between the CNCs surface and silica solution and facilitate the deposition of silica on the CNCs surface [24]. CTAB functioned as nuclei center for the growth of silica particles and played an important role in the synthesis of core-shell structure of the CNC/Silica hybrid. A schematic diagram to hybrid synthesis is shown in Fig. 6.2.
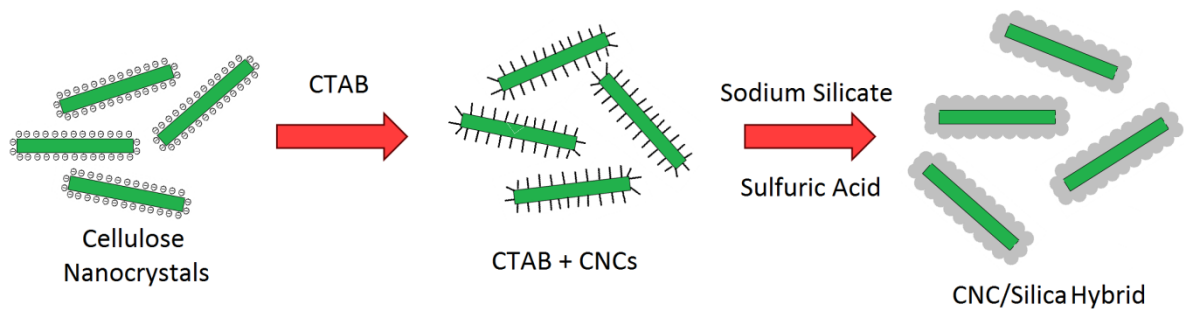

Figure 6.2: Schematic representation of mechanism of CNC/Silica hybrid synthesis

6.3.2 FTIR Analysis of CNC/Silica Hybrid

FTIR analysis was performed to confirm the synthesis of CNC/Silica hybrid and the formation of covalent bond between CNCs and silica. FTIR analysis of the hybrid was performed in comparison with pure CNCs and silica. FTIR spectra of CNCs, silica and CNC/Silica hybrid are shown in Fig. 6.3. The FTIR spectrum of CNC/Silica hybrid shows the characteristics peaks of both CNCs and silica. The peaks appeared at 1080 cm^{-1} and 800 cm^{-1} in the spectrum of silica correspond to the Si-O-Si asymmetric and symmetric stretching vibrations [25]. The stretching vibration of the Si-O-C or C-O-C bonds also appeared at 1100-1000 cm^{-1} and overlapped with the band of silica in the same spectral region [26,27]. An increase in the intensity of the peak at 1080 cm^{-1} was observed in the spectrum of the hybrid which shows a bond formation between CNCs and silica. Furthermore, it was also observed that the characteristic peaks of the CNCs appeared at
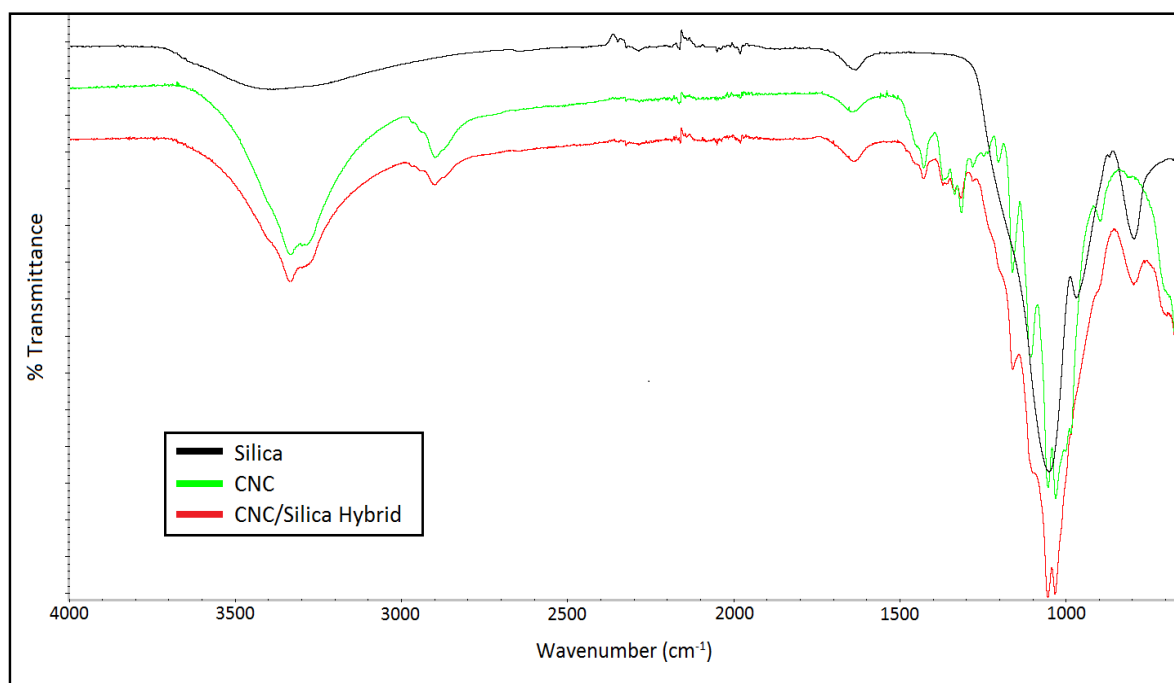
Figure 6.3: FTIR spectra of CNCs, silica and CNC/Silica hybrid

1155 cm^{-1}, 1105 cm^{-1} and 900 cm^{-1} corresponding to the stretching vibration of the C-C bond, C-O-C glycosidic ether bond, and C-O-C cellulose β-glycosidic linkage, respectively, were significantly weakened in the hybrid spectrum because these groups were covered by the layer of silica nanoparticles. Hence, these results showed that the silica was successfully decorated on the CNCs surface.

6.3.3 FESEM Analysis of CNC/Silica Hybrid

The morphology of the prepared CNC/Silica hybrid was studied by FESEM analysis. The FESEM images of the hybrids at different magnifications are shown in Fig. 6.4. A clear rod-like morphology of the CNC/Silica hybrid can be seen from these images, which shows that silica was successfully deposited on the surface of CNCs maintaining the original rod-like morphology of CNCs. The width of these rod-like particles ranges between 20 to 35 nm. As the original width of CNCs was from 5 to 20 nm, so these images show that silica layer of about 8-10 nm thickness was coated on the CNCs surface. The length of the hybrid was same as the length of CNCs i.e. 150-200 nm. These results confirmed the synthesis of core-shell structured CNC/Silica hybrid. A small degree of aggregation was observed in the

images that could be due to the formation of strong hydrogen bonding between the hydroxyl groups on the surface of silica.
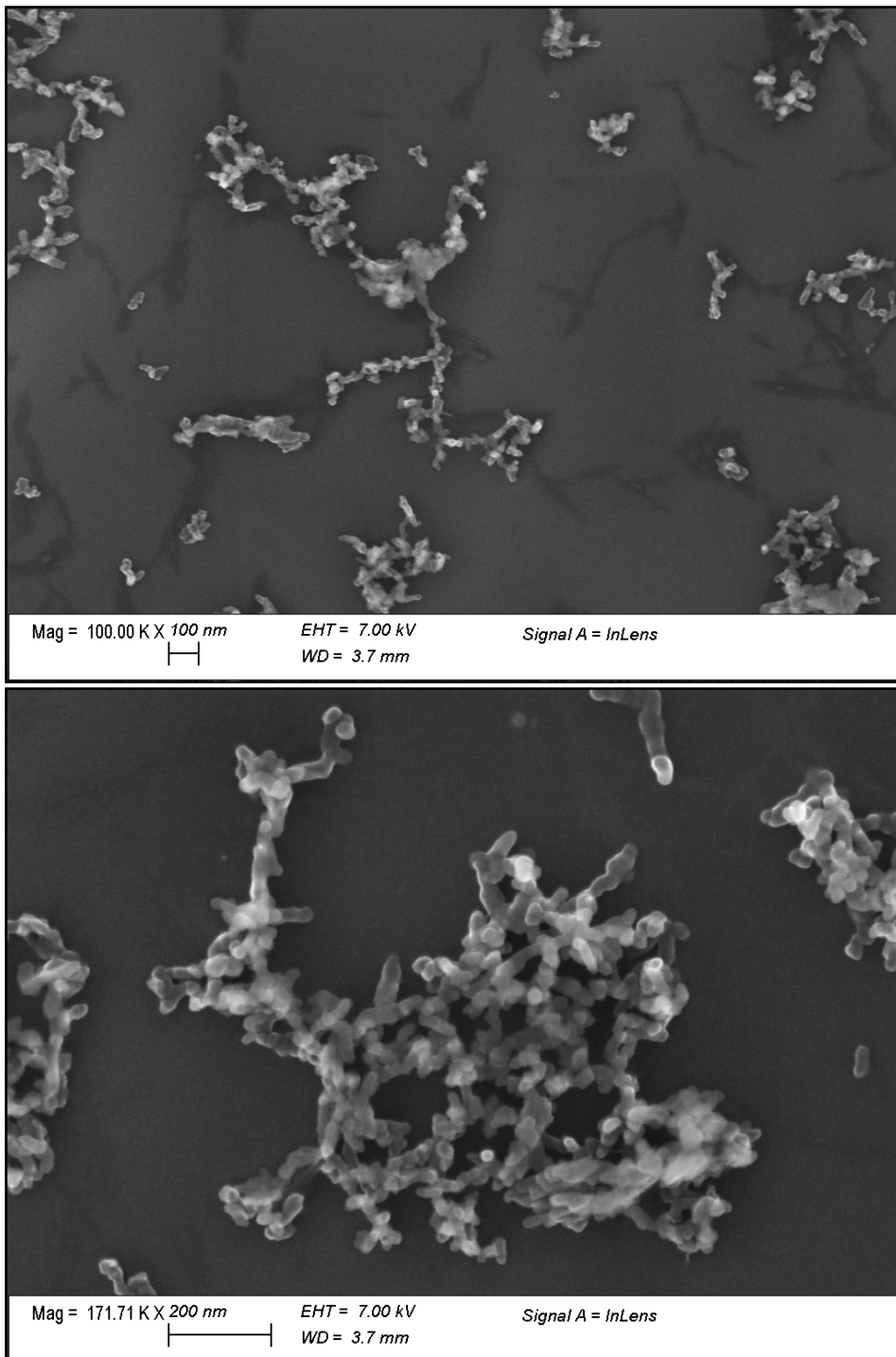

Figure 6.4: FESEM images of prepared hybrid at different magnifications

6.3.4 Nitrogen Physisorption Measurements of CNC/Silica Hybrid

The total surface area, external surface area, micropores area, and micropores volume of the CNC/Silica hybrid were measured before and after calcination at 600 $^\circ$C for 3 h. The values of the total surface area, external surface area, micropores area, and micropores volume are reported in Table 6.3. The total surface area of the pristine hybrid was 99.18 m^2/g, which was increased to 186.54 m^2/g after calcination which is due to the increase of micropores area. The micropores volume of the hybrid was also increased to about seven-fold after the calcination. It was proposed that the CNCs functioned as template in the synthesis of CNC/Silica hybrid, the removal of CNCs through calcination created the silica

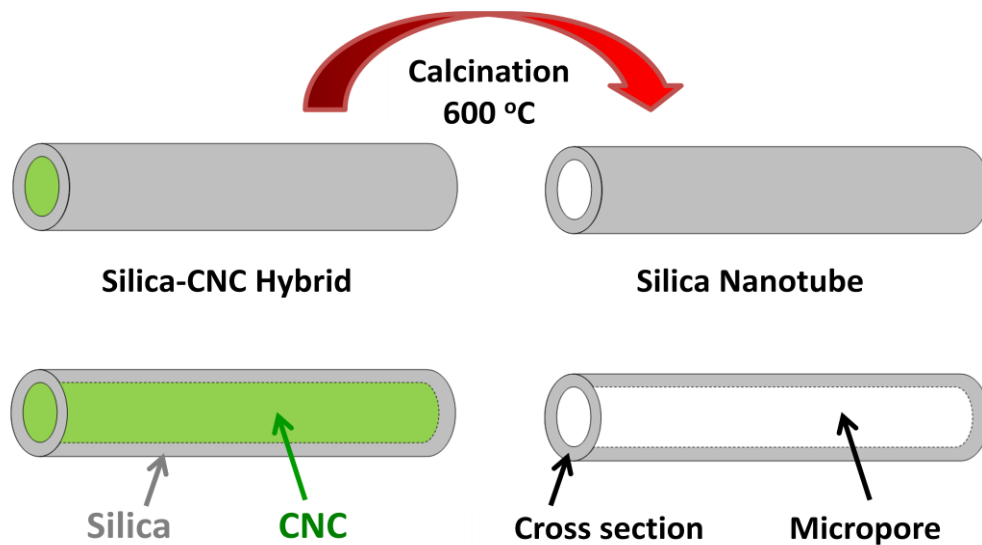**Figure 6.5:** Schematic representation of micropores creation after calcination

Table 6.3: Surface area and pore volume of the hybrid before and after calcination

Sample	Total Surface Area (m^2/g)	External Surface Area (m^2/g)	Micropores Area (m^2/g)	Micropores Volume (cm^3/g)
Hybrid	99.18	84.68	14.50	0.005613
Hybrid (Calcined)	186.54	114.78	71.76	0.039176

nanotubes with micro-channel or micropores. Due to the creation of this micro-channel, the micropores area and micropores volume were significantly increased. A schematic diagram representing the creation of micropores after the calcination of the pristine hybrid is shown in Fig. 6.5. These results support our proposal of formation of the core-shell structure of the CNC/Silica hybrid and are in good agreement with the FESEM results.

6.3.5 TGA Analysis CNC/Silica Hybrid

The thermal gravimetric analysis of the CNC/Silica hybrid was performed not only to measure the CNCs and silica contents but also to study the thermal stability of the prepared hybrid during the processing of the rubber compounds. It is important that the material must be thermally stable during the mixing and vulcanization process. Typically, the vulcanization process is carried out at temperatures of 140 - 170 ^{o}C for 10 - 30 min, so the material should withstand the high processing temperatures during this process. Therefore, the TGA analysis was performed in three steps with two isothermal
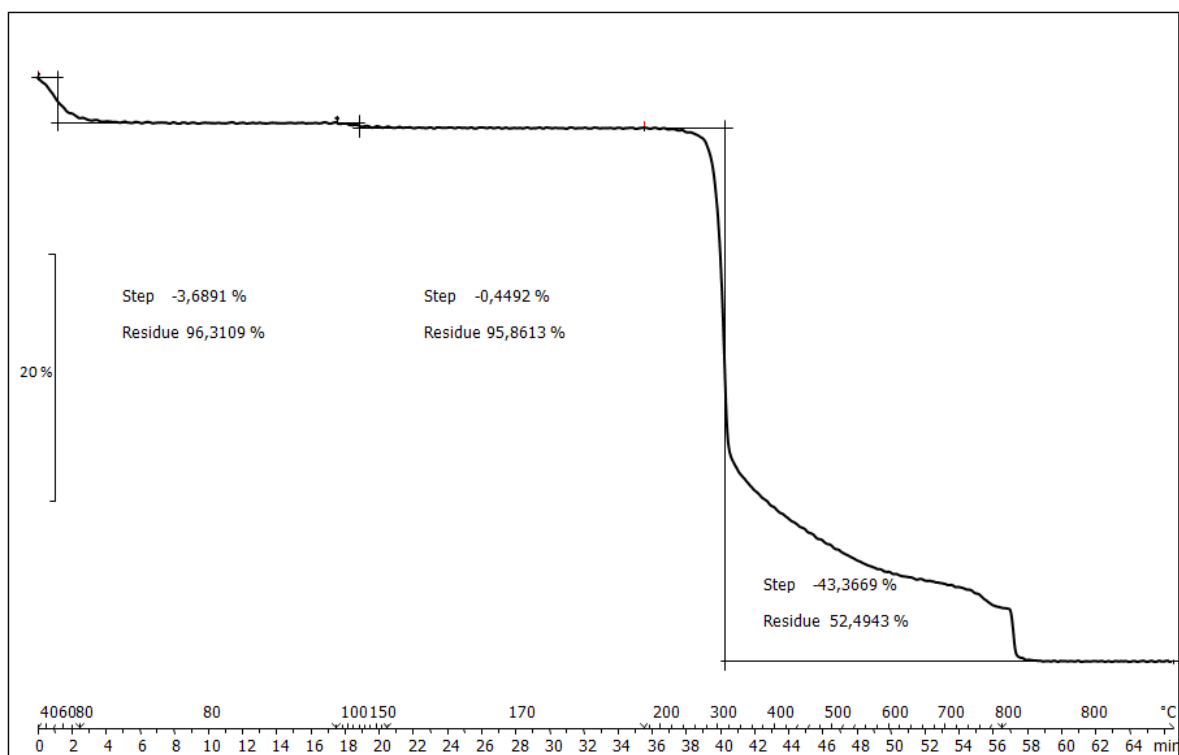

Figure 6.6: TGA curve of the CNC/Silica hybrid

134

conditioning periods, each one lasting for 15 min. The TGA curve of the prepared hybrid is shown in Fig. 6.6. The first step performed at 30-80 ^{o}C showed a weight loss of about 3.7 % due to the loss of adsorbed water. The presence of physisorbed water is very important and reactivity of silane with silica is strongly influenced by the physisorbed water [28–30]. The second step performed at 80-170 ^{o}C was carried out to access the thermal stability of the hybrid during the vulcanization process. The results showed a high thermal stability of the hybrid and only 0.44 % weight loss was observed which is due to the loss of water produced by the condensation of silanol groups on the silica surface. The third step performed between 170-800 ^{o}C was carried out to determine the loading of silica on CNCs surface. The prepared hybrid was thermally stable up to 280 ^{o}C, and then the CNCs started to decompose. From the results, it was calculated that the prepared CNC/Silica hybrid contains about 45 % of CNCs contents and about 55 % of silica contents.

6.3.6 XRD Analysis

The crystalline structure of the prepared hybrid was investigated by XRD. The XRD patterns of CNCs, silica and prepared hybrid are shown in Fig. 6.7. Broad peak observed in
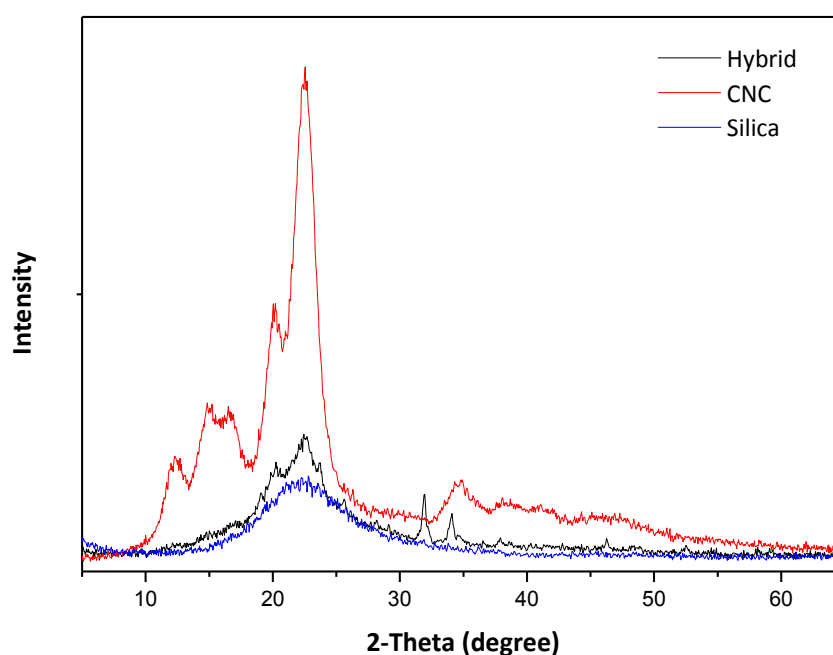

Figure 6.7: XRD patterns of silica, CNCs, and the hybrid

the XRD pattern of silica centered at 2-theta = 22.2^o shows the amorphous structure of the silica. The CNCs showed high crystallinity and XRD pattern of CNCs showed the characteristics peaks of the cellulose Iβ and cellulose II. Peaks observed at 2-theta = 14.8^o, 16.5^o, 22.5^o, and 34.6^o correspond to the cellulose Iβ and two other peaks observed at 12.2^o and 20.2^o correspond to the cellulose II. The XRD pattern of the hybrid displayed the combined reflection of CNCs and silica. The peaks observed at 2-theta = 20.2^o and 22.5^o correspond to the characteristic peaks of CNCs combined with the broad peak of silica. The crystallinity of the hybrid was reduced due to the presence of amorphous silica. A sharp small peak observed at 2-theta = 31.9^o is due to sodium sulfate, formed during the hybrid synthesis. The presence of a small percentage of sodium and sulfur was confirmed by the elemental analysis.

6.3.7 Rubber Compounds of CNC/Silica Hybrid

6.3.7.1   Properties of Rubber Compounds

Two different methods used for the preparation of rubber compounds demonstrated a significant effect on the dispersion of fillers in the rubber matrix. The dispersion of the filler in polymer matrix plays an important role in determining the reinforcement capability of the filler. The optical microscope images of the prepared rubber compounds, showing the filler dispersion in the rubber matrix, are shown in Fig. 6.8. Silica and hybrid agglomerates can be clearly seen as white dots and carbon black as black dots. Table 6.4 shows the data obtained from the automatic image analysis. A high agglomeration of the hybrid was observed in the dry-mixed compound while the hybrid was homogeneously dispersed in the co-precipitated compound. During the drying process of hybrid, the high surface area and high aspect ratio lead to aggregation of hybrid nanoparticles. The dry mixing process of this hybrid with natural rubber in the internal mixer was not able to break down these aggregates and resulted in the poor dispersion of hybrid in the rubber matrix. On the other hand, during the co-precipitation method, the hybrid suspension was not dried and mixed as such with natural rubber latex. This process resulted in a very high dispersion of hybrid in the rubber matrix. Processing method does not have considerable
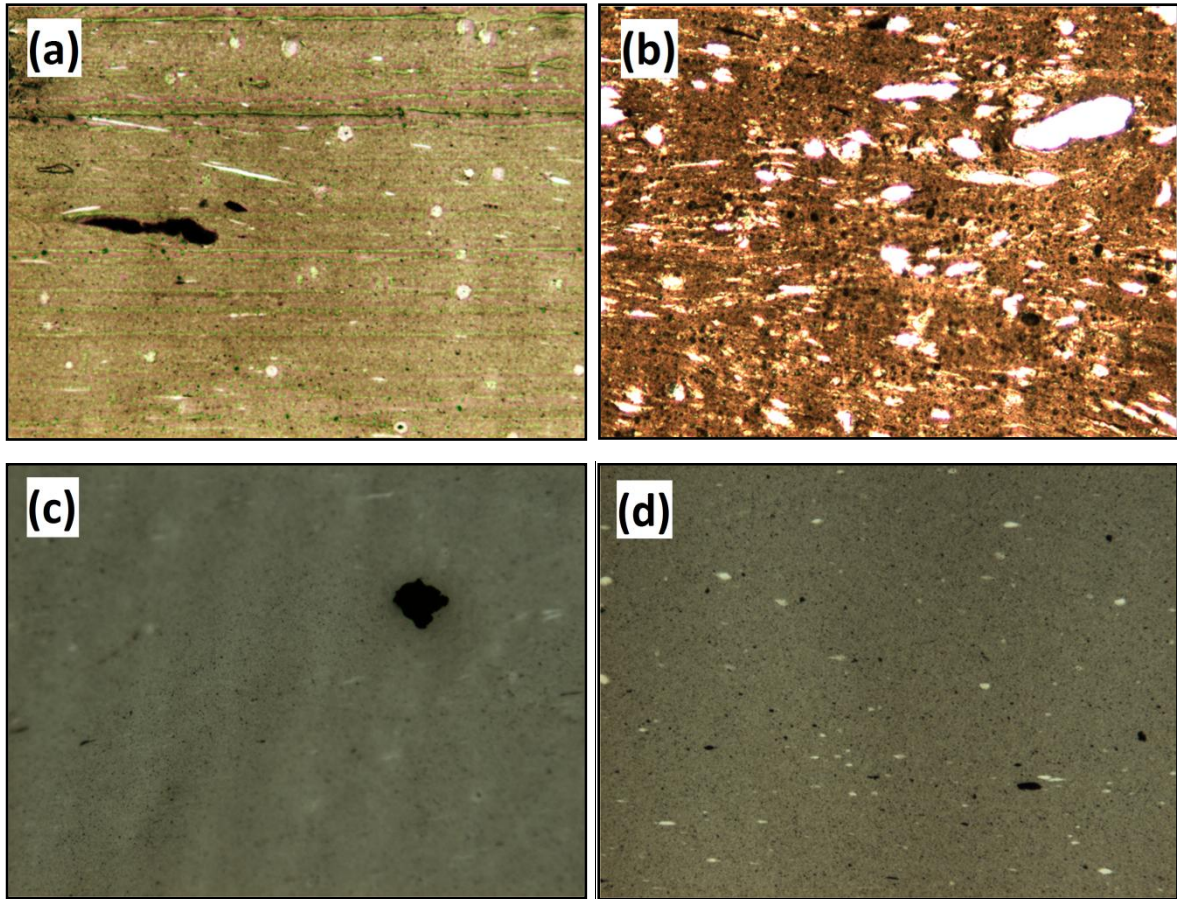
Figure 6.8: Optical microscope images of (a) Dry-Silica (b) Dry-CSH (c) Co-Silica (d) Co-CSH compounds at magnification of x100

Table 6.4: Automatic image analysis data of the prepared compounds

	Dry-Silica	Dry-CSH	Co-Silica	Co-CSH
Min diameter [μ]	9.47	7.36	9.75	7.82
Max diameter [μ]	30.80	95.37	26.08	18.25
No. of aggregates	25	374	21	34
Undispersed filler (Silica) [%]	0.23	15.93	0.44	0.43
Undispersed filler (CB) [%]	9.21	3.94	6.85	6.56

influence on silica dispersion, as commercial high dispersible silica was used, is the study. Therefore, silica was highly dispersed in both methods, but slightly better dispersion was observed in compound prepared through the co-precipitation method.

The vulcanization characteristics, such as scorch time (T_S2), optimum curing time (T_{90}), minimum (M_L), and maximum (M_H) values of torques of the prepared compounds, were calculated from vulcanization curves. The vulcanization curves of the prepared compounds are shown in Fig. 6.9. Table 6.5 shows the vulcanization parameters of the prepared compounds. The hybrid has almost the same vulcanization behavior irrespective of the preparation method. However, the behavior of hybrid is quite different from its corresponding reference silica compound. The hybrid has a significant effect on the scorch time and optimum curing time of the prepared compounds. T_S2 and T_{90} of the hybrid compounds are quite lower than the silica compounds. T_S2 and T_{90} are the two important parameters of vulcanization process and represent the time of initiating crosslinking reactions and the time required for the optimum value of curing. These two parameters determine the curing rate index (CRI) which is proportional to the average slope of cure rate in the steep region [CRI= $100/(T_{90}-T_S2)$] [31]. Vulcanization process of hybrid compounds was much faster and showed quite higher values of CRI than the corresponding silica compounds. Hence, these results show that the hybrid accelerated the process of vulcanization and reduced the time of initiating the curing process and time
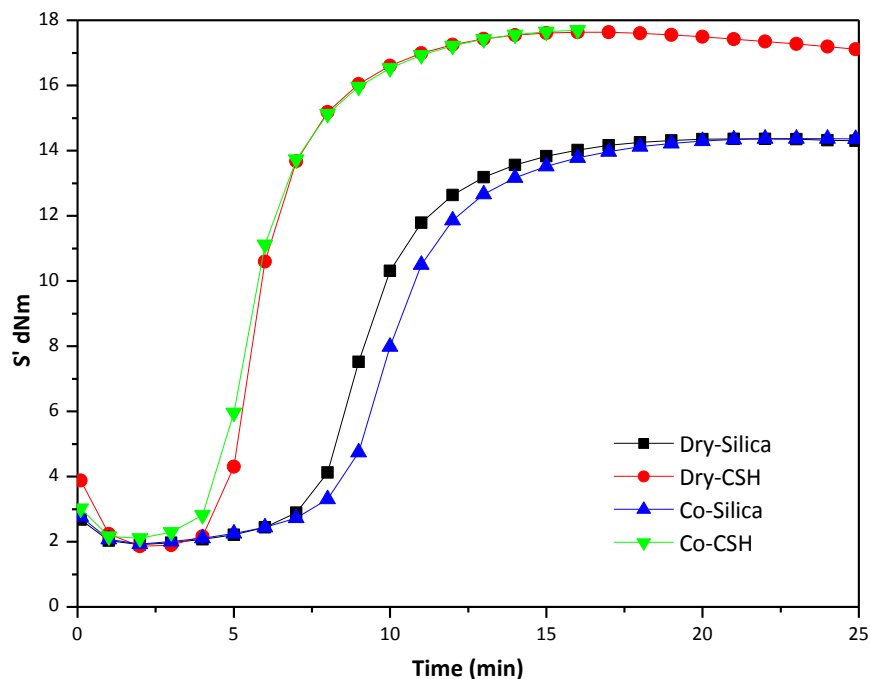

Figure 6.9: Vulcanization curves of the prepared compounds

Table 6.5: Vulcanization parameters of the prepared compounds

Parameter	Dry-Silica	Dry-CSH	Co-Silica	Co-CSH
T_S2 (min)	7.33	4.8	7.83	4.46
T_{90} (min)	12.87	9.02	13.92	9.28
CRI (min^{-1})	18.05	23.70	16.42	20.75
M_L (dNm)	1.91	1.86	1.93	2.06
M_H (dNm)	14.37	17.64	14.38	17.71
ΔM (dNm)	12.46	15.78	12.45	15.65

of curing and increased the curing rate of the rubber compounds. This is due to the fact that the silica could adsorb the vulcanizers which lead to the slowdown of vulcanization process [32]. Two other important parameters of the vulcanization process are M_L and M_H. M_L is directly related to the viscosity of the compounds in unvulcanized state at the test temperature. It was observed from the results that the M_L values are almost similar for all the compounds. This implies that the hybrid did not have a significant effect on the viscosity of the unvulcanized compounds. M_H predominantly depends on the crosslinking density and reinforcement of filler in the rubber matrix [33]. The M_H values of the hybrid compounds are much higher than the corresponding reference silica compounds. This observation is attributed to the increased crosslink density. The degree of crosslinking, calculated as the difference between the maximum and minimum torques ($\Delta M = M_H - M_L$), is quite higher for the hybrid compounds than silica compounds. This showed a higher reinforcement effect of the hybrid than silica [34,35]. These results showed that the hybrid has improved vulcanization characteristics than silica and preparation method of rubber compounds did not have a significant influence on vulcanization characteristics.

Dynamic mechanical analysis of the prepared rubber compounds was performed in shear stress mode before and after vulcanization. The effect of the hybrid as reinforcing filler in comparison with silica on the dynamic mechanical properties, such as storage modulus and tan δ, was studied. The effect of the processing methods of rubber compounds on these properties was also investigated. The strain sweep curves of the unvulcanized and vulcanized compounds are shown in Fig. 6.10. All the compounds either unvulcanized or

vulcanized showed viscoelastic behavior, characterized by the typical non-linear dependence of storage modulus G' on the applied dynamic strain. This strain softening is due to the breakdown of the filler network upon oscillatory shear. Based on this widely accepted mechanism, the modulus at low strain (G'_o) is the representative of filler-filler interactions. The modulus at high strain (G'_∞) comes from three strain independent contributions; polymer network, hydrodynamic effect and in-rubber structure (filler-polymer interactions). The higher G'_o values for the hybrid compounds than the silica compounds demonstrated the stronger filler-filler interactions and higher reinforcement effect. The strong filler network of hybrid is attributed to the high aspect ratio of the hybrid particles which enhanced the possibility to make strong hydrogen bonding between particles. Furthermore, the G'_∞ is higher for Co-CSH compound than other hybrid and silica compounds in unvulcanized and vulcanized states. At high strain, only different filler-rubber interactions could differentiate the dynamic mechanical characteristics of the compounds, as the filler particles are supposed to be not mutually interacting. This high value of G'_∞ for Co-CSH compound is due to better dispersion and the large contact area between the anisotropic hybrid particles and polymer. The behavior of the hybrid was strongly influenced by the compound preparation method. In the unvulcanized compounds, the Dry-CSH showed much higher G'_o value (high filler-filler interactions) than Co-CSH. This is due to the poor dispersion of the hybrid during the dry-mixing process which increased the interaction between the hybrid aggregates and resulted in high stiffness of the compound at low strain. It should be noted that a high value of G'_o does not mean the filler network is percolated throughout the specimen. Local subnetworks also contribute to the G'_o value and yield a Payne effect [36]. The hybrid prepared through the co-precipitation method was efficiently dispersed, which resulted in lower filler-filler interactions but higher filler-polymer interactions, as evident by the higher value of modulus for Co-CSH at high strain. The dispersion of the hybrid in prepared compounds was investigated and poor dispersion of the hybrid during dry mixing was observed. Also, the Payne effect of the Co-CSH compound is much lower than Dry-CSH compound which shows a high filler networking capability of the hybrid in dry mixing. On the other hand, after the vulcanization of hybrid compounds, the Co-CSH has higher G'_o than Dry-CSH but similar G'_∞ values. Due to the high degree of crosslinking of hybrid compounds, the

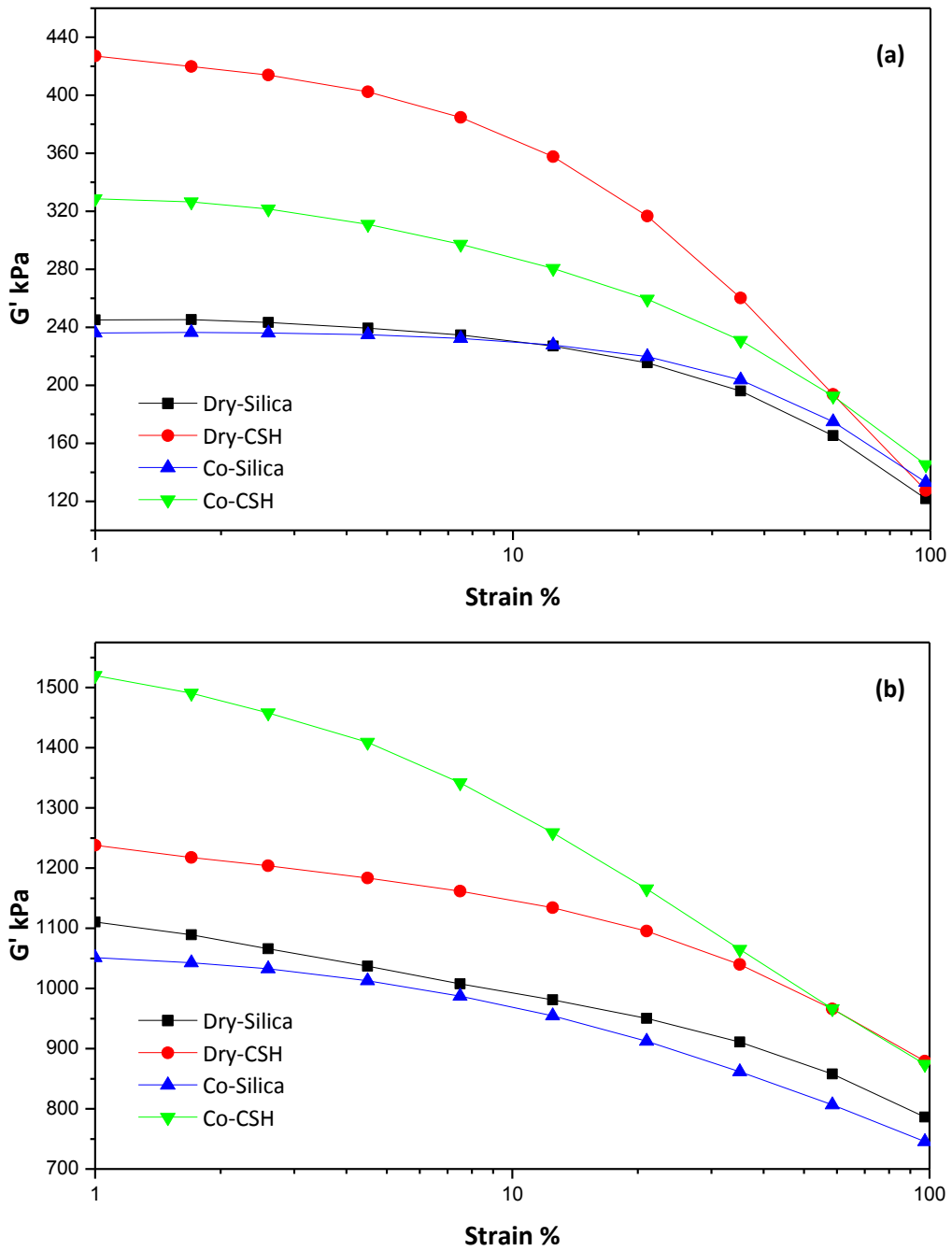**Figure 6.10:** Storage modulus *vs* strain of (a) unvulcanized (b) vulcanized compounds

Table 6.6: Payne effect of unvulcanized and vulcanized compounds

Compounds	Dry-Silica	Dry-CSH	Co-Silica	Co-CSH
Payne Effect ($\Delta G = G'_o - G'_\infty$)				
Unvulcanized	123.23	299.56	103.06	183.40
Vulcanized	324.06	359.09	305.66	646.22

difference of filler-polymer interactions between the two hybrids was diminished and showed similar modulus at high strain. The higher G'_o for Co-CSH could be due to the flocculation of the filler during the vulcanization process. At high temperature during the vulcanization, the low viscosity of the polymer enhances the mobility of the filler, which tends to aggregate and make strong filler network. As the hybrid was already agglomerated in the dry-mixed compound, filler network did not contribute significantly to the increase of modulus, as no considerable change in Payne effect was observed after vulcanization. The increase in modulus after the vulcanization is due to the formation of the crosslinked polymer network. A similar trend was observed in the case of silica compounds but the difference was very small because the silica was well dispersed in both compounds. A small difference in Payne effect of the two compounds was observed and Co-Silica compounds showed lower Payne effect than Dry-Silica compounds which is probably due to the better dispersion of silica by co-precipitation, which resulted in lower filler-filler but higher filler-polymer interactions. In the vulcanized compounds, two silica compounds showed the same behavior against increasing strain but a parallel shift of the curve of Co-Silica to lower values of the modulus. It was supposed that this parallel shift in the G' value was caused by a strain-independent contribution. As the filler and crosslink density of the two compounds are same, so this shift can only be due to in-rubber structure [36]. In-rubber structure is the measure for the rubber entrapped between the filler, term as occluded rubber, which is shielded from deformation and enhance the effective filler loading. During the co-precipitation, the structure of the silica was slightly lowered which resulted in a parallel shift to lower modulus values.

The effect of strain amplitude on the Tan δ of unvulcanized and vulcanized compounds is shown in Fig. 6.11. Tan δ is the ratio of loss modulus (G") to storage modulus (G'). For a viscoelastic material, the G' measures the stored energy and represents the elastic portion, while G" represents the energy dissipated as heat (viscous portion) and depend on the rates of filler network breakdown and reformation due to the strain amplitudes [37]. In the unvulcanized compounds at low and intermediate strains, the Tan δ remained constant then increased sharply with increasing strains and reached at highest value at high strain amplitude. At low strains, the filler network is capable to reform after deformation and the viscous polymer is stabilized by the filler network, hence a low hysteresis was observed.
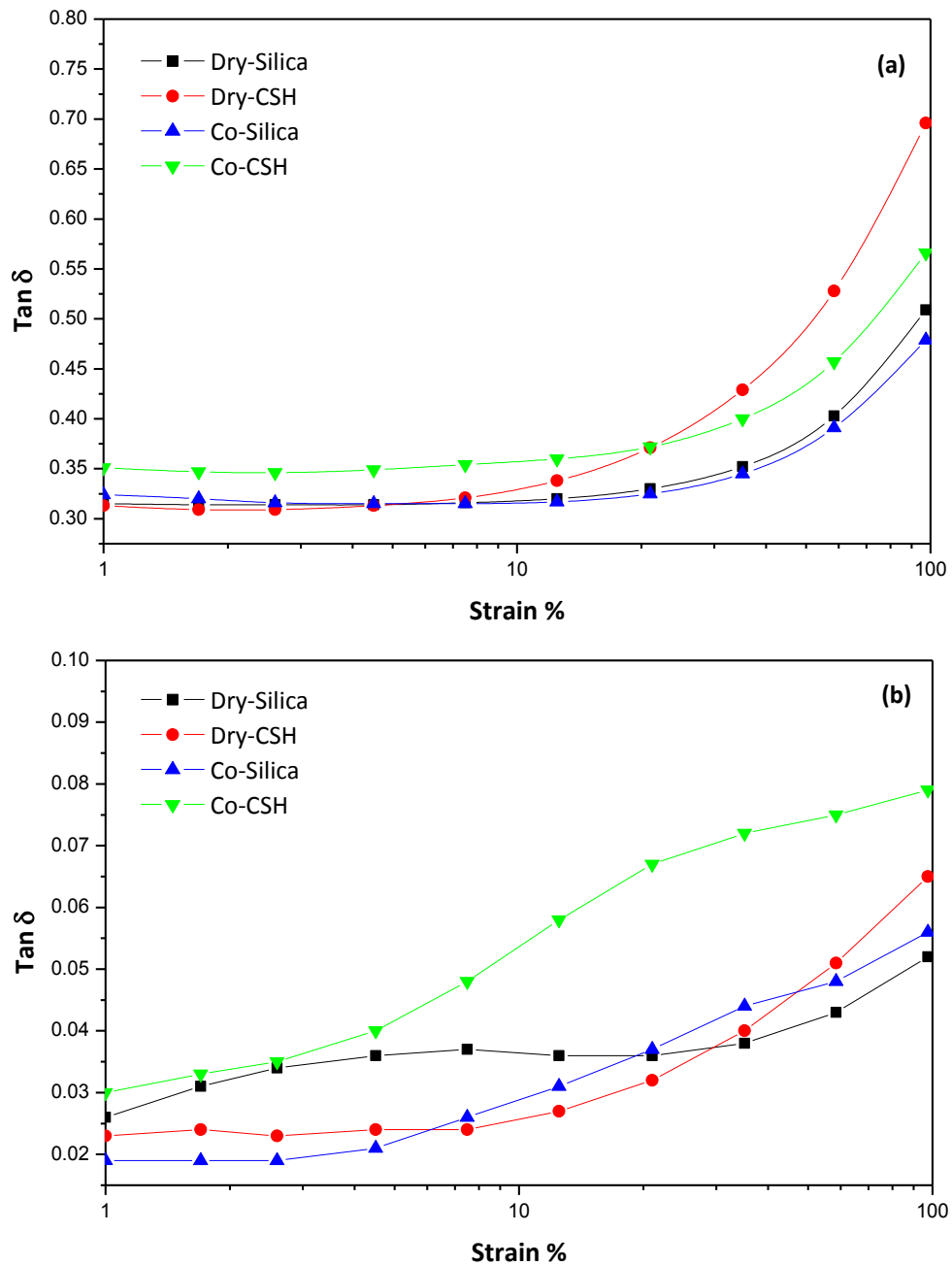
Figure 6.11: Tan δ *vs* strain of (a) unvulcanized (b) vulcanized compounds

While at high strain, filler network is broken down and not able to reform in the time frame of dynamic measurement, so polymer chains are no more stabilized by the filler and show more viscous behavior, hence a high hysteresis was observed. It was observed that the two silica compounds have almost same behavior, while the two hybrids showed quite different behavior. The Co-CSH compound showed higher hysteresis than the silica compounds. It can be explained as the hysteresis is resulted due to filler breakdown, so the disruption of a strong filler network during straining dissipates more energy.

Furthermore, the hysteresis for Co-CSH compounds was higher than Dry-CSH at low strain but lower at high strain amplitude. This is due to the fact that after the breakdown of filler network, Dry-CSH showed more viscous behavior while the viscous behavior of the Co-CSH was stabilized by the higher filler-polymer interaction which is in agreement with the results of storage modulus obtained through strain sweep. For a given filler, the absolute value of Tan δ drastically reduced after the vulcanization which is due to the less viscous nature of the crosslinked polymer matrix. After the vulcanization, the Co-CSH compound still has a higher value to Tan δ than other compounds, as the breakdown of strong filler network dissipates more energy. The two silica-filled compounds showed different behavior in vulcanized state. As the co-precipitation method slightly lowered the structure of silica, Dry-Silica compound has higher Tan δ at low strain than Co-Silica due to strong filler network of Dry-Silica which build up more heat during cyclic deformation, while at high strains due to improved filler-polymer interactions the Dry-Silica compound has lower Tan δ values.

The effect of hybrid as filler on the tensile mechanical properties of the rubber compounds, such as tensile strength (TS), elongation at break (Eb), modulus at 300 % strain, was investigated in comparison with silica. The effect of the processing method of compounds on these properties was also studied. Typical stress-strain curves of the prepared compounds obtained from the tensile tests are shown in Fig. 6.12. Modulus at different strain amplitudes, tensile strength, and elongation at break are given in Table 6.7. A clear difference between the tensile properties of the two hybrids and silicas compounds was observed due to the different processing method. Furthermore, tensile properties of the hybrid were quite different than corresponding silica compound. Significant improvement in the tensile properties of the hybrid compound prepared through the co-precipitation was observed and showed very high reinforcement as compared to silica compounds. Two hybrids compounds have very high modulus than silica compounds up to 100 % elongation, and then the modulus of Dry-CSH started to decrease as compared to Co-CSH. The agglomeration of hybrid in dry-mixed compounds lead to poor dispersion in the polymer matrix which resulted in lower tensile strength, elongation at break, and modulus at 300% strain. A higher modulus than silica at low strains up to 200 % elongation was due to the higher stiffness of rod-like rigid filler. On the other hand, when the
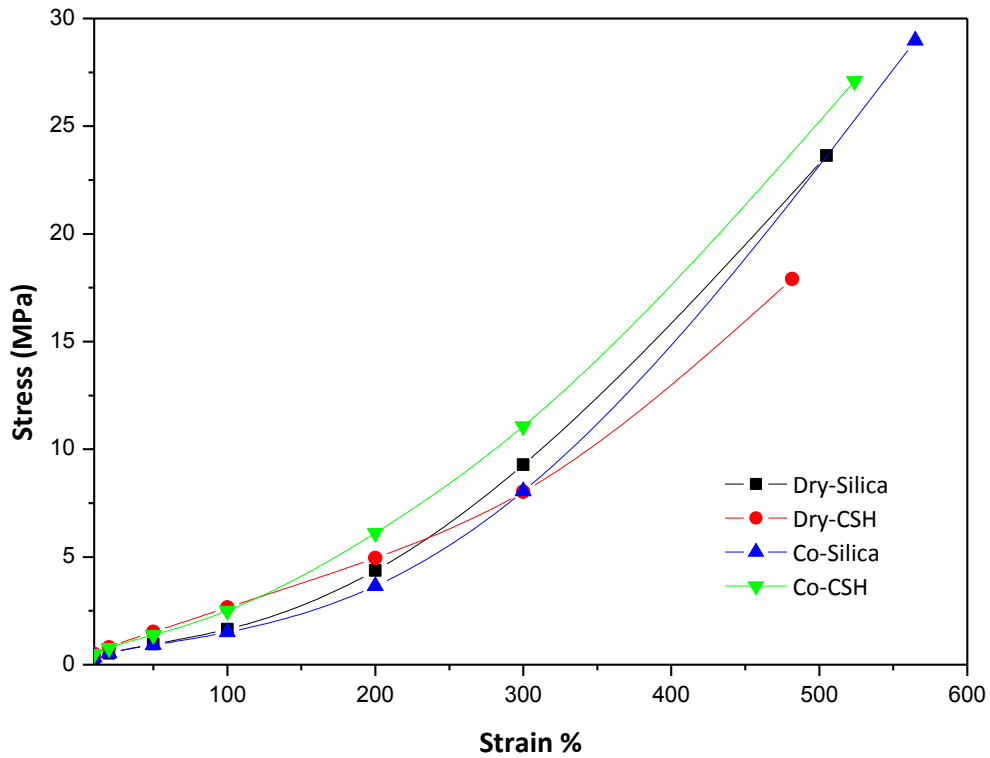
Figure 6.12: Stress-strain curves of the prepared compounds

Table 6.7: Tensile mechanical properties of the prepared compounds

Property	Dry-Silica	Dry-CSH	Co-Silica	Co-CSH
Stress 10% (MPa)	0.32	0.50	0.33	0.50
Stress 50% (MPa)	0.95	1.52	0.91	1.38
Stress 100% (MPa)	1.65	2.65	1.51	2.51
Stress 200% (MPa)	4.37	4.95	3.65	6.11
Stress 300% (MPa)	9.28	8.02	8.06	11.07
Elongation at break (%)	504.82	481.61	564.85	523.90
Tensile Strength (MPa)	23.64	17.90	28.97	27.09

compound was prepared through the co-precipitation, high dispersion of the hybrid in the rubber matrix was obtained. High dispersion of the filler increased the contact area between the anisotropic hybrid filler and the polymer resulted in stronger interfacial interaction between the hybrid filler and polymer, which allowed achieving the improved mechanical properties of the hybrid-filled rubber compounds. Furthermore, this high

reinforcing effect of Co-CSH can be assigned to well-known percolation phenomenon of high aspect ratio fillers, which formed a stiffer continuous network of these rod-like hybrid nanoparticles as compared to silica. The tensile behavior of the two silica compounds was slightly different which is due to the different processing method. The Dry-Silica compound showed better reinforcing effect than Co-Silica compound. The Silica was more uniformly distributed through the co-precipitation method, which improved the tensile strength and elongation at break but modulus at 300 % strain was lowered. In tire industry, the modulus at 300 % elongation is considered as the signature of reinforcement and considered more important than tensile strength and elongation at break. Modulus of the Co-CSH at 300 % elongation is much higher than both silica reference compounds which show the enhanced reinforcing ability of the hybrid. The orientation of the high aspect ratio filler particles under strain as well as the formation of strong filler network is attributed to the high level of reinforcement.

6.3.7.2 Effect of Filler Contents

The rubber compounds were prepared at a different loading of hybrid and reference silica to study the effect of filler contents on the properties of the rubber compounds. The compounds were prepared at 20, 30 and 40 phr of filler loading. The vulcanization parameters, such as scorch time (T_S2), optimum curing time (T_{90}), curing rate index (CRI), minimum (M_L) and maximum (M_H) values of torques, and degree of crosslinked (ΔM) are reported in Table 6.8. Results showed that the scorch time slightly decreased while the optimum curing time increased with the increase of filler contents. Hence, cure rate index (CRI) representative of vulcanization rate decreased with the increase of filler loading for both hybrid and silica compounds. The decrease of T_S2 and increase of T_{90} with increasing filler contents could be due to the fact that, at higher filler contents more silane coated filler is available which facilitate the early start of the vulcanization process [38]. It can be clearly seen from the ΔM values that the crosslink density is high at high filler contents so the vulcanization process took more time for completion, so high T_{90} was observed. For a given loading of filler, the T_S2 and T_{90} for the hybrid were lower while CRI was higher than the respective reference silica compound. Hence, hybrid compounds showed a higher rate of vulcanization than silica compounds. Two other important characteristics of

Table 6.8: Effect of filler loading on vulcanization parameters of prepared compounds

Parameter	Silica-20	Silica-30	Silica-40	CSH-20	CSH-30	CSH-40
T_S2 (min)	1.45	1.5	1.49	1.22	1.21	1.14
T_{90} (min)	3.01	3.41	3.42	2	2.43	2.72
CRI (min^{-1})	64.10	52.35	51.81	128.20	81.96	63.29
M_L (dNm)	0.81	1.32	1.98	0.69	0.88	2.09
M_H (dNm)	11.83	13.6	16.09	12.15	14.17	19.14
ΔM (dNm)	11.02	12.28	14.11	11.46	13.29	17.05

vulcanization process i.e. minimum (M_L) and maximum (M_H) torques also showed an increasing trend with the increase of filler loading in both silica and hybrid compounds. As the M_L is indicative of the effective viscosity of the unvulcanized compounds, at high filler contents the viscosity of the unvulcanized compounds increases which resulted in high M_L values. A high M_H value at high filler content shows an increase of crosslinking with the increase of filler contents. This is also clear from the value of ΔM, which increases with the increase of filler loading showing an increasing degree of crosslinking. The formation of crosslink between the filler and polymer through the coupling agent lead to the enhancement in crosslink density. At high filler loading, more silane is available for polymer-filler crosslinking, which resulted in increased crosslink density of the compounds. The crosslinking density of the hybrid is higher than silica compounds and this effect is more pronounced at high filler loading.

The effect of filler loading on the dynamic mechanical properties of the rubber compounds is summarized in Table 6.9. The storage modulus (G') and Tan δ at 9 % strain as a function of filler contents are shown in Fig. 6.13. Both G' and Payne effect increase with the increase of filler contents in silica as well as in hybrid compounds. This increase is due to the formation of increased filler network. The inter-particle distances decrease with the increase of filler contents and hence increased the possibility of the formation of the filler network. The hybrid showed higher G' and Payne effect than respective silica compounds and effect is more pronounced at high filler contents which are attributed to the high

Table 6.9: Effect of filler loading on dynamic mechanical properties of rubber compounds

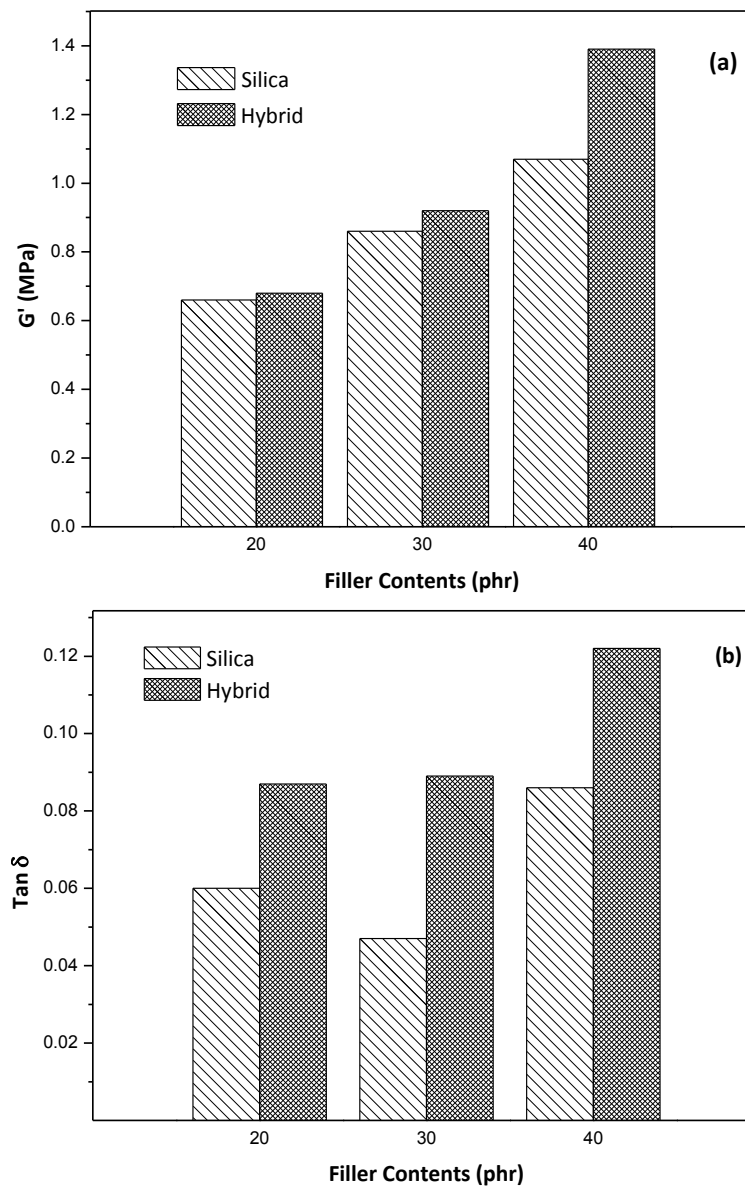| Parameter	Silica-20	Silica-30	Silica-40	CSH-20	CSH-30	CSH-40
G' (9%) [MPa]	0.66	0.86	1.07	0.68	0.92	1.39
G' (3%) [MPa]	0.69	0.9	1.17	0.73	0.95	1.6
ΔG' (0.5-10) [MPa]	0.28	0.34	0.49	0.25	0.44	0.98
Tan δ (9%)	0.06	0.047	0.086	0.087	0.089	0.122
Tan δ (3%)	0.064	0.06	0.097	0.089	0.091	0.119

Figure 6.13: Effect of filler contents on (a) Storage modulus (b) Tan δ at 9 % strain

aspect ratio of the hybrid particles which formed more stronger filler-network than silica. The Tan δ values also increase with the increase of filler contents. As the Tan δ represents the amount of energy dissipation during straining, at high filler loading, a strong filler network is formed. So, the disruption of increased filler network during the straining dissipates more energy.

The density of the prepared compounds is shown in Table 6.10. Hybrid compounds showed much lower density as compared to silica-filled rubber compounds, which is due to the lower density of the prepared hybrid than silica. Therefore, the negative effect of high density of silica was minimized by introducing the hybrid as filler in rubber compounds, in addition to the higher reinforcing effect of the hybrid than silica.

Table 6.10: Density of the prepared compounds

Parameter	Silica-20	Silica-30	Silica-40	CSH-20	CSH-30	CSH-40
Density (g/cm^3)	1.054	1.097	1.131	1.046	1.066	1.095

The effect of filler contents on the tensile mechanical properties of the rubber compounds was investigated. The Fig. 6.14 shows the stress-strain curves of the compounds prepared at different filler loadings. The modulus at 10, 50, 100, 200 and 300 % elongation, elongation at break, and tensile strength are summarized in Table 6.11. It can be clearly

Table 6.11: Effect of filler loading on tensile mechanical properties of prepared compounds

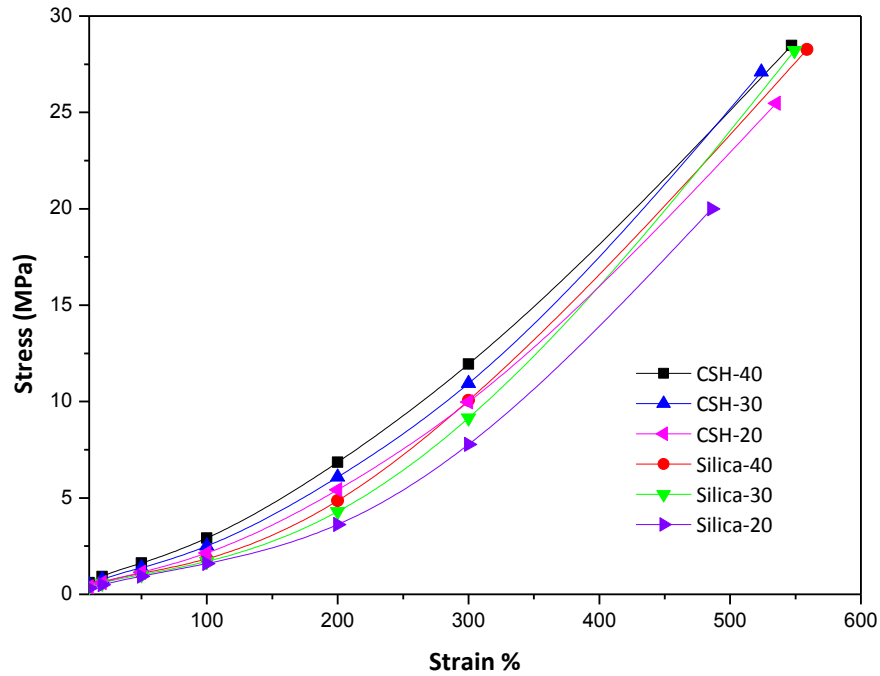| Parameter	Silica-20	Silica-30	Silica-40	CSH-20	CSH-30	CSH-40
Stress 10% (MPa)	0.32	0.38	0.41	0.38	0.5	0.61
Stress 50% (MPa)	0.94	1.02	1.09	1.14	1.38	1.64
Stress 100% (MPa)	1.6	1.71	1.84	2.14	2.51	2.94
Stress 200% (MPa)	3.62	4.29	4.86	5.42	6.08	6.85
Stress 300% (MPa)	7.77	9.15	10.08	9.98	10.94	12.04
Elongation at break (%)	486.89	549.21	562	535.3	523.9	543.46
Tensile Strength (MPa)	20.37	28.92	27.96	25.47	27.09	28.41

Figure 6.14: Stress-strain curves of the compounds at different filler contents

seen from the results that the reinforcement increases with the increase of filler contents. The reinforcement imparted by the addition of hybrid is considerably higher than those provided by the respective silica. It is interesting to note that, the compounds prepared with 20 phr of hybrid showed similar reinforcement as 40 phr of silica, however considerable improvement in the density of the final compound was observed.

6.4   Conclusions

A hybrid of CNCs and silica was synthesized and used as reinforcing filler in natural rubber compounds. The CNC/Silica hybrid was prepared by a simple and efficient co-precipitation method using CNCs as a template and the surface was coated with a silica layer. The core-shell structure of the prepared hybrid was confirmed by FESEM and surface area analysis. Silica layer of about 8-10 nm thickness was decorated on the surface of CNCs. The crystallinity of the hybrid was checked by XRD analysis, the crystal structure of the CNCs was preserved however decrease in crystallinity was observed due to the presence of amorphous silica part. TGA analysis demonstrated that the prepared CNC/Silica hybrid contains about 45 % of CNCs contents and about 55 % of silica contents. The hybrid was

incorporated as reinforcing filler in natural rubber using dry-mixing and co-precipitation methods and compared with standard high reinforcing silica used in the tire industry. Vulcanization characteristics, dynamic mechanical and tensile mechanical properties were investigated. The high aspect ratio of rod-like hybrid particles developed not only strong filler network but also strong filler-polymer interactions. The compounds prepared by the co-precipitation method showed the high dispersion of hybrid in the rubber matrix and demonstrated much higher reinforcing effect than dry-mixed hybrid compound as well as reference silica compounds. The effect of filler contents of hybrid on the physio-mechanical properties of the prepared compounds was studied and compared with reference silica. It was demonstrated that the compounds prepared with 20 phr of hybrid showed similar reinforcement as 40 phr of silica, however significant improvement in the density of the final compound was observed. Based on the obtained results, it was concluded that the hybrid can be used as a potential reinforcing filler in tire tread compounds with higher reinforcement and lower density than tradition silica filler.

References

[1]   A.P. Wight, M.E. Davis, Chem. Rev. 102 (2002) 3589–3614.

[2]   F. Hoffmann, M. Cornelius, J. Morell, M. Fröba, Angew. Chemie - Int. Ed. 45 (2006) 3216–3251.

[3]   C. Sanchez, P. Belleville, M. Popall, L. Nicole, Chem. Soc. Rev. 40 (2011) 696.

[4]   C. Sanchez, B. Julián, P. Belleville, M. Popall, J. Mater. Chem. 15 (2005) 3559.

[5]   S. Yano, Polymer (Guildf). 35 (1994) 5565–5570.

[6]   R.A. Zoppi, M.C. Gonçalves, J. Appl. Polym. Sci. 84 (2002) 2196–2205.

[7]   K. Tanaka, H. Kozuka, J. Mater. Sci. 40 (2005) 5199–5206.

[8]   R.S. Gill, M. Marquez, G. Larsen, Microporous Mesoporous Mater. 85 (2005) 129–135.

[9]   S. Sequeira, D. V. Evtuguin, I. Portugal, Polym. Compos. 30 (2009) 1275–1282.

[10]   S. Sequeira, D. V. Evtuguin, I. Portugal, A.P. Esculcas, Mater. Sci. Eng. C 27 (2007) 172–179.

[11]   H.S. Barud, R.M.N. Assunção, M.A.U. Martines, J. Dexpert-Ghys, R.F.C. Marques, Y. Messaddeq, S.J.L. Ribeiro, in:, J. Sol-Gel Sci. Technol., Springer US, 2008, pp. 363–367.

[12]   M.A. Tshabalala, P. Kingshott, M.R. VanLandingham, D. Plackett, J. Appl. Polym. Sci. 88 (2003) 2828–2841.

[13]   M. Abdelmouleh, S. Boufi, M.N. Belgacem, A. Dufresne, A. Gandini, J. Appl. Polym. Sci. 98 (2005) 974–984.

[14]   B. Ding, C. Li, Y. Hotta, J. Kim, O. Kuwaki, S. Shiratori, Nanotechnology 17 (2006) 4332–4339.

[15]   X. Chen, Y. Liu, H. Lu, H. Yang, X. Zhou, J.H. Xin, Cellulose 17 (2010) 1103–1113.

[16]   J. Alongi, M. Ciobanu, G. Malucelli, Cellulose 18 (2011) 167–177.

[17]   M. Kaushik, H.M. Friedman, M. Bateman, A. Moores, RSC Adv. 5 (2015) 53207–53210.

[18]   M. Rezayat, R.K. Blundell, J.E. Camp, D.A. Walsh, W. Thielemans, ACS Sustain. Chem. Eng. 2 (2014) 1241–1250.

[19]   X. Wu, C. Lu, Z. Zhou, G. Yuan, R. Xiong, X. Zhang, Environ. Sci. Nano 1 (2014) 71.

[20]   N. Rattanasom, S. Prasertsri, T. Ruangritnumchai, Polym. Test. 28 (2009) 8–12.

[21] H. Peng, L. Liu, Y. Luo, X. Wang, D. Jia, Polym. Compos. 30 (2009) 955–961.

[22] K.W. Stöckelhuber, A. Das, R. Jurk, G. Heinrich, Polymer (Guildf). 51 (2010) 1954–1963.

[23] W.H. Dokter, I.I.M. Tijburg, Precipitated Silica, a Process to Make It, and Its Use, WO2001007364 A1, 2001.

[24] J. Song, G. Fu, Q. Cheng, Y. Jin, Ind. Eng. Chem. Res. 53 (2014) 708–714.

[25] R.C. Schroden, C.F. Blanford, B.J. Melde, B.J.S. Johnson, A. Stein, Chem. Mater. 13 (2001) 1074–1081.

[26] S.R. and W. FX, in:, Spectrom. Identif. Org. Compd., 2010, pp. 71–143.

[27] M. Kacuráková, A.C. Smith, M.J. Gidley, R.H. Wilson, Carbohydr. Res. 337 (2002) 1145–53.

[28] F. Vilmin, I. Bottero, A. Travert, N. Malicki, F. Gaboriaud, A. Trivella, F. Thibault-Starzyk, J. Phys. Chem. C 118 (2014) 4056–4071.

[29] U. Goerl, A. Hunsche, A. Mueller, H.G. Koban, Rubber Chem. Technol. 70 (1997) 608–623.

[30] A. V. Krasnoslobodtsev, S.N. Smirnov, Langmuir 18 (2002) 3181–3184.

[31] E.M. Dannenberg, Rubber Chem. Technol. 48 (1975) 410–444.

[32] S.-S. Choi, B.-H. Park, H. Song, Polym. Adv. Technol. 15 (2004) 122–127.

[33] M.A. Kader, C. Nah, Polymer (Guildf). 45 (2004) 2237–2247.

[34] C.H. Chen, J.L. Koenig, J.R. Shelton, E.A. Collins, Rubber Chem. Technol. 55 (1982) 103–115.

[35] R.M. Russell, T.D. Skinner, A.A. Watson, Rubber Chem. Technol. 42 (1969) 418–440.

[36] J. Fröhlich, W. Niedermeier, H.D. Luginsland, Compos. Part A Appl. Sci. Manuf. 36 (2005) 449–460.

[37] M.A. Meyers, K. Chawla, Mechanical Behavior of Materials, Cambridge University Press, 2009.

[38] W. Bai, K. Li, Compos. Part A Appl. Sci. Manuf. 40 (2009) 1597–1605.

7.   Summary and Conclusions

The research presented in this thesis deal with the development of renewable and low-density fillers to replace the traditional fillers in the tire industry. Two selected biomasses i.e. rice husk and *Arundo donax* were fractionated through biorefinery process into value-added products. An integrated biorefinery process based on acidic leaching, alkaline treatment, and concentrated sulfuric acid hydrolysis was set up for the simultaneous recovery of lignin, hemicelluloses, silica, and cellulose nanocrystals (CNCs). The major appeal of the proposed process lies in the relative simplicity of the refining process that enabled the recovery of all the desired products with high purity and reasonable overall yield. Among the extracted materials, the reinforcing capability of the CNCs was initially investigated by partially replacing the silica with increasing contents of CNCs in rubber compounds prepared through the dry-mixing process. The dynamic and tensile mechanical studies of the prepared compounds showed an improved processability of the compounds, however, the reinforcing effect was reduced with the increasing content of CNCs. This behavior of CNCs was connected to the poor dispersion of the CNCs in the rubber matrix and inferior CNCs-polymer interactions. By changing processing method of rubber compounding from dry-mixing to co-precipitation, made it possible of obtaining the high dispersion of CNCs in the rubber matrix and functionalization of CNCs with silane coupling agents enhanced the interfacial interaction between the CNCs and polymer. Six different silane coupling agents containing similar hydrolyzable alkoxy group while different organic functionalities (polysulfide, acrylic, thiol, amine, and vinyl) demonstrated varying reactivity toward the natural rubber. Two different approaches used for the functionalization of CNCs significantly influenced the compatibilizing efficiency of silane coupling agents, which in turn affected the reinforcing capability of CNCs. Reduced reinforcement observed for pre-functionalized CNCs was related to their poor dispersion in the rubber matrix. However, very higher reinforcement observed for compounds filled with post-functionalized CNCs than silica-filled compound demonstrated the higher reinforcing capability of the CNCs than silica and can be used to replace the silica in the tire compounds. The potential of CNCs to replace silica in rubber compounds was additionally explored by preparing a CNC/Silica hybrid material by coating CNCs surface with a layer of

silica nanoparticles. The properties of the hybrid materials are not only the sum of the properties of their individual counterparts but the inner interface could also play an important role in obtaining improved and unique properties of the hybrid materials. The CNC/Silica hybrid incorporated in natural rubber through co-precipitation method was homogeneously dispersed into the polymer matrix and resulting compound showed much higher reinforcing effect than silica-filled compounds, in addition to the lower density. Furthermore, the high dispersion of the hybrid increased the contact area between the anisotropic hybrid filler and the polymer which resulted in stronger interfacial interaction between the hybrid filler and polymer and allowed achieving the improved mechanical properties of the hybrid-filled rubber compounds. Rubber compounds prepared with different filler contents demonstrated that compound filled with 20 phr of CNC/Silica hybrid have similar reinforcement as compound filled with 40 phr of silica but with a lower density of the final compound. Thus, the CNC/Silica hybrid can potentially replace silica in elastomeric compounds to produce greener and lighter tires.

List of Publications

1. Barana, D., Salanti, A., Orlandi, M., Ali, D. S., & Zoia, L. (2016). Biorefinery process for the simultaneous recovery of lignin, hemicelluloses, cellulose nanocrystals, and silica from rice husk and Arundo donax. *Industrial Crops and Products*, *86*, 31-39.

2. Patent Application

   Inventors: Ali S. D., Zoia L., Orlandi M., Castellani L., Hanel T.

   Title: Pneumatico per ruote di veicoli comprendente una carica di rinforzo composita

   Application No.: 102017000102274

   Filing date: 13 Sep, 2017